Organization of olfactory signal transduction – a molecular analysis

Inaugural-Dissertation to obtain the academic degree

Doctor rerum naturalium (Dr. rer. nat.)

submitted to the Department of Biology, Chemistry and Pharmacy

of Freie Universität Berlin

by **Bastian Henkel**

from Schwelm

July 2014

This work was prepared from 1st June 2010 to 31 July 2014 under the supervision of Prof. Dr. Eva Neuhaus as part of the Cluster of Excellence NeuroCure at Charité - Universitätsmedizin Berlin.

1st Reviewer: **Prof. Dr. Eva Neuhaus**
Institute for Pharmacology and Toxicology
Jena University Hospital

2nd Reviewer: **Prof. Dr. Stephan Sigrist**
Institute of Biology
Department of Biology, Chemistry and Pharmacy
Freie Universität Berlin

Date of defense: 16.01.2015

Acknowledgments

A four year PhD-project is surely not the solely work of a single person. I received valued feedback, input and support from a myriad of different persons. Here, I want to express my thanks to all of you and name at least a few who specifically contributed to this work.

First and foremost, I would like to thank my supervisor Eva Neuhaus. When she moved her lab to Berlin and I expressed my wish to join the team, she immediately offered me a PhD position and thereby provided me with the great opportunity to study in this excellent research environment. Thank you for sharing your expertise, for your support and for the great freedom you endowed me with to conduct this project. I certainly learned a lot in this time.

I would like to thank Stephan Sigrist for taking over responsibilities as second reviewer of my thesis and being part of my thesis committee. Furthermore, the people from his lab supplied me with materials and knowledge to establish the dual color STED technique used in this thesis. Without him, this work would not have been possible.

Special thanks goes to the whole Neuhaus Group. Willem Bintig, Sonja Oberland, Thomas Pelz, Niels de Wit and Dina Reihnhart. Thank you for your support and encouragement, your input, feedback and comments.

Thanks to all members of our weekly Tuesday Journal Club / Progress Report Group, especially group leaders, Sarah Shoichet, Hans-Christian Kornau, Britta Eickholt and Gregory Wulczyn. Thank you for the opportunity to present my research and hone my presentation skills. Thank you for the productive discussions, valuable feedback and critical comments concerning my work.

I thank Marc Spehr, Tobias Ackels and Daniela Drose for the successful collaboration on the Anocatmin project. They recorded the electrophysiological

data from Anoctamins presented here. Your contribution added significantly to this work. Thank you for all your support, feedback and ideas.

A heartfelt thanks goes to all my friends in Berlin who have made this such a great time here, especially Michael and Nina. I do not know what I would have done without our countless evenings of board gaming. You are the best!

My parents and family, thank you for all your love and support. Without you, this would not have been possible.

Then I would like to mention my long term friends Sina who always helps me not to get lost in this mess called life and of course Kim. Thank you for being a friend even in rough times. I will always admire your strength and character.

Finally, my loving wife Melanie. Thank you for listening to all those things which did not work out and enduring me in this final stage of writing. Thank you for believing in me and all your support and love. You are the best wife a man could wish for!

Contents

1 Introduction

The capability to perceive the surrounding environment is a fundamental trait of all biological life. Based on the necessity to detect, process and react to a myriad of different stimuli, organisms developed a multitude of complex sensory systems. Even single celled organisms discern between numerous chemical stimuli. They react to changes in osmotic or pH conditions or they get into contact with other cells. Higher organisms like mammals evolved complex sensory systems, which detect different environmental conditions and convert them to signals the brain can process, ultimately affecting or even controlling their behavior.

1.1 The olfactory system

The olfactory system conveys a tremendous amount of information and is often underestimated from our human point of view. Most vertebrate species use it extensively not only to evaluate food (Yeomans, 2006) or detect potential dangers (Dielenberg & McGregor, 2001), but also in terms of social communication. Kin recognition, mate choice and social status are just a few examples for intra-species communication mediated by the olfactory system (Tirindelli et al., 2009).

Over the last decades, the knowledge about the olfactory system grew profoundly on anatomical and physiological levels. However, many processes and features are still not understood in detail. Some olfactory stimuli, for example, trigger behavioral or physiological reactions which are to some extent innate (Kobayakawa et al., 2007). How much of these unconscious responses are still present in humans remains elusive. The sense of smell is mediated through olfactory receptors (Buck & Axel, 1991). The olfactory receptor gene family is the largest gene family in the animal genome and every olfactory neuron expresses only one olfactory receptor from this family (Chess et al., 1994). Understanding of this extreme gene selection is still incomplete. The olfactory system is one of the very few places in the vertebrate brain where neurons are constantly re-

placed (Brann & Firestein, 2010; Graziadei & Monti Graziadei, 1983). The process of continuously integrating newly generated neurons into a fully developed circuit is astonishing and far from comprehensively investigated. All these characteristics render the olfactory system a fascinating and practical model system to study fundamental neurological questions.

1.1.1 Morphology of the main olfactory system and the vomeronasal organ

The enormous range of sensory information gathered by the olfactory system states the concept of the nose being a single organ a gross oversimplification. The mammalian olfactory system is comprised of separate subsystems (Munger et al., 2009) (Fig. 1.1).

The subsystems differ in their expression of receptors, their employed signaling mechanisms and ultimately in their primary chemosensory stimuli. These stimuli include airborne volatile odors, hormones and single peptides. Some of these subsystems, like the main olfactory epithelium (MOE) or the vomeronasal organ (VNO) are well studied. Others, like the Grueneberg ganglion (GG) or the septal organ (SO) are less well characterized (Munger et al., 2009).

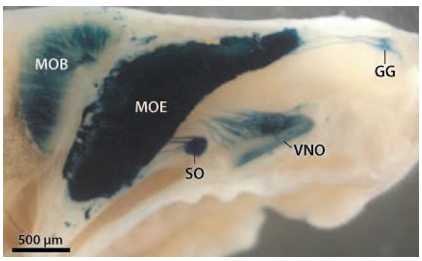

Figure 1.1: Olfactory subsystems. Sagital vibratome slice of a mouse head showing olfactory neurons labeled with β-galactosidase in olfactory subsystems. Neurons located in the main olfactory epithelium (MOE), the vomeronasal organ (VNO), the septal organ (SO) and the Grueneberg ganglion (GG) project their axons to the main olfactory bulb (MOB) (Munger et al., 2009).

The main olfactory epithelium primarily mediates the classic sense of smell. It detects more than 1 trillion volatile odorants (Bushdid et al., 2014). The main olfactory systems spreads out on cartilaginous lamellae called turbinates in-

side the upper part of the nasal cavity (Breer et al., 2006) (Fig. 1.2 B). The epithelium is comprised of different cell layers. One basal cell layer of constantly dividing stem cells on the basal lamina (Huard & Schwob, 1995), one layer of immature olfactory sensory neurons in various stages of differentiation (Kott & Westrum, 1996), the layer with fully mature olfactory sensory neurons (OSN) with their dendrites protruding into the nasal cavity (Moulton & Beidler, 1967) and one apical layer of supporting cells forming the physical barrier of the epithelium (Suzuki et al., 1996) (Fig. 1.2 C). The mature olfactory sensory neurons use their dendrites to reach into the nasal cavity and detect volatile odorants. The dendrites end in a thick dendritic knob with around 20 - 30 very fine cilia protruding into the nasal cavity. The olfactory sensory neurons project their axons directly to the olfactory bulb (Fig. 1.2 D).

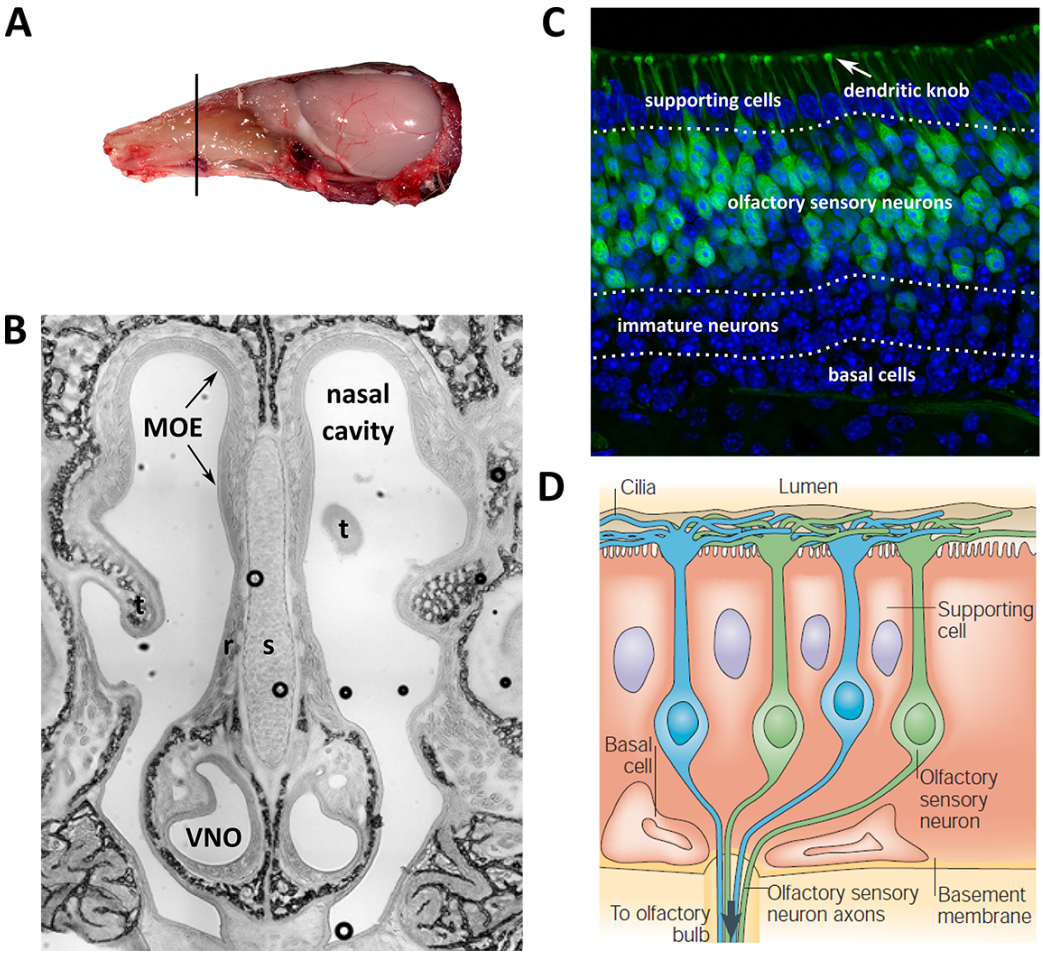

Figure 1.2: Morphology of olfactory system. **A:** Skinned mouse head sagittal split in half. Line indicate position of coronal section. **B:** Coronal section of mouse nose with labeled structures. MOE = main olfactory epithelium, VNO = vomeronasal organ, r = respiratory epithelium, s = nasal septum, t = turbinates. **C:** Cryosection of olfactory epithelium from OMP-GFP mouse (Potter et al., 2001) with different cell layers labeled. Mature olfactory sensory neurons are labeled by GFP expression. **D:** Schematic representation of cellular organization in the olfactory epithelium A-C: modified from (Oberland, 2014), D: modified from (Mombaerts, 2004).

The vomeronasal organ is located at the base of the nasal cavity above the upper denture. It is a pairwise crescent-shaped tube, blind ending and fluid filled (Fig. 1.2 B). The whole organ is embedded in a cartilage capsule (Halpern & Martinez-Marcos, 2003). The vomeronasal organ does not only detect volatile stimuli but also peptides and proteins (Dulac & Torello, 2003). These ligands serve for intra-species communication and trigger behavioral or physiological processes (Zufall et al., 2002). The concave side of the vomeronasal organ is

covered with sensory epithelium. The cellular organization is quite similar to the main olfactory epithelium. In contrast, the vomeronasal sensory epithelium harbors two layers of mature vomeronasal sensory neurons (VSN) (Chamero et al., 2012). These two cell populations differ in their choice of receptor expression and partially in their utilized signaling cascades and they detect different classes of ligands (Spehr & Munger, 2009).

One population is found in the apical part and expresses receptors from the vomeronasal receptor family type 1 (V1). The other population resides in basal parts of the epithelium and expresses receptors from vomeronasal receptor family type 2 (V2). The V1 receptor family is tuned for volatile pheromones (Leinders-Zufall et al., 2000). V2 receptors detect small peptide ligands which provide information about the genetic equipment of conspecifics (Kimoto et al., 2005; Leinders-Zufall et al., 2004).

1.1.2 Signal transduction in the main olfactory epithelium and vomeronasal organ

Olfactory sensory neurons in the main olfactory epithelium feature non-motile cilia at their dendritic ends (Menco, 1984). They function as specialized signal transduction compartments. Technically, olfactory cilia represent electro-diffusional cables which transmit electrical signals to cell body (Kleene et al., 1994; Lindemann, 2001).

The olfactory cilia harbor all relevant signal transduction proteins (Kleene, 2008). A schematic display can be found in Fig. 1.3. Receptors from the olfactory receptor family are expressed (Buck & Axel, 1991) together with G protein $G_{\alpha olf}$ (Jones & Reed, 1989). Upon ligand binding the G protein activates an adenylate cylcase type III (Bakalyar & Reed, 1990). This enzyme produces second messenger cAMP to activate the olfactory cyclic nucleotide-gated (CNG) channel, a non-specific cation channel (Zheng & Zagotta, 2004). Activation of the CNG channel depolarizes the cell and inflowing calcium activates a calcium-gated chloride channel (Kleene & Gesteland, 1991). Anoctamin 2 was recently identified as the calcium-gated chloride channel in olfactory cilia (Billig et al., 2011; Rasche et al., 2010; Stephan et al., 2009).

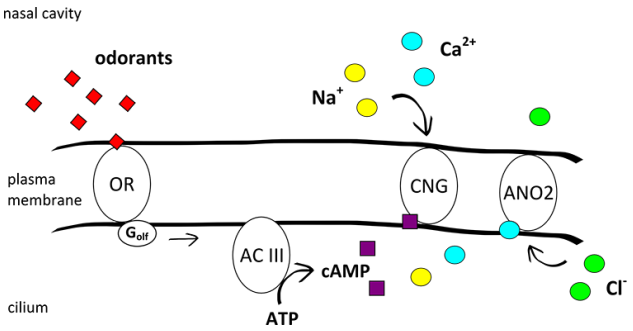

Figure 1.3: Signal transduction in the main olfactory epithelium. Signal transduction takes place in cilia of olfactory sensory neurons. Odorants bind to olfactory receptors (OR), the G protein $G_{\alpha olf}$ activates an adenylate cylcase type III (AC III) which leads to production of cAMP. cAMP activates a cyclic nucleotide-gated cation channel (CNG). The influx of cation depolarizes the cell and calcium activates calcium-gated chloride channel Anoctamin 2 (ANO2) leading to chloride efflux and further depolarization.

Vomeronasal signal transduction also takes place in specialized cell compartments, the neuronal microvilli. They protrude from the dendritic knob into the vomeronasal duct to probe for ligands and harbor the complete vomeronasal signaling cascade (Trotier et al., 1998). Like olfactory cilia, neuronal microvilli represent electro-diffusional cables which transmit an electrical signal to the cell body upon receptor stimulation.

Two different cell populations expressing different receptor families, namely V1 and V2 receptors, are found in the vomeronasal organ (Munger et al., 2009). The expression of these receptor families is linked to the expression of two different G proteins. V1 receptors are coupled to $G_{\alpha i2}$ protein while V2 receptors use $G_{\alpha o}$ for signal transmission (Jia & Halpern, 1996). Further signal transduction is supposed to be identical in both cell populations. The participating proteins of vomeronasal signal transduction have not been conclusively identified on genetic level. Hence the exact process of vomeronasal signaling is not fully understood. A schematic display can be found in Fig. 1.4.

Ligand binding confers a conformation change in vomeronasal receptors. This change activates the corresponding G protein which in turn activates phospholipase C (PLC), which cleaves phosphoinositol-phosphate-2 (PIP2) into inositol-phosphate-3 (IP3) and diacylglycerol (DAG) (Zufall et al., 2005). These two second messengers activate TrpC2 (transient receptor potential C2) channels, which leads to cation influx and subsequent depolarization of the cell (Lu-

cas et al., 2003). The elevated calcium levels activate a calcium-gated chloride channel. This leads to chloride efflux with further depolarization of the cell and ultimately to the generation of an action potential (Kim et al., 2011). The identity of this calcium-gated chloride channel is currently unknown, but expression of Anoctamins has also been shown in the vomeronasal organ (Billig et al., 2011; Rasche et al., 2010).

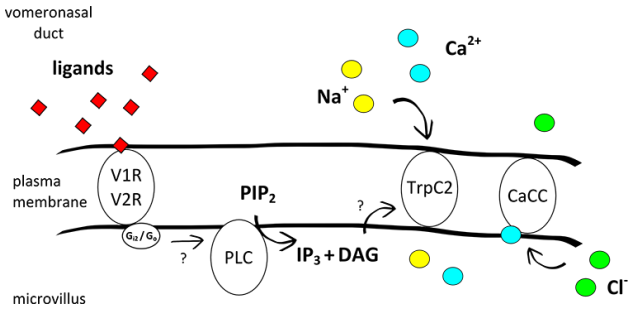

Figure 1.4: Signal transduction in the vomeronasal organ. Signal transduction takes place in microvilli of vomeronasal sensory neurons. Ligands bind to vomeronasal receptors type 1 or type 2 (V1R, V2R). The G protein $G_{\alpha i2}$ is associated with V1 receptors, $G_{\alpha o}$ with V2 receptors. Both G proteins activate a phospholipase C (PLC) which leads to production of IP3 and DAG. These second messenger molecules activate a TrpC2 channel. The influx of cation depolarizes the cell and calcium activates an unknown calcium-gated chloride channel (CaCC) leading to chloride efflux and further depolarization. ? indicate parts of the cascade which details remain elusive.

1.1.3 Common principles in olfactory subsystems

Although the olfactory subsystems meet very different needs, their anatomy and physiology share a number of common attributes. All olfactory epithelia are organized in cell layers. All sensory neurons express a single olfactory receptor. The olfactory sensory neurons in all systems project their unbranched axons directly to the olfactory bulb (Klenoff & Greer, 1998). All axons from neurons expressing a certain receptor converge in only a few defined spots of the olfactory bulb(Mombaerts, 2004; Spehr & Munger, 2009).

Olfactory sensory neurons in all systems have receptors localized at the dendritic tip to probe the periphery for stimuli. These dendrites end in a thick dendritic knob featured with either non-motile cilia or microvilli (Menco, 1984). In all cases these extensions are specialized cell compartments for olfactory signal transduction.

Although the cells use different proteins, the basic principle of signal transduction in most olfactory neurons remains the same (Kleene, 2008; Munger et al., 2009) (Fig. 1.5). Olfactory neurons express G protein-coupled 7 transmembrane receptors from the olfactory receptor or vomeronasal receptor gene family. These receptors detect ligands from the periphery and docking leads to conformation change of the receptor with activation of the G protein. The G proteins activate downstream enzymes leading to production of second messenger molecules. These molecules activate a non-specific cation channel which is followed by cation influx and subsequent depolarization of the cell. Entering calcium opens a calcium-gated chloride channel, which leads to chloride efflux und further depolarization of the cell.

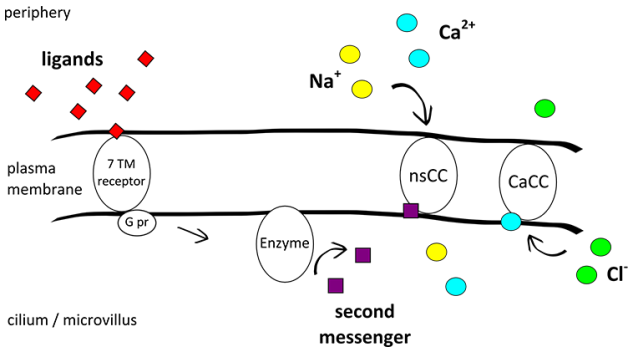

Figure 1.5: General principle of olfactory signal transduction. Olfactory signal transduction takes place in specialized cell compartments, namely cilia or microvilli. Odorants bind to G protein-coupled 7 transmembrane receptors, the G protein activates an enzyme leading to the production of second messenger molecules. These molecules activate a non-specific cation channel (e.g. olfactory CNG channel, TrpC2). The influx of cation depolarizes the cell and calcium activates a calcium-gated chloride channel (e.g. ANO2) leading to chloride efflux and further depolarization.

It is worth mentioning that the described schema does not fully apply to all olfactory neurons. A small (and less well studied) subpopulation does not express 7 transmembrane G protein-coupled receptors but the receptor guanylyl cyclase GC-D (Fuelle et al., 1995). Likewise, a small set of olfactory sensory neurons from the main olfactory epithelium does not express olfactory receptors but receptors from the trace amine-associated receptor (TAAR) family (Liberles & Buck, 2006). Some vomeronasal sensory neurons do not express vomeronasal receptors but one of five formyl peptide receptors (FPR) (Riviere et al., 2009).

1.1.4 Olfactory cilia vs. neuronal microvilli

In contrast to the olfactory sensory neurons, the dendritic knobs of vomeronasal sensory neurons feature microvilli instead of cilia (Eisthen, 1992). The functional reason for this variation is completely unknown (Elsaesser & Paysan, 2007). Technically, both cell compartments are able to fulfill similar functions. They represent cable-like structures with a high surface-to-volume ratio (Kleene et al., 1994; Lindemann, 2001). Both are ideally outfitted to probe the cell periphery for signaling molecules and to transmit electrical signals to the cell body. However, cilia are considered complex separate cell organelles where microvilli basically represent protrusions of the plasma membrane (Fath & Burgess, 1995; Ishikawa & Marshall, 2011).

On phylogenetic level olfactory sensory neurons are remarkably unselective in regard of their signaling compartment. While e.g. sharks have only microvilliar olfactory neurons, frogs and snakes only posses ciliated neurons (Eisthen, 1992). In salamander olfactory epithelium both cell types reside next to each other and birds even posses cells featuring microvilli and cilia on the same olfactory neuron (Eisthen, 1992; Kolnberger, 1971).

1.2 The evolving model of signaling cascades

The rather sophisticated signal transduction pathways involving G protein-coupled receptors were first imagined with free diffusing proteins meeting on occasion of a signaling event (Singer & Nicolson, 1972). This model led to the term "signaling cascade" (Fung et al., 1981; Liebman & Pugh Jr, 1979). The concept got well established in the visual system of the fly (Zuker, 1996). Nonetheless, certain response dynamics could not be explained with a model of free floating proteins (Ranganathan et al., 1991).

This observation led to the idea that signaling cascades need to include additional organizing elements. Triggered through very brief stimuli a complex set of proteins would need to interact with each other. This process takes part in spatially restricted cell compartments, like olfactory cilia or microvilli. These requirements challenged the free-floating diffusion model.

Today, the free-floating diffusion model gets more and more replaced by a model of complex structural organization (Huber, 2001). This organization is mediated by so called scaffolding proteins. The function of scaffolding proteins in sensory systems was first described in the visual system of *Drosophila melanogaster* (Pak et al., 1970; Shieh & Zhu, 1996). Scaffolding proteins feature protein-protein interaction domains which enable them to cluster proteins in close spatial proximity and in defined stoichiometry (Huber, 2001). In addition, they often interact with the cytoskeleton to serve as anchors for their interaction partners (Wu et al., 1998). Many scaffolding proteins also interact with each other to form complex hubs for protein-protein interactions (Montell, 1998). Inactivation no after potential (INAD) provides these functions in *Drosophila* photoreceptor cells. INAD recruits members of the visual signaling cascade into a functional complex and tethers this complex to the cytoskeleton (Hardie & Raghu, 2001) (Fig. 1.6).

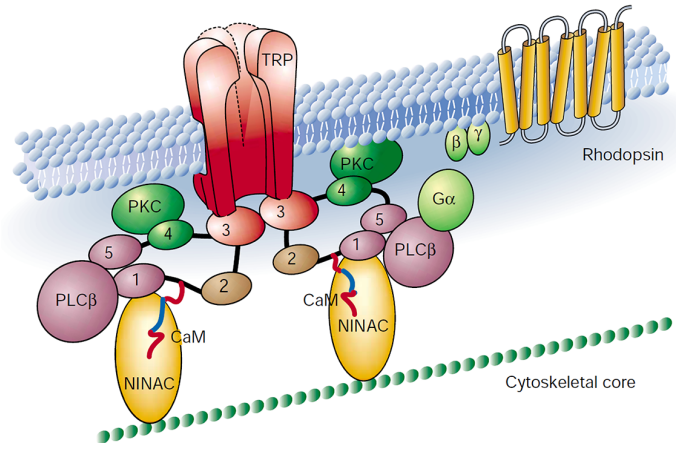

Figure 1.6: INAD signaling complex in *Drosophila* photoreceptor cells. INAD recruits different proteins from *Drosophila* visual signaling cascade into one functional complex. Interaction with NINAC tethers the complex to the cytoskeletal core, PDZ-PDZ interaction between PDZ domains 3 and 4 mediates multimerization of single INAD proteins into a signaling network. (Hardie & Raghu, 2001)

Moreover, scaffolding proteins have also been found to organize sensory transduction in vertebrate visual system (Roepman & Wolfrum, 2007), in auditory system (Verpy et al., 2000) and olfactory system (Baumgart et al., 2014; Dooley et al., 2009). Apart from sensory systems, scaffolding proteins were

extensively studied for their substantial role in synaptic transmission (Feng & Zhang, 2009).

1.2.1 Signaling microdomains

Signaling scaffolds operate as regulatory elements in signaling networks. Scaffolding proteins organize members of signaling cascades into functional microunits. These units form individual working entities in signaling compartments of cells, so called signaling microdomains (Good et al., 2011; Zeke et al., 2009).

Assembling relevant proteins into functional complexes provides several benefits. Trafficking of proteins is simplified if only one assembled complex has to be transported (Good et al., 2011). Binding partners are often either catalytic or regulatory elements (Pawson & Nash, 2003). These proteins get grouped together in optimized stoichiometry (Huber, 2001). Moreover, combination of new scaffold proteins or recombination of existing components provides a powerful way to create new circuits (Bhattacharyya et al., 2006).

Several examples of functional microunits have been described. Scaffolding proteins regulate intracellular GTPase signaling (Kozubowski et al., 2008), or cell-cell interaction at tight junctions (Funke et al., 2005; Jelen et al., 2003). However, apart from INAD signaling complex in the *Drosophila* eye (Zuker, 1996), no signaling complex in sensory neurons has been investigated in detail.

1.3 PDZ scaffolding proteins

Postsynaptic-density-95/Disc-large/zonula occludens-1 (PDZ) domain scaffolding proteins represent one of the most versatile scaffolding protein classes and are present in all multi-cellular organisms. 150 PDZ domain-containing proteins with over 250 non-redundant PDZ domains have been identified in the human proteome (Wang et al., 2010). They are ubiquitously expressed and among the most abundant proteins in the human proteome (Huber, 2001). PDZ scaffolding proteins are significantly involved in numerous cellular processes: Assembly of neuronal synapses, establishment and maintenance of epithelial cell

polarity, forming of cell shapes via interactions with the cytoskeleton and signal transduction in sensory neurons (Feng & Zhang, 2009; Huber, 2001; Ye & Zhang, 2013).

PDZ domains consist of 80 - 90 amino acids. They appear as a compact globular fold with a core of 6 β-strands and 2 α-helices (Fig. 1.7 left). PDZ ligands bind to a carboxylated binding loop called βA - βB loop. This loop contains the crucial GLGF motif defining the PDZ domain binding pocket (Karthikeyan et al., 2001) (Fig. 1.7 right). PDZ domains recognize most suitable PDZ ligands at the very C-terminus of the protein. Residues in the domain binding pocket interact with the four C-terminal amino acids of a ligand (Lenfant et al., 2010).

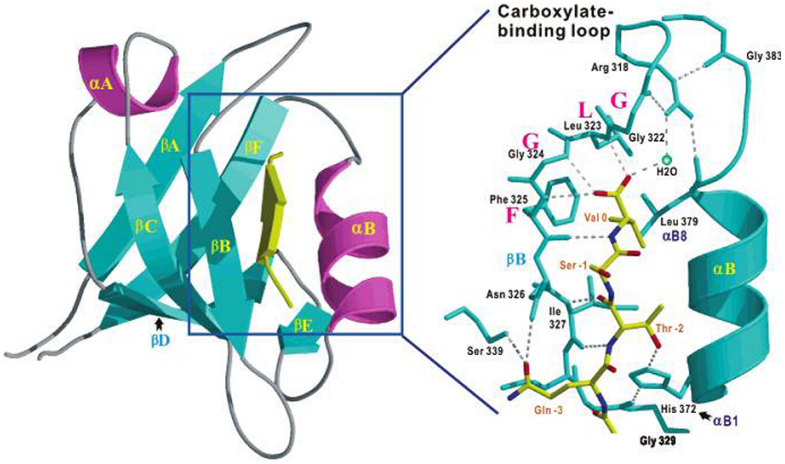

Figure 1.7: Canonical PDZ ligand binding. Crystal structure of the PDZ3 domain from PSD95 with bound PDZ ligand (yellow). Right image shows ligand binding pocket with conserved GLGF motif in detail. Hydrogen bonds are indicated by grey dashed lines. PDZ ligand oxygen atoms are depicted in red, nitrogen in blue, carbon atoms in yellow. (Zhang & Wang, 2003)

Initially, PDZ ligands were grouped into three classes based on their C-terminal motifs (Songyang et al., 1997). Class I with S/T - X - ϕ, Class II with ϕ - X - ϕ and Class III with D/R - X - ϕ, where ϕ represents a hydrophobic amino acid and X any amino acid.

It became, however, apparent that C-terminal tail peptides with only a few residues are too restrictive to fully account for the functional and structural characteristics of PDZ interaction. Investigations of PDZ interactions identified critical residues upstream of canonical PDZ motifs (Yan et al., 2009; Zhang et al.,

2008). Thus, high throughput approaches using structural modeling of PDZ interaction tried to develop a comprehensive classification for PDZ domain binding characteristics (Stiffler et al., 2007; Tonikian et al., 2008). Still, a new simple and applicable classification remains elusive and the idea of PDZ interaction as a simple lock-key-principle gets more and more rebutted.

PDZ domains are more than simple beads-on-a-string or passive glue between proteins. Two or more PDZ domains connected often display distinct properties from single, isolated PDZ domains (Ye & Zhang, 2013). PDZ domains engage in PDZ-PDZ domain interaction to form PDZ domain tandem pairs or even scaffolding protein oligomers which modulate PDZ ligand binding specificity (Chang et al., 2011). Thus, PDZ domains regulate interaction not only through their binding pocket sequence but also through intra-and extramolecular interaction.

PDZ domain interactions are also determined by their context. The context can be defined by the cellular environment or be encoded in the sequence (Stein & Aloy, 2008). Several examples are described for the PDZ domain sequence. Apart from the normal binding groove, the $\beta 2$ - $\beta 3$ loop can form an additional peptide binding pocket to accommodate upstream peptide residues from the PDZ ligands (Mostarda et al., 2012). The 90 amino acid PDZ domain only represents the conserved core domain. 40% of PDZ domains feature extension sequences at both termini of the canonical domain boundaries. They form conserved α helices or β strands and contribute to PDZ ligand binding in multiple ways (Wang et al., 2010). Gradually, more and more individual examples of extended core domains or C-terminal binding motifs emerge, extending the catalog of non-canonical PDZ interactions (Luck et al., 2012).

1.3.1 NHERF1

PDZ domain scaffolding protein NHERF1 was first identified as a regulator of Na^+/H^+-exchanger isoform 3 (NHE3) in brushboarder cells of kidney. Subsequently it was named NHE3-regulating factor 1 (NHERF1) (Weinman et al., 2006). Later, a second group isolated a 50 kDa protein associated with Ezrin from human placenta lysate and named it Ezrin-binding-protein 50 (EBP50) (Reczek

et al., 1997). The two proteins turned out to be identical but still both names are in use. Since the protein was first identified in kidney, we refer to it as NHERF1.

The NHERF protein family is comprised of 4 PDZ scaffolding proteins (Fig. 1.8). NHERF1 and NHERF2 feature two PDZ domains and an Ezrin/Radixin/Moesin (ERM) binding domain. NHERF3 and NHERF4 possess 4 PDZ domains, and no ERM domain. The C-terminal Class I PDZ motif is a unique feature of NHERF1 (Ardura & Friedman, 2011).

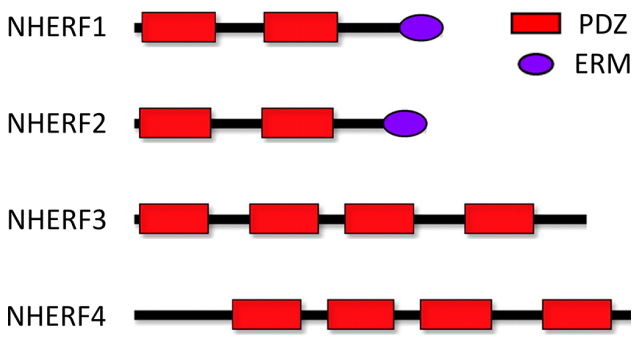

Figure 1.8: NHERF family of scaffolding proteins. Schematic display of characteristic functional domains of NHERF family scaffolding proteins. Modified from (Ardura & Friedman, 2011).

NHERF1 is highly expressed in kidney, placenta, brain, liver, the gastrointestinal tract and the airway epithelium. Basically, NHERF1 is present in every tissue with extensively polarized epithelia (Ediger et al., 1999; Ingraffea et al., 2002). The subcellular localization of NHERF1 is strictly regulated. Mistargeting of NHERF1 is discussed as a tumor-inducing factor (Georgescu et al., 2008). NHERF1 co-localizes with ERM proteins at the apical cell surface and is associated with actin-rich cell structures like filopodia or microvilli (Ardura & Friedman, 2011).

NHERF1 is essential for microvilli formation by recruiting different proteins to the apical plasma membrane (LaLonde et al., 2010). NHERF1 also plays a substantial role in signaling processes by forming multiprotein-complexes including G protein-coupled receptors (GPCR) (Ardura & Friedman, 2011) or ion channels (Hall et al., 1998).

Moreover, NHERF1 interacts with other scaffolding proteins through heterodimerization, either through interaction of two PDZ domains (Lau & Hall, 2001) or through direct binding of another scaffolding protein as PDZ ligand (LaLonde

et al., 2010). In addition, NHERF1 putatively forms homo-dimers through PDZ-PDZ domain interaction (Fouassier et al., 2000).

Two knockout mouse models have been described for NHERF1 (Morales et al., 2004; Shenolikar et al., 2002). Loss of NHERF1 leads to defective microvilli formation and ostenopenia through renal phosphate and calcium wasting. The latter due to loss of ion transporters in the apical membrane of brushboarder cells in kidney. Apart from gastrointestinal effects, NHERF1$^{-/-}$ mice also display defective G protein-coupled receptor signaling (Capuano et al., 2007; Weinman et al., 2006).

1.3.2 DLG1

The scaffolding protein DLG1 is part of the MAGUK (membrane-associated guanylate kinase) protein super-family. Members of this family feature several protein-protein interaction domains always including PDZ domains, one SH3 domain and one GK domain (Fig. 1.9) (Fujita & Kurachi, 2000). Given that DLG proteins are predominantly expressed in synaptic connections, some DLG proteins are also called synapse associated proteins (SAP), hence DLG1 is also known as SAP97.

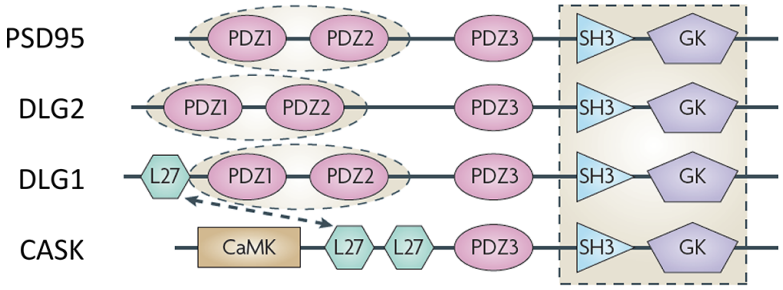

Figure 1.9: MAGUK family scaffolding proteins. Schematic display of characteristic functional domains of MAGUK family scaffolding proteins. Marked domains label functional units for scaffolding processes. Arrows illustrate multimerization through L27 domains. Modified from (Nourry et al., 2003).

SAP proteins are now well established for their part in forming the postsynaptic density in excitatory synapses (Feng & Zhang, 2009). This mesh of scaffolding proteins below the postsynaptic membrane organizes receptors, ion channels and cell adhesion molecules.

DLG1 was first identified as a PSD95 homolog (another SAP protein) from a cDNA library encoding components of synaptic connections and was found to be localized to presynaptic nerve terminals (Muller et al., 1995). Later, DLG1 was also identified as part of the postsynaptic density (Valtschanoff et al., 2000).

DLG1 interacts with G protein-coupled receptors (He et al., 2006) and regulates their trafficking and internalization through PDZ interaction (Gardner et al., 2007; Nooh et al., 2013). Furthermore, DLG1 forms heteromers with other members of the MAGUK family or homomers through its L27 domain (Feng et al., 2004; Lee et al., 2002; Nakagawa et al., 2004). DLG1 is also part of supra-molecular scaffold complexes including several scaffolding proteins and recruits these complexes to the plasma membrane (Colledge et al., 2000; Oliveria et al., 2003). Such complex formation is essential to ensure DLG1-mediated localization of G protein-coupled receptors at the plasma membrane (Valentine & Haggie, 2011). DLG1 is also expressed in epithelial cells (Muller et al., 1995), but its function in these cells is less well understood (Reuver & Garner, 1998; Wu et al., 1998).

1.4 The Anoctamin family

The family of Anoctamins (ANO) consists of 10 different proteins (Fig. 1.10 A). All proteins contain eight transmembrane spanning domains with intracellular N-and C-termini (Yang et al., 2008), hence the name Anoctamins (Fig. 1.10 B). Before they were named for that characteristic, the family was called TMEM16 family. In 2008, three independent groups used different approaches and identified Anoctamin 1 (ANO1) as a calcium-gated chloride channel (Caputo et al., 2008; Schroeder et al., 2008; Yang et al., 2008). Calcium-gated chloride channels confer a vast number of different physiological processes and are present in nearly every cell type. Their molecular identities however are often unknown (Hartzell et al., 2005). Thus, the identification of a large new family of potential calcium-gated chloride channels attracted a great deal of attention.

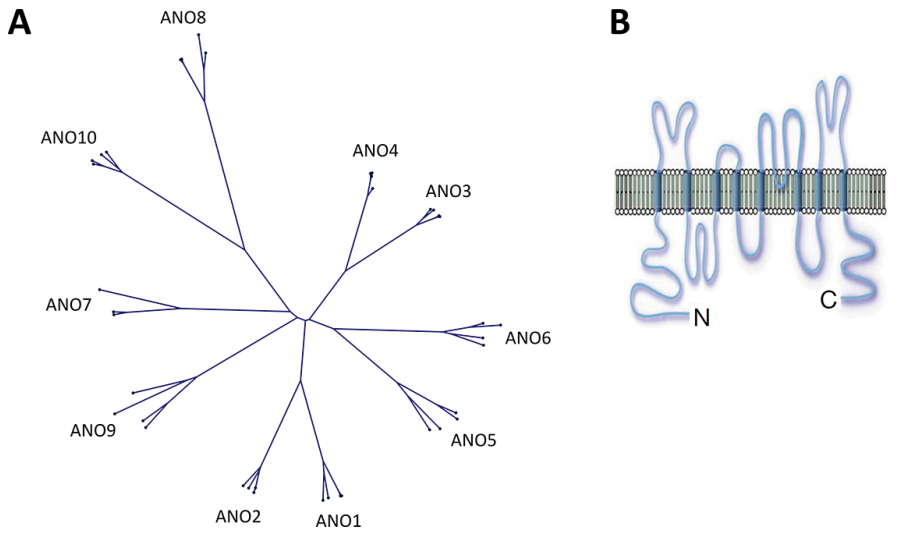

Figure 1.10: The Anoctamin family. A: Phylogenitic tree of Anoctmin proteins from human, mouse, rat, cow and dog. **B:** Membrane topology of Anoctamin proteins. Modified from (Yang et al., 2008).

The Anoctamin family, most of all ANO1, became extensively studied and their role as calcium-gated chloride channels was confirmed (Tian et al., 2012). The electrophysiological properties of ANO1 have been examined in detail (Xiao et al., 2011; Yu et al., 2012). Anoctamin 1 is expressed in a multitude of different tissues (Yang et al., 2008). Most studies focused on its role in epithelia cells (Jang & Oh, 2014; Kunzelmann et al., 2011). ANO1 was also found to play a crucial role in neuronal synaptic transmission (Cho et al., 2014; Jeon et al., 2013) and neuronal excitation in calcium microdomains of dorsal root ganglia (Jin et al., 2013). Moreover, ANO1 elicits chloride currents in smooth muscle cells (Dam et al., 2013; Heinze et al., 2014; Sanders et al., 2011; Thomas-Gatewood et al., 2011).

Apart from ANO1, the physiological roles of other family members were also investigated. Several studies identified ANO2 (Pifferi et al., 2009; Rasche et al., 2010; Stephan et al., 2009) and ANO6 (Martins et al., 2011) as *bona fide* calcium-gated chloride channels. Anoctamin 2 was identified in cilia of olfactory neurons (Rasche et al., 2010; Stephan et al., 2009) and ribbon synapses of photoreceptors (Stoehr et al., 2009). Apart from ion channel activity, ANO6 was also identified as a major factor in lipid scrambling processes (Suzuki et al.,

2010). Thus, the function of ANO6 as calcium-gated chloride channel is currently under debate (Kunzelmann et al., 2014). The physiological relevance of other Anoctamins is less well understood (Pedemonte & Galietta, 2014).

Anoctamin proteins are conserved throughout the animal phyla (Milenkovic et al., 2010). Outside the phylum of vertebrates, homologs have been described e.g. in *Drosophila* (Wong et al., 2013) and *C. elegans* (Wang et al., 2013). A distant homolog was also found in yeast cells (Kim et al., 2005). Individual Anoctamin proteins are conserved throughout evolution. Sequence analysis revealed greater sequence similarities between individual Anoctamins from different species, than between different Anoctamins from the same species (Fig. 1.10 A) (Milenkovic et al., 2010).

1.5 Aims of the study

In the present work, we sought to understand macro-molecular organization of olfactory signal transduction. Therefore, we conducted two research projects. We elucidated the role of PDZ scaffolding proteins in the vomeronasal organ and investigated the function of Anoctamin proteins in olfactory subsystems. This work is comprised the following subprojects:

Identification of PDZ scaffolding proteins in the vomeronasal organ. We applied biochemical and molecular methods to search for scaffolding proteins which could organize vomeronasal signal transduction. We analyzed the localization of identified candidates in the vomeronasal organ and investigated which PDZ proteins are expressed in microvilli of vomeronasal sensory neurons and therefore could possibly affect vomeronasal signaling.

Interaction of NHERF1 and DLG1 with vomeronasal proteins. We utilized molecular and biochemical methods to investigate the interaction of PDZ scaffolding proteins NHERF1 and DLG1 with vomeronasal signaling proteins. We analyzed if NHERF1 and DLG1 interact with potential PDZ ligands from vomeronasal organ and thereby potentially organize vomeronasal signal transduction.

Subcellular organization of olfactory signaling proteins. We established a dual color STED technique to analyze the subcellular organization of olfactory signaling components in super-resolution. Furthermore, we applied this technique to investigate the organization of NHERF1 in vomeronasal sensory neurons. Moreover, we analyzed the organization of Anoctamin proteins in olfactory signaling compartments. We sought to answer if olfactory signal transduction is organized in signaling microdomains mediated by PDZ scaffolding proteins.

Functional characterization of Anoctamin co-expression. We elucidated the macromolecular composition of different Anoctamin proteins via BRET assay and characterized their electrophysiological properties. We analyzed if co-expression of different Anoctamins in the same cell compartment could have physiological relevance.

2 Materials

2.1 Chemicals, Consumables & Devices

The following chemicals, consumables and machines have been used in this study. All chemicals were purchased in p.a. quality, if available. The Kits were used according to the manufactures instructions.

Table 2.1: Chemicals

Substance	Cat. No.	Company
Acetic Acid	7332	Roth
Agar	05339	Sigma
Agarose	161-3101	Biorad
Amonium persulfate	01216	Merck
Boric acid	B7901	Sigma
Bromphenol blue	B8026	Sigma
$CaCl_2$	29097	Sigma
CHAPSO	G9551	Sigma
Coelenterazine 400a	Sc-280647	Santa Cruz
DMEM GlutaMax	61965-026	Life Technologies
DMSO	41647	Sigma
DTT	D9779	Sigma
EDTA	E5134	Sigma
Ethidium bromide	161-0433	Biorad
Glycerol	49767	Sigma
Glycin	1.04169	Merck
HEPES	H3375	Sigma
2-Propanol	9866	Roth
KCl	60130	Sigma
KH_2PO_4	60218	Sigma

Continued on next page

Substance	Cat. No.	Company
Lysozyme	L3790	Sigma
Methanol	7342	Roth
$MgCl_2$	63064	Merck
Milk Powder	170-6404	Biorad
Na_2HPO_4	4984	Roth
NaCl	1.06404	Merck
Penicillin / Streptomycin	30-002-Cl	PAA
Pluronic F-127	P-6866	Life Technologies
Ponceau S	78376	Sigma
Prolong Anitfade Gold	P36930	Sigma
Protease Inhibitor Cocktail	11836170001	Roche
SDS	D6750	Sigma
Sucrose	4621	Roth
Tissue Freezing Medium	47050418	Jung
Tris-BASE	648310	Calbiochem
Triton X-100	1.12298	Merck
Turbofect	R0531	Thermo Scientific

Table 2.2: Consumables

Consumable	Cat. No.	Manufacturer
50ml Centrifuge Tubes	525-0155	VWR
15ml Centrifuge Tubes	525-0150	VWR
2ml Centrifuge Tubes	0030420.094	Eppendorf
1,5ml Centrifuge Tubes	72.690.001	Sarsted
Tissue Culture Dish 35x10mm	83.1800	Sarsted
Cell Culture Flask 75ml	132494	Thermo Scientific
Cell Culture Flask 25ml	134381	Thermo Scientific

Continued on next page

Consumable	Cat. No.	Manufacturer
Plasmid Miniprap Kit	A1460	Promega
Plasmid Maxiprap Kit	A2393	Promega
PCR Cleanup Kit	A9281	Promega
RNeasy	74004	Quiagen
Nitrocellulse Membrane	10401196	GE Healthcare
Blotting Paper	742131	Machery-Nagel
Hyperfilm ECL	28906837	GE Healthcare

Table 2.3: Devices

Device	Model	Manufacturer
37° C Incubator	Function line	Heraus
37° C Shaking Incubator	Certomat IS	Braun
Blotting Chamber	Transblot Cell	Biorad
Cell Counting Chamber	Neubauer improved	Brand
Centrifuge	Avanti J-20	Beckman Coulter
Centrifuge	Centrifuge 5417R	Eppendorf
Centrifuge	Centrifuge 5424	Eppendorf
Centrifuge	Minispin	Eppendorf
Centrifuge	Varifuge 3.0R	Heraeus
Chemiluminescence Imaging System	Fusion FX7	Vilber Lourmat
Clean Bench	HSP12	Kendro
CO_2 Incubator	Hera Cell	Heraeus
Confocal Microscope	TCS SPE	Leica
PCR Cycler	IQ5	Biorad
pH Meter	pH 540 GLP	WTW
Photometer	6100 Spectrometer	Jenway
Platereader	Mithras LB940	Berthold

Continued on next page

Device	Model	Manufacturer
Power Supply	Power Pac	Biorad
Scales	ATL2202	Acculab
Scanner	V750 Pro	Epson
Shaker	Polymax 1040	Heidolph
Sonicator	UP100H	Hielscher
Thermomixer	Thermomixer comfort	Eppendorf
UV Imaging System	Biodoc Analyzer	Biometra
STED Microscope	SP5 II, STED CW	Leica

2.2 Solutions

Buffer solutions, growth media and staining solutions to conduct this study, which were not commercially purchased, are listed below. Ready-to-use media and solutions are listed in Chemicals, Consumables & Devices on page 31.

Table 2.4: Solutions

Solution	Concentration	Substance
	2.7 mM	KCl
	1.5 mM	KH_2PO_4
$PBS^{+/+}$	137 mM	NaCl
pH 7.3 - 7.5	8.1 mM	Na_2HPO_4
	0.9 mM	$CaCl_2$
	0.48 mM	$MgCl_2$
TBS	50 mM	Tris-BASE
pH 7.4	150 mM	NaCl

Continued on next page

Solution	Concentration	Substance
TN Buffer pH 7.4	50 mM 100 mM	Tris-BASE NaCl
Solubilizing Buffer pH 7.5	200 mM 50 mM 1% (w/v)	NaCl HEPES CHAPSO
Bacterial Lysis Buffer pH 7.4	2 % (w/v) 1 % (w/v)	Lysozyme Triton X100
Transfer Buffer pH 8.6	150 mM 1 % (v/v) 20 mM	Glycine Methanol Tris
SDS-PAGE Running Buffer pH 8.3	191.8 mM 0.1 % (w/v) 25 mM	Glycine SDS Tris
Laemmli Buffer	0.02 % (w/v) 20 % (v/v) 200 mM 4 % (w/v) 125 mM	Bromphenol blue Glycerol DTT SDS Tris
Ponceau S	1 % (v/v) 0.5 % (w/v)	Acetic Acid Ponceau S
WB Blocking Buffer	1 % (w/v)	Milk in TBS
Seperating Gel Buffer	1.5 M	Tris

Continued on next page

Solution	Concentration	Substance
pH 8.8	0.4 % (w/v)	SDS
Gathering Gel Buffer	1 M	Tris
pH 6.8	0.8 % (w/v)	SDS
	0.025 % (w/v)	Bromphenol blue
DNA Sample Buffer	100 mM	EDTA
(5x)	20 % (w/v)	Ficoll PM400
	0.025 % (w/v)	Xylencyanole
	450 mM	Boric Acid
TBE	10 mM	EDTA
(5x)	450 mM Tris	
	10 mM	$CaCL_2$
	15 % (v/v)	Glycerol
RF1 Buffer	30 mM	Potassium Acetat
pH 5.8	50 mM	$MnCl_2$
	100 mM	RbCl
	75 mM	$CaCL_2$
RF2 Buffer	15 % (v/v)	Glycerol
pH 6.8	10 mM	MOPS
	10 mM	RbCl
	0.5 % (w/v)	Yeast Extract
LB Medium	1 % (w/v)	NaCl
pH 7.4	1 % (w/v)	Tryptone
PFA	4 % (w/v)	para Formaldehyde
pH 7.2		in $PBS^{+/+}$

Continued on next page

Solution	Concentration	Substance
IHC	0.1 % (v/v)	Triton X-100
Blocking Buffer	1 % (v/v) Gelatin in $PBS^{+/+}$	

2.3 Oligonucleotides & Vectors

The oligonucleotides used to perform RT-PCR experiments and DNA-sequencing analysis and to amplify genes of interest for this study are listed below. The vectors used for cloning and expressing genes of interest, either in mammalian or bacterial cells can be found in the corresponding table.

Table 2.5: BRET-Primers

Name	Sequence
BRET-GFP-fwd	GCAAGCTTACCATGGAATTCGTGAGCAAGGGCGAGGAGCTGTTCACC
BRET-GFP-rev	GCCTCGAGTTAAGCGGCCGCCTTGTACAGCTCGTCCATGC
BRET-Luc-fwd	GCCTCGAGTTAAGCGGCCGCCTGCTCGTTCTTCAGCACTCTCTCC
BRET-Luc-rev	GCCTCGAGTTAAGCGGCCGCCTGCTCGTTCTTCAGCACTCTCTCC
Ano1-Cterm-fwd	GCAAGCTTACCATGAGGGTCCCCGAGAAGTACTCG
Ano1-Cterm-rev	GCGAATTCCCAGCGCGTCCCCATGGTACTCG
Ano2-Cterm-fwd	GCGAATTCCACTTTCACGACAACCAGAGGAAAGTC
Ano2-Cterm-rev	GCGAATTCTACATTGGTGTGCTGGGAC
Ano2-Nterm-fwd	TTGCGGCCGCTCACTTTCACGACAACCAGAGGAAAGTC
Ano2-Nterm-rev	TTAGCGGCCGCTACATTGGTGTGCTGGGAC
Ano6-Cterm-fwd	GCGAATTCCAGATGATGACTAGGAAGGTCC
Ano6-Cterm-rev	GCGAATTCTTCGAGTTTTGGCCGC

Continued on next page

Name	Sequence
Ano6-Nterm-fwd	TTGCGGCCGCTCAGATGATGACTAGGAAGGTCC
Ano6-Nterm-rev	TTAGCGGCCGCTTCGAGTTTTGGCCGC

Table 2.6: Sequencing-Primers

Name	Sequence
CMV	CGCAAATGGGCGGTAGGCGTG
BGH-rev	TAGAAGGCACAGTCGAGG
Luc-C	GCTTCGTGGAGAGAGTGC
Luc-N	GGAAGATCACGGCGTTCTCGGCG
GFP2-N	GCTCCGACCAGGATGGGCACC
GFP-C	CCGCCGCCGGGATCACTCTCGGC
5-pGEX	GGGCTGGCAAGCCACGTTTGGTG
3-pGEX	CCGGGAGCTGCATGTGTCAGAGG
Ano1-1200-rev	GGTTATCAAAAAGGTGACTGGCACG
Ano1-1200-fwd	CCTCTGTGTGACAAGACCTGC
Ano1-1100-fwd	GTATGGAGATGTGTGACCAG
Ano1-1900-rev	GCTCAGCTGGATACAGAGC
Ano1-2400-rev	CCATTCTGACTGTACATGTAGAGG
Ano2-900-fwd	GGATGTGCAACAATCGAGG
16b-mid-fwd	CAATCCAGCCACCGTCTTCTTTTCCATCTTC
16b-mid-rev	GATGGAAAAGAAGACGGTGGCTGGATTG
Ano2-1800-fwd	GGCAAGCAGCTGATCCAGAAC

Continued on next page

Name	Sequence
Ano6-500-fwd	GGTTCACCAAGGTCCTCCG
Ano6-700-rev	GCTTTGTAGATTCCAGAGCTGACC
Ano6-1900-fwd	CCACGATGGGAACAGGATTACC
Ano6-2100-rev	GGTTGTGAGCTTCCACGCG

Table 2.7: PDZ screening-Primers

Name	Sequence
DGL-2-fwd	TTATGGGCCACCGGATATTA
DLG-2-rev	GGAGAGTCACTGAAGGCTGG
Gipc1-fwd	CATCAAGGAAGGCAGTGTGA
Gipc1-rev	ATTCATCTGGGAATGCGAAG
Shank2-fwd	GCTATCCCCGGAATTCTCTC
Shank2-rev	GAAGTCCCCGGTCCTTAGTC
Erbin-fwd	TTGCGAGACGGAAGAGGTTCT
Erbin-rev	GGCCACTTTCAGCATCAAAT
Syntenin-fwd	ATGTGTGTGAGGTGAACGGA
Syntenin-rev	AACCAGGTCCCAAGTCTGTG
ZO-1-fwd	CAAAACGCTCTACAGGCTCC
ZO-1 rev	GAAGAGCTGGACAGAGGTGG
PICK1-fwd	GCGAACTTCCACCAACACTT
PICK1-rev	GATGCTGATCCCAATCAGGT
PATJ-fwd	AAGCTAAGAGGCACGGAACA
PATJ-rev	TCCTTATTGCCAGCGAGACT
NHERF1-fwd	AAGCTGGGCGTCTCGATCCG
NHERF1-rev	GAGCTCGCGCAAGTGGCTCTT
PSD95 fwd	GAGGGGAGGAACAAAACTCC
PSD95-rev	CCGTTCACCTGCAACTCATA

Table 2.8: PDZ-Primers, Capital letter indicate added restriction sides and tags.

Name	Sequence
NHERF1-HA-HindIII-fwd	GCAAGCTTACCATGtacccatacgatgttccagattacgctAGCGCGGACGCAGCGGCCGG
NHERF1-EcoRI-rev	CGGAATTCTCAGAGGTTGCTGAAGAGTTC
NHERF1-BamHI-fwd-PDZ1	AAGGATTCagcgcggacgcagcggccgg
NHERF1-XhoI-rev-PDZ1	AACTCGAGggtgcagagccggggccggagctcg
NHERF1-BamHI-fwd-PDZ2	AAGGATTCaagaaaggccccaatggctatgg
NHERF1-XhoI-rev-PDZ2	AACTCGAGgaggttgctgaagagttcatttttcttgc
NHERF1-BamHI-fwd-PDZ1-HA	AAGGATTCtacccatacgatgttccagattacgctagcgcggacgcagcggccgg
NHERF1-BamHI-fwd-PDZ2-HA	AAGGATTCtacccatacgatgttccagattacgctaagaaaggcccccaatggctatgg
NHERF1-XhoI-rev-PDZ1-HA	AACTCGAGagcgtaatctggaacatcgtatgggtaggtgcagagccggggccggagctcg
NHERF1-XhoI-rev-PDZ2-HA	AACTCGAGagcgtaatctggaacatcgtatgggtagaggttgctgaagagttcatttttcttgc
NHERF1-XhoI-rev-PDZ2-HA-EB	AACTCGAGagcgtaatctggaacatcgtatgggtactgcggggccctcttgctactgc
DLG1-PDZ1-fwd	AAGAATTCGCAGATTATGAATATGAGG
DLG1-PDZ1-rv-HA	AACTCGAGTCAagcgtaatctggaacatcgtatgggtaGGCTGGCTTCCGCCTTTTCAC
DLG1-PDZ2-fwd	AAGAATTCGCCTCAGAAAAAATCATGG
DLG1-PDZ2-rv-HA	AACTCGAGTCAagcgtaatctggaacatcgtatgggtaTGCATAGCCATCATTTATATAC
DLG1-PDZ3-fwd	AAGAATTCGCAGTGCTTGGAGATGATGAG
DLG1-PDZ3-rv-HA	AACTCGAGTCAagcgtaatctggaacatcgtatgggtaAGCTTCAAAACGACTGTACTC

Table 2.9: PLC RT PCR-Primers

Name	Sequence
PLCβ4-rt-fwd	GGACGGGGTTATTGCAGCCACG
PLCβ4-rt-rev	TCCGTATGGTGTCGGTGGGCA
PLCβ3-rt-fwd	GACCAGCGGGCCAAGCAACTA
PLCβ3-rt-rev	GGTTGGAGGGGAGCTGTGACC
PLCβ1-rt-fwd	ATCCCTTGCACCCAAGCCGC
PLCβ1-rt-rev	AGCTCTTCGATGGTTTGCGCC
PLCϵ1-rt-fwd	CCCTGCAATCGGTCTGCCTCG
PLCϵ1-rt-rev	AGCCCCAGGTCGGAGACGTT
PLCη1-rt-fwd	TGACAAGAGCCTTCTGGGGGC
PLCη1-rt-rev	CTTGTCTCCTGCTTGCGCTGCT
PLCγ2-rt-fwd	TTCCGTCTGTGGCTGTGCGG
PLCγ2-rt-rev	AGGACGTAGCCTGTTCGCCCA
PLCγ1-rt-fwd	GCGCGGACAAAATCGAGGGGT
PLCγ1-rt-rev	TGATCTGGCCGGAAGGCAGG
PLCδ1-rt-fwd	TGAGGTCCCCGGAGTCGCAG
PLCδ1-rt-rev	GGAGAAGCATCGGTCCTCGGGT
PLCβ4c-fwd-rt	AAAGAAAGAGACTGGCGATGAAGCA
PLCβ4c-rev-rt	TTGGGACACTGCATGACAGG
PLCβ4b-fwd-rt	GACAACGGATCACAAATCTAAG
PLCβ4b-rev-rt	CTTCTTAGTGTTGCTGCTGTTC
PLCβ4b-fwd-rt	GAGAAGGCGATGAAGAAGAAGG
PLCβ4b-rev-rt	CCTTGCTTTCCCTTAGATTTGTG
rt-PLC-η1-fwd	GGGGCTTTGTCGCTGCCCAT
rt-PLC-η1-rev	TGTCTCCTGCTTGCGCTGCTTC
rt-PLC-η2-fwd	GCAGCAGCAGCCCCCGAG

Continued on next page

Name	Sequence
rt-PLC-η2-rev	GGCCCAGGGCTGGTTCCTC

Table 2.10: Vectors

Name	Cat. No.	Supplier
pcDNA3.1	V790-20	Life Technologies
pGEX 6T1	28-9546-48	GE Healthcare
BioSensor pGFP2-MCS-Rluc(h)	9600496	PerkinElmer

2.4 Enzymes

The following enzymes were used in this study to amplify or modify nucleic acids. This comprises digesting DNA with restriction enzymes, amplifying DNA with Polymerases, ligating DNA with ligases and modifying DNA with alkaline phosphatases. RNA was transcripted to cDNA with the help of reverse transcriptase enzyme supplied as a ready-to-use kit (see Tab 2.2 on page 31).

Table 2.11: Restriction Enzymes

Name	Cat. No.	Supplier
EcoRI	ER0271	Thermofisher Scientific
XhoI	ER0691	Thermofisher Scientific
BamHI	ER0051	Thermofisher Scientific
NotI	ER0591	Thermofisher Scientific
HindIII	ER0501	Thermofisher Scientific

Table 2.12: Cloning Enzymes

Name	Cat. No.	Supplier
FastAP	EF0654	Thermofisher Scientific
T4 DNA Ligase	EL0014	Thermofisher Scientific

Table 2.13: PCR Enzymes

Name	Cat. No.	Supplier
GoTaq Flexi DNA Polymerase	M8301	Promega
Phusion High-Fidelity DNA Polymerase	M0530S	NEB
KAPAHiFi DNA Polymerase	07-KK2100-01	peqLab

2.5 DNA-Constructs

During this study several DNA-constructs were generated to express genes of interest in either mammalian cell lines or bacterial cells. All constructs were generated as described in section Cloning on page 48 and are listed below.

Table 2.14: BRET Constructs

Construct	Gene	Restriction sites	Tag	Backbone
BRET GFP	GFP	HindIII - XhoI	-	pcDNA3.1
BRET Luc	Luciferase	HindIII - XhoI	-	pcDNA3.1
Ano1 GFP-C	Anoctamin 1	HindIII - XhoI	GFP C-Terminal	pcDNA3.1
Ano1 Luc-C	Anoctamin 1	HindIII - XhoI	Luc C-Terminal	pcDNA3.1
Ano1 A169P GFP-C	Anoctamin 1	HindIII - XhoI	GFP C-Terminal	pcDNA3.1
Ano1 A169P Luc-C	Anoctamin 1	HindIII - XhoI	Luc C-Terminal	pcDNA3.1
Ano1 WT	Anoctamin 1	HindIII - XhoI	-	pcDNA3.1
Ano2 GFP-C	Anoctamin 2	EcoRI - EcoRI	GFP C-Terminal	pcDNA3.1
Ano2 Luc-C	Anoctamin 2	EcoRI - EcoRI	Luc C-Terminal	pcDNA3.1

Continued on next page

Construct	Gene	Restriction sites	Tag	Backbone
Ano2 GFP-N	Anoctamin 2	NotI - XhoI	GFP N-Terminal	pcDNA3.1
Ano2 Luc-N	Anoctamin 2	NotI - XhoI	Luc N-Terminal	pcDNA3.1
Ano2 WT	Anoctamin 2	HindIII - EcoRI	-	pcDNA3.1
Ano6 GFP-C	Anoctamin 6	EcoRI - EcoRI	GFP C-Terminal	pcDNA3.1
Ano6 Luc-C	Anoctamin 6	EcoRI - EcoRI	Luc C-Terminal	pcDNA3.1
Ano6 GFP-N	Anoctamin 6	NotI - XhoI	GFP N-Terminal	pcDNA3.1
Ano6 Luc-N	Anoctamin 6	NotI - XhoI	Luc N-Terminal	pcDNA3.1
Ano6 WT	Anoctamin 6	HindIII - EcoRI	-	pcDNA3.1

Table 2.15: PDZ-Microarray Constructs

Construct	Gene	Restriction sites	Tag	Backbone
NHERF1-PDZ1	NHERF1	BamHI - XhoI	HA	pGEX 6T1
NHERF1-PDZ2	NHERF1	BamHI - XhoI	HA	pGEX 6T1
NHERF1-PDZ3	NHERF1	BamHI - XhoI	HA	pGEX 6T1
DLG1-PDZ1	DLG1	EcoRI - XhoI	HA	pGEX 6T1
DLG1-PDZ2	DLG1	EcoRI - XhoI	HA	pGEX 6T1
DLG1-PDZ3	DLG1	EcoRI - XhoI	HA	pGEX 6T1

2.6 Antibodies

The following antibodies were used in this work to conduct immunohistochemical stainings and Western blot experiments. For detailed methodical instructions see section Immunohistochemistry on page 54 and Western Blotting on page 55. Primary antibodies were used to detect a protein of interest, subsequently secondary antibodies were used for labeling.

Table 2.16: Primary Antibodies

Antigene	Cat. No.	Supplier	Host	Dilution
Acetylated Tubulin	T6793	Sigma	Mouse	1 : 10.000
Adenylate Cyclase Type III	sc-588	Santa Cruz	Rabbit	1 : 100
Ahnak	Marg et al. 2010	Selfmade	Rabbit	1 : 20
Anoctamin 1	ab53212	Abcam	Rabbit	1 : 100
Anoctamin 2	Rasche et al. 2010	Selfmade	Rabbit	1 : 300
Anoctamin 6	Martins et al. 2011	Selfmade	Rabbit	1 : 300
CNG-A2	APC-045	Alomone Labs	Rabbit	1 : 100
CNG-A4	-	Selfmade	Guinea Pig	1: 100
DLG1	610874	BD	Mouse	1 : 300
NHERF1	ab3452	Abcam	Rabbit	1 : 1.000
GAPDH	ab8245	Abcam	Mouse	1 : 30.000
GFP	11814460001	Roche	Mouse	1 : 10.000 (WB) 1 : 1.000 (IHC)
$G_{\alpha i2}$	sc-13534	Santa Cruz	Mouse	1: 500
Gipc1	ab5951	Abcam	Goat	1 : 100
$G_{\alpha o}$	sc-387	Santa Cruz	Rabbit	1: 500
GST	27-4577-01	GE Healthcare	Goat	1 : 5.000
HA	MMS-101P	Covance	Mouse	1 : 1.000
Lin7c	51-5600	Invitrogen	Rabbit	1 : 100
OMP	544-10001	Wako	Goat	1 : 2.000
PDZK1	sc-27289	Santa Cruz	Goat	1 : 100
PLCβ3	sc-13958	Santa Cruz	Rabbit	1 : 100
PLCβ4	sc-166132	Santa Cruz	Mouse	1 : 100
PSD95	LV1359450	Chemicon	Mouse	1 : 100
Renilla - Luciferase	MAB4400	Millipore	Mouse	1 : 10.000 (WB) 1 : 1.000 (IHC)
TrpC2	Liman et al. 1999	Selfmade	Rabbit	1 : 500

Table 2.17: Secondary Antibodies

Conjugate	Target	Cat. No.	Supplier	Host	Dilution
Alexa 488	Mouse	A21202	Invitrogen	Donkey	1 : 500
Alexa 488	Rabbit	A21206	Invitrogen	Donkey	1 : 500
Alexa 488	Rat	A21434	Invitrogen	Goat	1 : 500
Oregon Green 488	Rabbit	O11038	Invitrogen	Goat	1 : 200
V500 Streptavidin	Biotin	561419	BD	-	1 : 50
Alexa 568	Goat	A11057	Invitrogen	Donkey	1 : 500
Alexa 568	Mouse	A10037	Invitrogen	Donkey	1 : 500
Alexa 568	Rabbit	A10042	Invitrogen	Donkey	1 : 500
Alexa 568	Rat	A11077	Invitrogen	Goat	1 : 500
Phalloidin - Alexa 568	Actin	A-12380	Invitrogen	*Amanita phalloides*	1 : 500
Alexa 633	Mouse	A21052	Invitrogen	Goat	1 : 500
Alexa 633	Rabbit	A21070	Invitrogen	Goat	1 : 500
Alexa 633	Rat	A21094	Invitrogen	Goat	1 : 500
Biotin	Goat	AP180B	Millipore	Donkey	1 : 200
Biotin	Mouse	715-065-150	Jackson	Donkey	1 : 200
Biotin	Rabbit	711-065-152	Jackson	Donkey	1 : 200
HRP	Goat	sc-2056	Santa Cruz	Donkey	1 : 10.000
HRP	Mouse	170-6516	Biorad	Goat	1 : 10.000
HRP	Rabbit	170-6515	Biorad	Goat	1 : 10.000

3 Methods

3.1 Tissue collection

The animals used in this work were housed and sacrificed according to animal welfare standards. The collection of tissue from the olfactory epithelium and from the vomeronasal organ are discribed below. The preparation of slices for immunehistochemistry can be found in section 3.7 on page 54.

3.1.1 Collecting tissue from main olfactory epithelium

Mouse olfactory tissue was collected by removing the head, freeing it from skin and hair, removing the lower yaw and splitting the head in two halves. The now visible olfactory epithelium was gathered from the nasal septum and the olfactory turbinates.

3.1.2 Collecting vomeronasal organ tissue

The vomeronasal organ resides below the nasal cavity. It is a pairwise, crescent-shaped organ enwrapped in an ossified capsule. The mouse head was removed, skinned and the lower yaw was removed. Now the palate was detached, so that the bone capsule carrying the vomeronasal organ becomes visible. The left and right maxillary bones adjacent to the vomeronasal organ were cut and the alveolar bone holding both incisors was fractured, so that both anterior parts of the maxillary bones could be removed. The bone capsule carrying the vomeronasal organ was gathered and transferred to a dish with $PBS^{+/+}$. Next, the vomeronasal organ bone capsule was carefully cracked and the residing vomeronasal organ tissue was harvested.

3.2 Neuron dissociation

Vomeronasal sensory neurons were dissociated using neuronal tissue dissociation kit from Milteny Biotec according to the manufacturers instructions. Vomeronasal tissue was harvested as described in section Collecting vomeronasal organ tissue on page 46. Dissociated vomeronasal sensory neurons were seeded on a polylysine covert glass slide, fixed with 4% PFA solution for 15 min at room temperature and stained as described in section Immunohistochemistry on page 54.

3.3 Molecular biology techniques

Molecular biology techniques were applied to generate expression constructs with genes of interest for this study or to validate expression of proteins of interest in different mouse tissue. The methods used to generate expression constructs are explained in the section Cloning. Expression of different proteins in mouse tissue was detected as described in section Verification of protein expression.

3.3.1 Bacterial cell strains

The following bacterial cell strains were used to express proteins of interest or to clone desired DNA-constructs.

Table 3.1: Bacteria

Name	Cat. No.	Supplier
E. coli XL10 Gold	200315	Agilent Technologies
E. coli BL21 (DE3)	C6000-03	Life technologies

3.3.2 Generating chemically competent bacteria

Successful transformation of plasmid DNA depends on the ability of used bacteria to absorb plasmids. This process can be improved by making bacteria chemically competent as described by (Hanahan, 1983).

3 ml of E. coli XL10 Gold were cultured over night at 37°C and transferred into 250 ml LB media. The new culture was grown to an $OD_{595\,nm}$ of 0.4. After centrifugation cells were resuspended in 80 ml ice cold RF1 buffer and incubated for 1 hour on ice. Following a second centrifugation step cells were resuspended in ice cold RF2 buffer, incubated for 15 min on ice and subsequently aliquoted for storage at -80°C.

3.3.3 Transformation of plasmid-DNA

Plasmid-DNA was transformated into chemically competent bacteria by incubating bacteria together with plasmid-DNA for 30 min on ice. Afterwards cells were heat-shocked for 90 s at 42°C, supplemented with LB media and grown for 1 hour at 37°C. Following a centrifugation step cells were plated on agar plates containing a selective antibiotic.

3.3.4 Cloning

Genes of interest for this work were cloned into suitable expression vectors (see p. 41) and either expressed in mammalian cell lines or bacterial cells. This process started with the transcription of RNA to cDNA from tissue expressing the desired protein using an RNA extraction kit followed by a cDNA synthesis kit according to the manufactures instructions. The cDNA was used as template for amplifying the gene of interest via PCR using specific oligonucleotides (see p. 36). The reaction was run according to the polymerase suppliers instructions. The oligonucleotides introduced restriction sides flanking the gene of interest to clone the amplified DNA into a digested and dephosphorylated expression vector. The vector-insert combination was subsequently ligated by T4 DNA ligase over night at 4°C.

The ligated DNA was transformated into chemical competent bacteria and cells were plated on agar plates containing an antibiotic to select for transformated cells after growing over night at 37°C. Grown colonies were picked and cultured over night in a liquid culture at 37°C. Afterwards success of cloning was verified by extracting DNA from grown cultures and sending extracted plasmids for sequence analysis.

3.3.5 Verification of protein expression

Expression of proteins of interest were verified by performing a PCR with specific oligonucleotides using cDNA from different tissues. cDNA was generated from tissue total-RNA with the help of cDNA synthesis kit from Thermo Scientific. RNA was extracted from tissue using RNA extracion kit from Quiagen. All kits and enzymes were used according to manufactures instructions.

3.4 Cell Culture

3.4.1 Mammalian cell lines

The following mammalian cell line was used to express proteins of interest in order to perform BRET assays and Western Blot experiments.

Table 3.2: Mammalian Cells

Name	Reference
HEK293	Graham et al. 1977

3.4.2 General cell culture

The mammalian HEK (human embryonic kidney) cell line was used in this work to express mammalian proteins of interest. The cells were cultured in DMEM GlutaMAX media supplemented with 10% FCS and 1% Pen-Strep solution and

grown in cell culture flask from Thermo Scientific. Upon 80% confluence cells were passaged. Cells were grown on 5x5 mm glass slides inside Ø 35 mm tissue culture dishes for immunocytochemical staining.

3.4.3 Transfection

Generated expression plasmids were introduced into mammalian cells by transfection, to express genes of interest. All cells were transfected using Turbofect reagent from Thermo Scienfific according to the manufactorers instructions.

3.5 Protein expression & purification

Biochemical experiments like the PDZ interaction microarray require a large amount of purified protein. For that purpose proteins of interest were expressed in *E. coli* BL21 cells and purified via trap beads. *In vitro* experiments with proteins of interest were conducted in mammalian cell lines. Expression of mouse proteins in mammalian cells ensures a related, yet controlled environment with protein expression and modification machinery comparable to the native tissue.

3.5.1 Protein expression in bacterial cells

E. coli BL21 cells are optimized for protein expression. Genes of interest were cloned into inducible pGEX 6T1 vector and transformated into bacteria. Cells were grown in 5 ml LB media over night, transferred to 250 ml LB media at the next day and further cultured at 37°C to an $OD_{595\,nm}$ of 0.4. Protein expression was now induced by supplementing the media with 100 mM IPTG and further culturing the cells for 3 h. Subsequently cells were pelleted by centrifugation and protein was purified as described in section 3.5.2.

3.5.2 Protein purification from bacterial cells

Pelleted bacteria were resuspended in ice cold bacterial lysis buffer and incubated an ice for 30 min. Followed by sonification with a Hielsscher Sonicator (80% power 15x 1 s) cell debris were pelleted by centrifugation (14.000g, 20 min) and the supernatant containing expressed proteins was collected.

The pGEX 6T1 vector fuses the protein of interest to a removable GST-tag. This tag was used to purify the expressed protein from the supernatant via GST-trap beads. The supernatant was mixed with solubelized Glutathion Agarose beads able to bind GST, incubated for 1 h at 4°C on a rotatory shaker. Afterwards, beads were pelleted by centrifugation (1.000g, 3 min) and the supernatant was removed.

The fused GST-tag from pGEX 6T1 vector offered a unique cleavage site for PreScission Protease from GE Healthcare. Protein loaded Glutathion Agarose beads were washed 3x with cleavage buffer and incubated with PreScission Protease on a rotatory shaker at 4°C for 4 h. Following the cleavage step, beads were pelleted by centrifugation and protein containing supernatant was collected and stored at -20°C.

3.5.3 Protein expression in mammalian cells

Mammalian cell lines provide a suitable and controlled environment for plasmid-based expression of mammalian proteins. In this study HEK293 cells were used to express mouse proteins. The generated plasmids were introduced via transfection (see p. 50). The protein expression was driven by CMV promotor located on the expression plasmid. 24 h after transfection cells harvested, fixed and stained or otherwise used in an experiment.

3.5.4 Protein purification from mammalian cells

Harvested cells were pelleted by centrifugation and pellet was resuspended in ice cold $PBS^{+/+}$. All following steps were carried out on ice. Centrifuges were cooled to 4°C. After another centrifugation step the cell pellet was resuspended in ice cold TN buffer and cells were subjected to sonification (70% power, 10x

1s). Cell debris were pelleted by centrifugation (1.650g, 15 min) and the supernatant was collected. In order to enrich solubilized membrane fractions the supernatant was centrifuged again for 30 min at 20.000g. The membrane pellet was dried and resuspended in solubilizing buffer and stored at -20°C.

3.5.5 Protein purification from mouse tissue

The collected tissue was doused in TN buffer and cells were mechanically broken up with the help of a tissue-grinding douncer. Subsequently the tissue was subjected to the same treatment as described in section 3.5.4, to isolate membrane proteins.

3.6 PDZ interaction microarray

A PDZ interaction microarray was used to screen for interactions between single PDZ domains of different scaffolding proteins and potential PDZ ligands from vomeronasal organ. The selection of suitable candidates from vomeronasal organ is described in the section Data bank research.

Peptide microarrays with 288 single spots were purchased from intavis (for a complete list, see appendix). Every petide spot from intavis custom peptide microarray features peptides up to 15 amino acids length. As PDZ ligands interact with their very C-terminus, the last 15 amino acids from proteins of interest were used to design the petide spots.

3.6.1 Data bank research

All listed sequences of mouse vomeronasal type 1 and type 2 receptors were gathered from ncbi gene data bank (*http://www.ncbi.nlm.nih.gov/gene/*). Double listed receptors were eliminated from the list and C-termini of the remaining receptors were checked for a potential PDZ ligand binding motif. Those receptors were selected and their last 15 amino acids were checked for sequence identity, as the designed array features up to 15 amino acid per spot and the PDZ ligand motif is found at the very C-terminus of the protein. Receptors with

identical sequences were grouped, which yielded a list of 42 type 1 receptor- and 34 type 2 receptor-ligands

Additionally, vomeronasal organ microarray data was used to select further proteins of interest from vomeronasal organ (irrespective of their PDZ ligand status) to be checked for PDZ protein interaction. These proteins included described and presumed signaling proteins, different ion channels and ion transporters, proteins potentially regulating signal transduction and transmembrane proteins of unknown function. The complete array included different 286 peptide spots.

3.6.2 Using intavis custom peptide microarray

PDZ domains were cloned (3.3.4), expressed in bacteria (3.5.1) and purified (3.5.2) as decscribed above. Concentration of purified PDZ domain protein was determined using Coomassie Protein Assay Kit from Thermo Scientific. Miroarray slides were blocked with blocking solution made of 3% 3K-Eiweiss Protein Shake diluted in TBST for 2 h at room temperature. Proteins were diluted in blocking solution up to a final concentration of 200 ng/µl. The diluted proteins were dispensed on the array. The array was incubated over night at 4°C in a humidity chamber. After washing with TBST the array was probed with HA antibody (1 : 1.000,4°C, over night) diluted in blocking solution. Following 3x washing with TBST the array was incubated with HRP-coupled secondary antibody diluted in blocking buffer (1 : 4.000) for 1 h at room temperature. After 3x washing with TBST the array was probed for HRP activity by applying ECL substrate and recording luminescence with Vilber Lourmat FX7 Fusion system.

3.6.3 Analysis of peptide microarray data

PDZ domains bound to PDZ ligands on the microarray were detected via HRP-coupled antibodies and ECL substrate luminescence intensities for each spot were quantified using a Vilber Lourmat FX7 Fusion system. Proteins of interest were ranked according to their luminescence intensity levels. The background was defined as the arithmetic mean of empty spots on the array. The intensity

cut-off for positive hits in one experiment was defined as > background intensity + 2x standard deviation of background intensity. Every peptide meeting the defined criteria in at least 3 independent experiments was considered as positive hit and potential interaction partner for the tested PDZ domain.

3.7 Immunohistochemistry

Proteins of interest were labeled for microscopic assessment in olfactory tissue or vomeronasal organ slices, as they were in protein-expressing cell lines. The methods for labeling proteins using specific and fluorescent-labeled antibodies and the preparation of cryosections are described below.

Preparation of main olfactory epithelium slices

Adult mice were sacrificed and decapitated according to animal standards. After the nasal bones (*os nasale*) were removed the skinned head was incubated in 4% PFA at 4°C for 2h and subsequently in 30% sucrose over night. The fixed head was embedded in tissue freezing medium and stored frozen at -80°C. Cryosections (10 µm) of the main olfactory epithelium were prepared and mounted onto Superfrost glass slides.

Preparation of vomeronasal organ slices

Vomeronasal organs were prepared as described in 3.1.2 on page 46. Only the bone capsule was left intact and subsequently fixed, embedded and cut as described for the main olfactory epithelium slices.

3.7.1 Antibody staining

Main olfactory epithelium, vomeronasal organ slices or fixed cells on cover slips were blocked with blocking solution for 1h at room temperature and incubated with primary antibodies diluted in blocking solution over night at 4°C. Afterwards sections or cover slips were washed and incubated with fluorescence labeled secondary antibodies and mounted in Prolong Antifade Gold.

3.7.2 Dual color STED staining

Cryosections obtained as described above were blocked with blocking solution for 1h at room temperature and incubated with diluted primary antibodies at 4°C over night. On the next day sections were washed 3x with PBS for 5 min and incubated with diluted biotin-coupled secondary antibody for 2h at room temperature. Again sections were washed 3x with PBS and incubated with streptavidin-coupled V500 in the same manner. Afterwards, sections were washed again 3x and incubated with OregonGreen 488 coupled secondary antibody for 2h at room temperature. Following again with 3 washing, sections were mounted in Prolong Antifade Gold.

3.8 Western Blotting

Proteins from tissue or cell lines were detected by Western Blot using specific antibodies. The methods for extracting proteins from tissue or cell lines are explained in detail in section 3.5.4 and section 3.5.5 on page 51. For Western blotting protein concentration of cell or tissue lysates was determined by using Coomassie Protein Assay Kit from Thermo Scientific. The gel buffers were used to create polyacrylamid gels with the desired percentage according to the protein size of interest. The same amount of proteins were diluted in 10 µl of SDS-loading buffer, loaded onto the gels and blotted to nitrocellulose membrane. Membranes were blocked with WB blocking buffer and probed for immunoreactivity with primary antibodies diluted in 50% WB blocking buffer at 4°C over night. After washing the membrane 3x with TBST it was probed with HRP-coupled secondary antibodies diluted in 50% WB blocking buffer for 1 h at room temperature. Following 3x of washing the membrane was probed for HRP activity using ECL substrate and ECL Hyperfilms.

3.9 Co-immunoprecipiation

GST-tagged NHERF1 PDZ domains or GST were expressed in *E.coli* BL21 cells. Proteins were purified as described in Protein expression & purification. Vome-

ronasal receptor C-terminus was expressed in HEK293 cells and isolated as described in Western Blotting. All following steps were conducted at 4°C. Bacterial lyasate with GST-tagged NHERF1 PDZ domains or GST as control were pooled with vomeronasal receptor cell lysates. The pooled lysates were incubated for 3 h on a rotating shaker. GST-trap beads were added to bind either NHERF1 PDZ domains or GST. Therefore, the lysate was again incubated for 1 h on a rotating shaker. Afterwards, beads were pelleted by centrifugation and washed 3x with TNN buffer. Beads were diluted in SDS-loading buffer and subjected to Western Blot analysis. GST-tag antibody was used to control for successful loading of beads with PDZ domains or GST control. Precipitated vomeronasal receptor C-terminus was detected with GFP-antibody.

3.10 BRET assay

12.000 HEK293 cells per well were seeded in 100 µl of DMEM + Pen/Strp and grown in white 96-well plates for 2 days to 90% confluence for BRET assays. Cells were transfected with either luciferase or GFP fusion plasmid of Anoctamins, different combinations of both or control plasmids. Each well was transfected with 200 ng of plasmid using 0,4 µl of Turbofect reagent. For double transfections, the total amount of plasmid and Turbofect was raised accordingly. After 24 h of protein expression cells were probed for BRET activity. Before measurements cells were washed with PBS and subsequently incubated in 30 µl of PBS containing 7.5 µM coelenterazine 400a and 0.1% Pluronic F-127. Bioluminescence and fluorescence signals were detected with a Berthold Mitras LB940 platereader using Berthold BRET2 emission filter pack.

3.11 Dual color STED Microscopy

In this study, we used super resolution microscopy to investigate subcellular organization of different proteins. We established a protocol to use not only one, but two fluorophores simultaneously in super-resolution mode with a STED microscope. When using super-resolution microscopy to investigate co-localisa-

tion of different proteins in the same subcellular compartment it is mandatory to ensure that neither cross-talk nor bleed-through between both channels occur. Thus, we evaluated the characteristics of several fluorophores as dual color STED dyes under identical conditions (Fig. 3.1).

The principal of dual color STED imaging requires two dyes excited with different wavelengths of the same laser, which is simultaneously depleted. The different emission spectra of these dyes are subsequently detected at defined wavelengths. So the considered dyes must meet certain criteria. First, the dye must be excitable with the argon laser of the setup at either 458 nm or 514 nm, to work as short wave length fluorophore (SWF) or long wave length fluorophore (LWF). Second, its emission must be quenched by the depletion laser coupled to the argon laser to utilize the STED effect. Third, the emission for SWFs tested needs to be sufficient for detection between 458 nm and the beginning of the emission spectrum of the LWF (usually around 500 nm), as the LWF will be readily excited by the 458 nm laser. The emission spectrum for the LWF should be detectable between 514 nm and the depletion laser at 592 nm. Forth, all used fluorophores need to display high photo stability against the powerful depletion laser at 592 nm, as for the sake of image quality a certain amount of signal averaging is necessary.

We tested Alexa 488, Oregon 488 and Oregon 514 as potential LWFs together with V500 and Abberior STAR 440SX as potential SWFs by staining olfactory cilia with acetylated tubulin antibodies and comparing signal quality. While all three LWF dyes showed sufficient signal intensity when excited with a 514 nm laser (Fig. 3.1 B, E, H), Oregon 514 severely lacked in photo stability (Fig. 3.1 I) and Alexa 488 tended to show bleed-through to the SWF channel (Fig. 3.1 D). Oregon 488 displayed adequate signal intensity, no bleed-through and enough photo stability with the applied settings to acquire STED images (Fig. 3.1 A-C).

The fluorescence of V500 and Abberior 440SX excited with a 458 nm laser were clearly separable between the SWF (Fig. 3.1 J, M, P) and the LWF (Fig. 3.1 K, N, Q) channel. Both dyes displayed the same amount of photo stability when exposed to the depletion laser (Fig. 3.1 L, O, R), but the signal intensity of V500 was clearly superior to that of Abberior 440SX. Due to the lack of a rabbit hosted antibody against acetylated tubulin the signals of V500 and Abberior 440SX were

evaluated with stainings of adenylate cyclase III in olfactory cilia. Comparison between V500 stainings with acetylated tubulin and adenylate cyclase clearly demonstrate that signal properties are independent from primary antibodies used (Fig. 3.1 J - O).

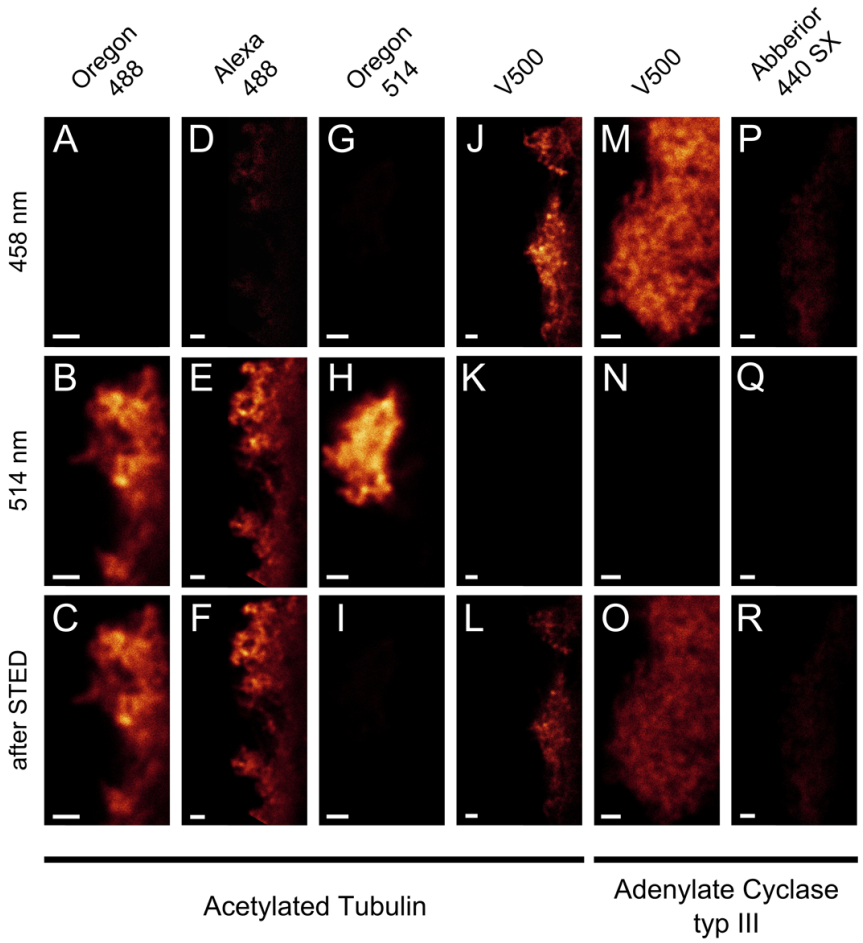

Figure 3.1: Evaluation of different fluorescent dyes for dual color STED microscopy. Oregon 488, Alexa 488 and Oregon 514 were tested as potential 514 nm fluorophores, V500 and Abberior 440 SX as potential 458 nm fluorophores. The upper row shows excitation with 458 nm laser light, the middle row shows simultaneous excitation with the 514 nm laser. The lower row illustrates decrease of signal intensity in the channel of interest after exposure to the depletion laser by taking one STED picture. All figures depict staining of olfactory cilia from the same animal. A - L show staining of acetylated tubulin. The Images J - O show V500 stainings to compare the signal quality with different primary antibodies. Due to lack of a rabbit hosted acetylated tublin antibody M - R show staining of adenylate cylcase type III to compare Abberior 440 SX staining with V500 signal. Image acquisition settings were used as described in methods section and kept equal for every tested dye. Scale bar = 2 µm.

4 Results

4.1 PDZ domain scaffolding proteins are expressed in the vomeronasal organ

PDZ scaffolding protein MUPP1 influences signal transduction in the main olfactory epithelium and interacts with olfactory receptors and several proteins from the signaling cascade (Baumgart et al., 2014). Thus, MUPP1 presumably recruits olfactory signaling proteins into functional complexes.

A similar mechanism is not known for vomeronasal signal transduction but both signaling pathways share common principles (Munger et al., 2009). Therefore, we analyzed deep RNA sequencing data and mRNA microarray data of vomeronasal epithelium for expression of scaffolding proteins with PDZ domains. The microarray data was gathered in the context of the SPP 1392 "Integrative analysis of olfaction" in collaboration with M. Spehr, RWTH Aachen. We found high expression levels for various scaffolding proteins in the vomeronasal organ (Fig. 4.1 A). The majority of the identified proteins was detected with both methods.

We investigated transcription of predominantly expressed genes or known scaffolding genes in more detail using RT-PCR (Fig. 4.1 B). Thereby, we excluded false positive candidates such as Shank2 or PICK1. Moreover, we confirmed the expression of NHERF1, which function was further analyzed in the vomeronasal organ.

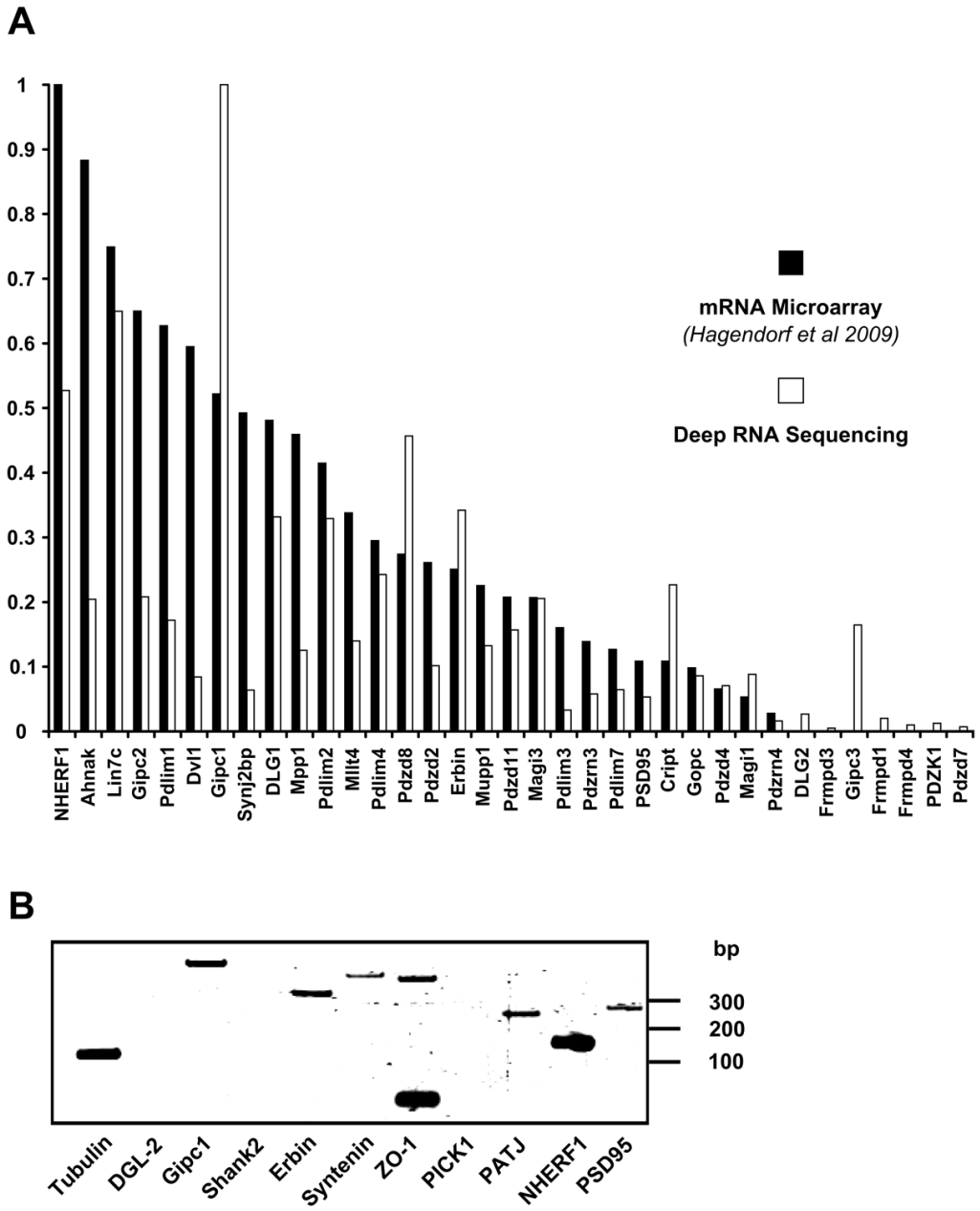

Figure 4.1: Numerous scaffolding proteins are transcribed in the vomeronasal organ. A: Transcription levels of PDZ domain scaffolding proteins in mouse vomeronasal organ analyzed by deep Sequencing and mRNA microarray analysis. Results were normalized to the highest signal found in each experiments. **B:** RT-PCR analysis of gene candidates from analysis in A as indicated.

4.2 NHERF1 protein in the vomeronasal organ

We identified high levels of NHERF1 transcription in the vomeronasal organ with two independent methods (Fig. 4.1 A). NHERF1 interacts with G protein-coupled receptors (GPCR), forms functional complexes of GPCRs and ion channels, and tethers these complexes to the cytoskeleton (Naren et al., 2003; Taouil et al., 2003). Furthermore, NHERF1 plays a role in phoshpholipse C (PLC) mediated calcium signaling after G protein-coupled receptor activation (Capuano et al., 2007; Mahon & Segre, 2004). Since signal transduction in the vomeronasal sensory neurons is based on G protein-coupled receptors and involves phospholipase C activity (Munger et al., 2009), we investigated the role of NHERF1 in the vomeronasal organ regarding its potential role in organizing signal transduction.

4.2.1 NHERF1 expression in the vomeronasal organ rises with maturation

The vomeronasal organ is present but not fully functional at birth and continues to develop until sexual maturity is reached (Coppola et al., 1993; Horowitz et al., 1999). If NHERF1 plays a role in vomeronasal signal transduction, expression levels may develop in parallel with the functional maturating of the organ.

Thus, we compared NHERF1 expression levels in premature P8 and adult P90 mice using Western Blot analysis (Fig. 4.2). Vomeronasal signaling proteins TrpC2 and $G_{\alpha o}$ were included as expression controls (Munger et al., 2009). GAPDH was used as loading control. We pooled lysates from 6 individual P8 and 3 individual P90 animals for each experiment.

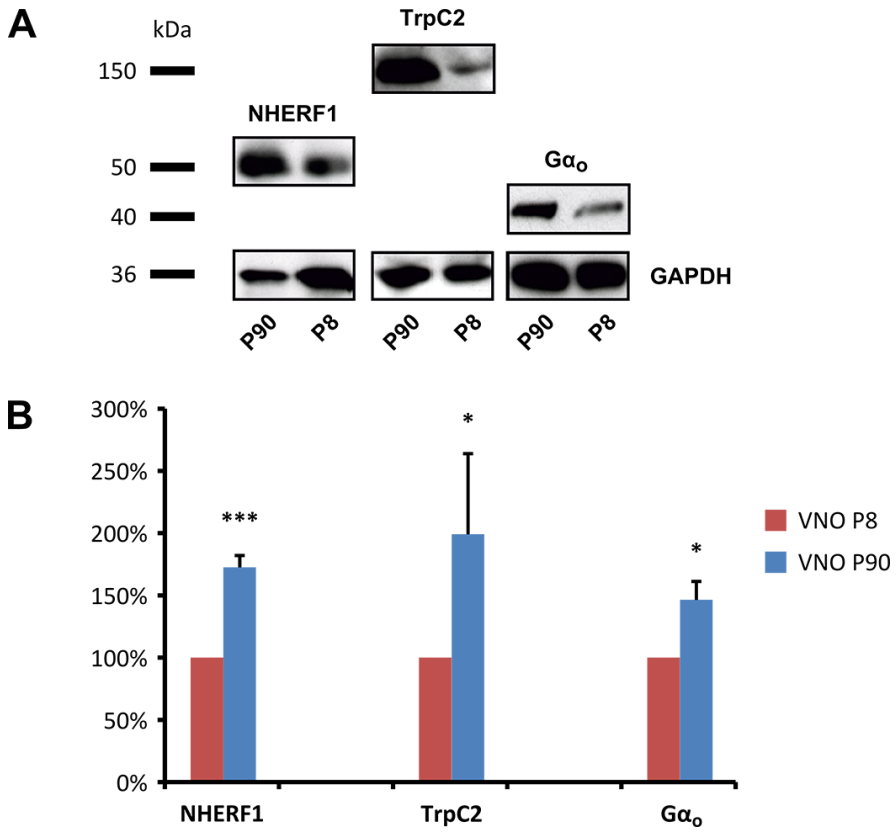

Figure 4.2: NHERF1 expression rises in parallel with vomeronasal signaling protein expression. A: Western Blots showing proteins found in lysate from adult and juvenile mice with loading control GAPDH. **B:** Relative expression of NHERF1 and signaling proteins TrpC2 and $G_{\alpha o}$ were compared between juvenile and adult mice. P8 values were set to 100%. GAPDH was used as a loading control. Student's t-test was used to compare juvenile and adult mice. NHERF1 $p < 0.0003$, n=3, TrpC2 $p < 0.047$, n=5, $G_{\alpha o}$ $p < 0.041$, n=3

We found NHERF1 expressed in P8 and P90 vomeronasal tissue, as we found TrpC2 and $G_{\alpha o}$ (Fig. 4.2 A). We quantified protein levels in both age stages and set values from juvenile mice to 100% (Fig. 4.2 B), to compare expression levels between both age stages. We observed an increase in NHERF1 expression to 173% $\pm$ 10% in adult mice. TrpC2 expression increased to 199% $\pm$ 65% and expression of $G_{\alpha o}$ increased to 146% $\pm$ 15%. NHERF1 expression increased with maturation of the vomeronasal organ, as did expression of vomeronasal signaling proteins. These data may indicate a role for NHERF1 in vomeronasal neuron activity.

4.2.2 NHERF1 is expressed in the microvillar layer of the vomeronasal organ

Signal transduction in vomeronasal sensory neurons takes place in the sensory microvilli (Trotier et al., 1998). We therefore hypothesized that scaffolding proteins which affect the signaling cascade should co-localize with signaling proteins in the microvilli. We assessed the localization of different scaffolding proteins in the vomeronasal organ by immunostaining of vomeronasal cryosections (Fig. 4.3). We focused on NHERF1, Lin7c, Ahnak, Gipc1 and DLG1 proteins, since these proteins were highly abundant in the vomeronasal organ (Fig. 4.1 A).

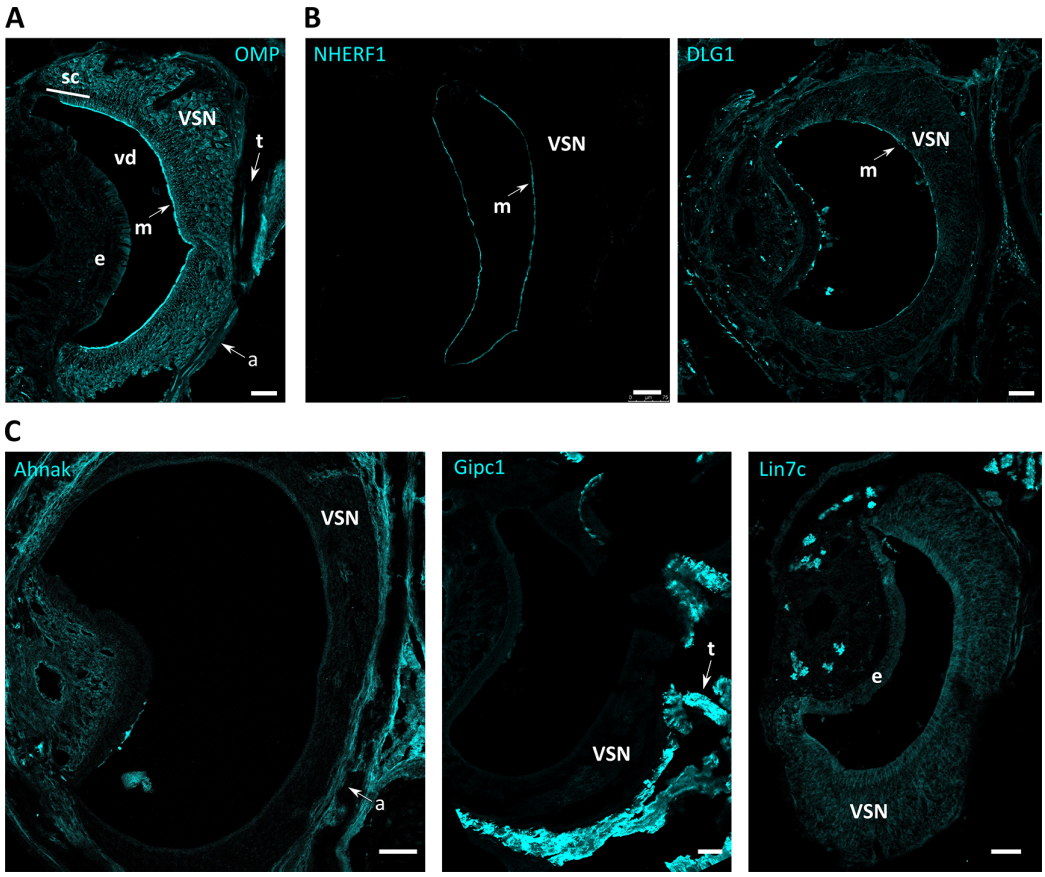

Figure 4.3: Localization of different scaffolding proteins in the vomeronasal organ. A: Overview image of a cryoslide through the vomeronasal organ. Vomeronasal sensory neurons were stained for olfactory marker protein OMP. Relevant structures were labeled for orientation. **B:** Enriched expression of NHERF1 and DLG1 in vomeronasal microvilli. **C:** Expression of Ahnak, Gipc1 and Lin7C in the vomeronasal organ. VSN = vomeronasal sensory neurons, sc = supporting cell layer, vd = vomeronasal duct, m = microvillar layer, e = non-neuronal epithelium, t = connective tissue, a = vomeronasal neuron axons, Scale bars = 50 µm, Age = P85 - P90

The olfactory marker protein OMP is specifically synthesized in mature olfactory neurons (Kott & Westrum, 1996). We illustrated the organization of the vomeronasal organ by labeling vomeronasal neurons with OMP (Fig. 4.3 A).

We found NHERF1 expression exclusively in the microvillar layer of the vomeronasal organ. DLG1 was expressed in microvillar layer and in dendrites of vomeronasal sensory neurons (Fig. 4.3 B). Ahnak was not expressed in neuronal cell bodies or dendrites, but we detected expression in axons. Lin7c was expressed in all cell bodies and microvilli including supporting cells. We found Gipc1 highly expressed in the connective tissue embedding the vomeronasal

organ, but Gipc1 is not expressed in the organ itself (Fig. 4.3 C).

With NHERF1 and DLG1, we identified two scaffolding proteins expressed in vomeronasal microvillar layer. Therefore, localization of NHERF1 supports our hypothesis that NHERF1 may contribute to signaling in the vomeronasal sensory neurons. The localization of DLG1 identified another scaffolding protein with a possible role in vomeronasal signaling. Neither Ahnak nor Gipc1 nor Lin7c displayed distinct vomeronasal microvilli expression. These results argue against a significant role of these proteins in vomeronasal signal transduction.

4.2.3 NHERF1 is expressed in vomeronasal sensory neurons

The vomeronasal sensory neurons reside in the crescent-shaped part of the vomeronasal epithelium (Fig. 4.3 A). The supporting cells cover the complete vomeronasal duct (Menco et al., 2001). Both cell populations project their microvilli into the vomeronasal duct. Thus, the microvillar layer is comprised of microvilli from two different cell populations in the neuronal part (Menco et al., 2001). Since we found NHERF1 localized to the complete microvillar layer, we investigated whether NHERF1 is also expressed in neuronal microvilli or only in those of supporting cells.

We stained cryosection from vomeronasal organ for mature olfactory neuron marker OMP to lable sensory neurons and simultaneously probed for NHERF1 expression. We identified NHERF1 expression in microvilli of supporting cells but co-localization with OMP also argued for NHERF1 expression in neuronal microvilli (Fig. 4.4).

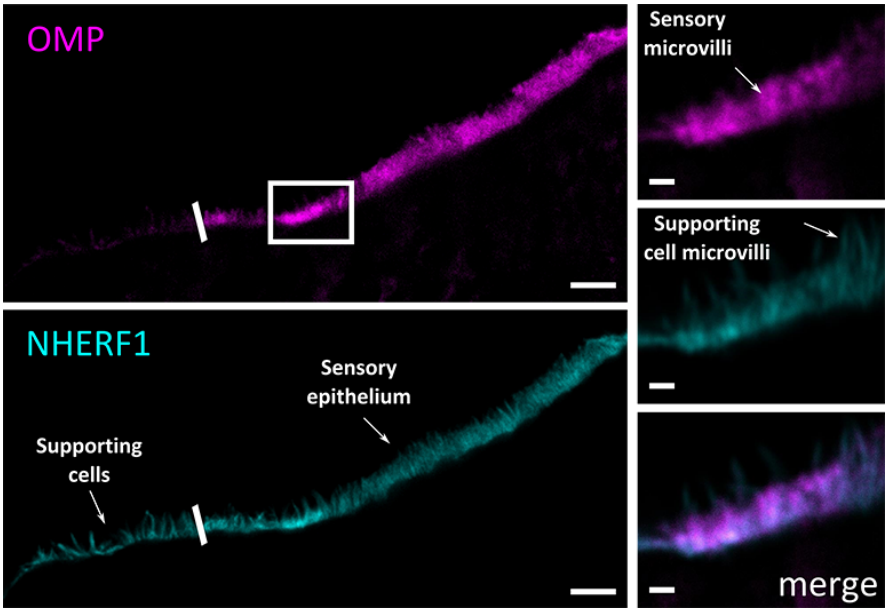

Figure 4.4: NHERF1 is expressed in vomeronasal microvilli. Detailed images of NHERF1 expression in vomeronasal microvilli. Vomeronasal sensory neurons were marked with OMP. The border between sensory epithelium and supporting cells is marked. High magnification images show NHERF1 expression and OMP expression in microvilli of sensory neurons. No OMP expression was detected in microvilli of the supporting cells. Scale bars: large = 5 µm, small = 1 µm

Due to microvilli density, differentiation between microvilli of supporting cells and neuronal microvilli was not possible (Fig. 4.4 merge). In order to image microvilli from single sensory neurons, we dissociated cells from vomeronasal tissue. We used $G_{\alpha i2}$ and TrpC2 from the vomeronasal signaling cascade to label neuronal microvilli (Munger et al., 2009), and stained dissociated cells for NHERF1 in combination with $G_{\alpha i2}$ or TrpC2 (Fig. 4.5).

We found NHERF1 expression in microvilli from dissociated vomeronasal sensory neurons. Signaling proteins like $G_{\alpha i2}$ (Fig. 4.5 A) and TrpC2 channel (Fig. 4.5 B) did co-localize with NHERF1 in the neuronal microvilli. The results from dissociated neurons show that NHERF1 is expressed in neuronal microvilli of the vomeronasal organ. Therefore, NHERF1 could possibly influence vomeronasal signaling in neuronal microvilli.

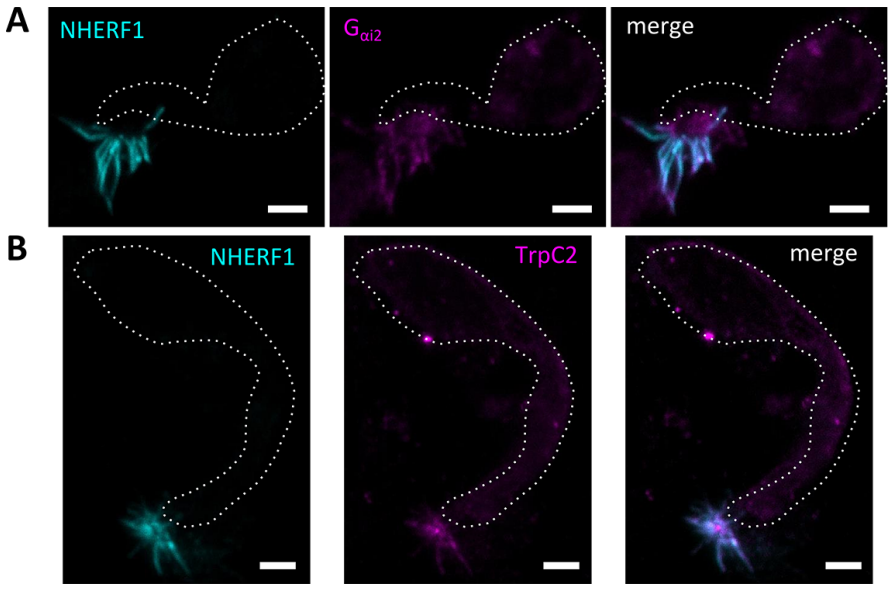

Figure 4.5: NHERF1 is found in vomeronasal neuron microvilli. Dissociated neurons from vomeronasal organ were stained for NHERF1 together with different signaling proteins. **A:** with $G_{\alpha i2}$ **B:** with TrpC2. Scale bars: = 2 µm. Dotted lines indicate cell bodies and dendrite.

4.2.4 NHERF1 is organized in segregated domains in vomeronasal microvilli

The hypothesis of scaffolding proteins organizing functional microdomains in olfactory systems was already proposed by L'Etoile & Bargmann (2000) in their work on *C. elegans* olfaction, but up to now there is no evidence for any scaffolding protein organizing signal transduction in the vomeronasal system. We showed evidence for NHERF1 expression in neuronal microvilli. Thus, we investigated the possibility that NHERF1 affects vomeronasal signal transduction by forming signaling microdomains.

Since signaling microdomains consist of only few proteins (Huber, 2001), their dimensions are beyond the resolution limit of conventional confocal microscopy. Therefore, we stained dissociated vomeronasal sensory neurons for NHERF1 (Fig. 4.6 A) and used super-resolution STED microscopy to analyze subcellular organization in microvilli. Confocal images (Fig. 4.6 B) showed a blurry unfocused NHERF1 staining. In contrast, STED microscopy revealed NHERF1 was not distributed homogeneously along the sensory microvilli but forms seg-

regated domains along sensory microvilli (Fig. 4.6 B). These domains may be single signaling microdomains, where NHERF1 possibly contributes to the organization of the vomeronasal signaling cascade.

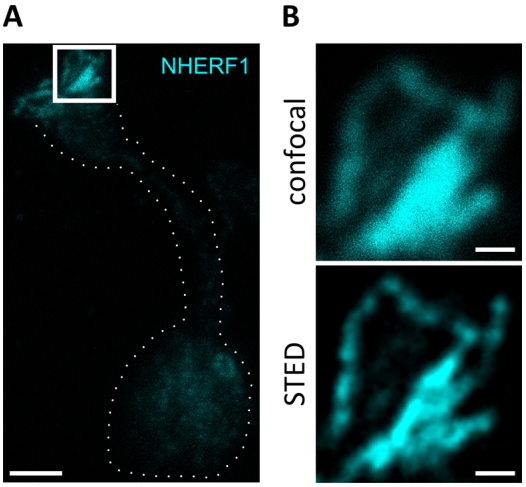

Figure 4.6: NHERF1 is organized in microdomains. Dissociated neurons from vomeronasal organ were stained for NHERF1. **A:** Z-Stack of a dissociated vomeronasal sensory neuron. Dotted line indicates cell body, dendrite and dendritic knob. Box indicates area shown in B. **B:** High magnification of sensory microvilli. conventional confocal image vs. super-resolution STED image. Scale bars: A = 3 µm, B = 500 nm

Based on the focused localization of NHERF1, we addressed the question if NHERF1 assembles signaling proteins into functional complexes. Therefore, we looked for co-localization of signaling protein $G_{\alpha i2}$ with NHERF1 microdomains. We established a dual color STED microscopy technique to resolve two distinct proteins on super-resolution level (see Dual color STED Microscopy on p. 56).

We applied the double staining technique to cryosections and started with imaging TrpC2 and $G_{\alpha i2}$ (Fig. 4.7 A, B), to analyze two proteins from the same signaling cascade only expressed in neuronal microvilli (Menco et al., 2001). This control experiment yielded two results. First, super-resolution images showed a clear difference in subcellular organization between TrpC2 and $G_{\alpha i2}$. $G_{\alpha i2}$ was arranged in distinct domains, TrpC2 channel expression was evenly distributed along the sensory microvilli (Fig. 4.7 B). Second, although both proteins are localized to the same compartment they only partially co-localize in super-resolution images (Fig, 4.7 B, lower row). This results demonstrate, signaling pro-

tein $G_{\alpha i2}$ is organized in segregated domains in neuronal microvilli and does not completely co-localize with TrpC2.

Next, we stained sections for NHERF1 together with $G_{\alpha i2}$ (Fig. 4.7 C), to compare the organization of scaffolding and signaling protein. The distribution of NHERF1 in sensory microvilli appeared in distinct microdomains, like in dissociated neurons. These microdomains partially co-localize with $G_{\alpha i2}$ domains (arrows). This demonstrates, we were able to image two proteins in neuronal microvilli in super-resolution.

Proteins localized to the same cell compartment often appear to fully co-localize in conventional confocal microscopy images. However, using super-resolution STED microscopy we revealed heterogeneity in distribution even for proteins of a mutual cascade. (Fig. 4.7 B). Imaging NHERF1 together with $G_{\alpha i2}$ showed a similar pattern which may indicate an influence of NHERF1 on this cascade.

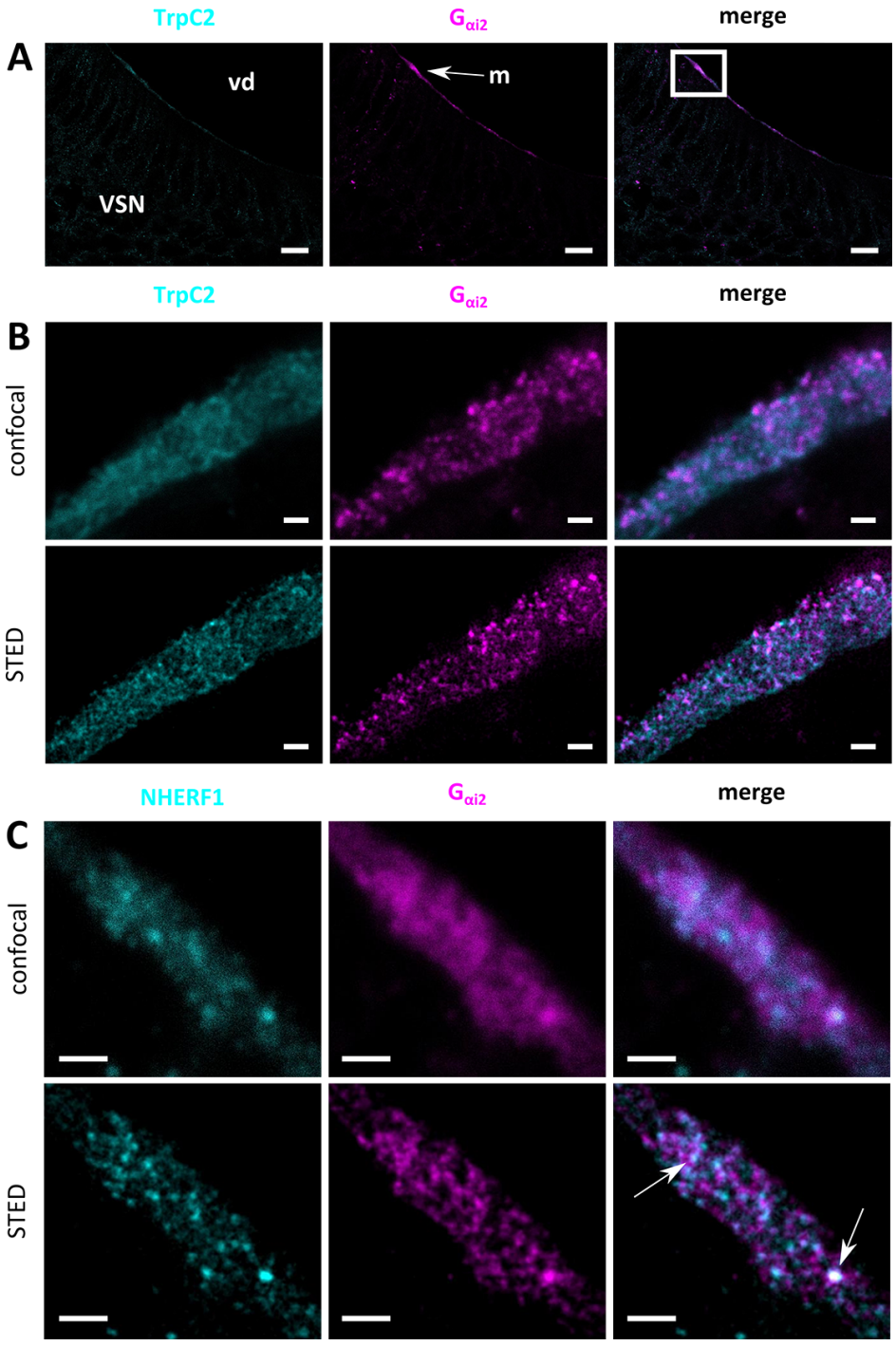

Figure 4.7: NHERF1 forms partially overlapping microdomains with $G_{\alpha i2}$ in neuronal microvilli. cryosections of adult vomeronasal organ were stained for NHERF1 and signaling proteins $G_{\alpha i2}$ and TrpC2. The microvillar layer was imaged in super-resolution. **A:** Low-magnification-overview with labeled structures. Boxed area exemplifies magnification. VSN = vomeronasal sensory neurons, vd = vomeronasal duct, m = microvillar layer **B:** Microvilli stained for TrpC2 and $G_{\alpha i2}$. Upper row with confocal images. Lower row with corresponding STED images. **C:** High magnification of microvilli stained for NHERF1 and $G_{\alpha i2}$. Upper row with confocal images. Lower row with corresponding STED images. Scale bars: A = 10 µm, B,C = 1 µm

4.3 Interaction of NHERF1 PDZ domains with vomeronasal proteins

With indications for a possible role of NHERF1 in vomeronasal signal transduction, we focused on the question whether NHERF1 can interact with PDZ ligands found in vomeronasal sensory neurons. We designed a PDZ interaction microarray with 288 potential ligands to identify NHERF1 interaction partners.

4.3.1 Numerous vomeronasal receptors are classical PDZ ligands

NHERF1 regulates G protein-coupled receptor signaling in multiple ways(Ardura & Friedman, 2011). For example, NHERF1 recruits β-adrenergic receptor and CFTR channel into one functional complex and tethers this complex to the cytoskeleton (Naren et al., 2003) or NHERF1 recycles somatostatin receptor 5 to the plasma membrane (Bauch et al., 2014). Moreover, GPCRs like β-adrenergic receptor type 2, κ-opioid receptor and parathyroid hormone receptor are PDZ ligands of NHERF1 (Huang, 2004; Mahon & Segre, 2004).

The vomeronasal signaling cascade is initiated by ligand binding to vomeronasal receptors. Vomeronasal receptors are divided into two distinct families (Spehr & Munger, 2009). Type 1 (V1) receptors are narrowly tuned to detect small natural ligands from conspecifics, type 2 (V2) receptors detect peptide and protein pheromones influencing social behavior (Munger et al., 2009). V1 receptors are Class-A G protein-coupled receptors, V2 receptors are part of the Class-C family (Spehr & Munger, 2009). NHERF1 could possibly interact with vomeronasal receptor PDZ ligands and organize vomeronasal signal transduction. We investigated this possibility and looked for conserved PDZ ligand motifs (Nourry et al., 2003) in vomeronasal type 1 and type 2 receptors.

19% of the annotated V1 receptors featured a PDZ ligand motif. 10% of V1 receptors were class II ligands and 8% class III ligands. Only 1% were class I ligands (Fig. 4.8 left). 38% of the annotated V2 receptors displayed a PDZ ligand motif. We found 20% of V2 receptors with class I, 16% with class II and only 2%

with class III motifs (Fig. 4.8 right). This results show, a subset of vomeronasal receptors from both families are PDZ ligands, and could therefore interact with PDZ domain scaffolding proteins such as NHERF1.

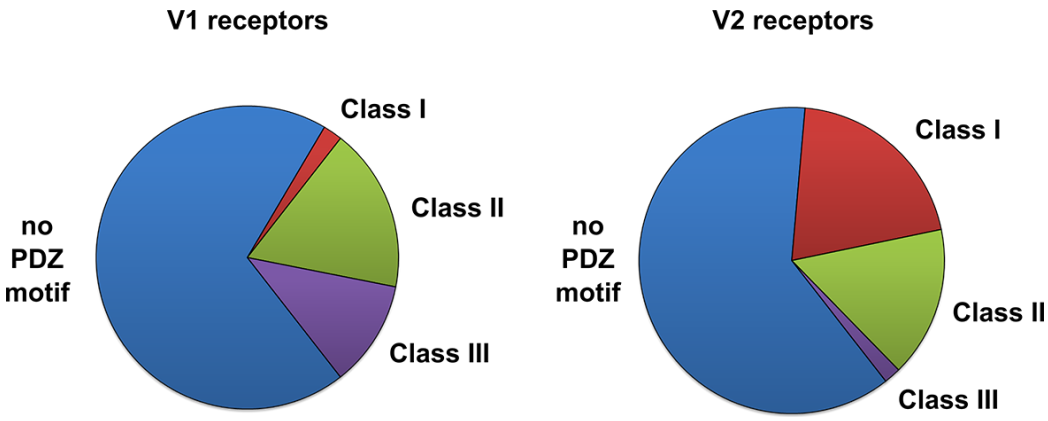

Figure 4.8: Distribution of PDZ liand motifs in V1 and V2 receptors. Class I (red), Class II (green), Class III (purple), no PDZ motif (blue).

4.3.2 NHERF1 PDZ domains interact with vomeronasal receptors type 1

We used the identified vomeronasal receptors with PDZ ligand motifs to design a custom-made PDZ ligand microarray. Besides vomeronasal receptors, the microarray featured olfactory signaling proteins and other proteins of interest (complete list, see appendix).

We cloned NHERF1 PDZ domains with added HA-tag as described by Huang (2004) into a GST-tag vector. Both PDZ domains were expressed in *E.coli* BL21 cells using an IPTG-inducible system. We purified the protein from bacterial lysate by binding to GST-trap beads and removed the GST-tag using a specific protease. No protein expression could be detected prior to IPTG induction. After induction we identified both PDZ domains fused to the GST-tag via Western Blot analysis. The Western Blot signals were reduced after incubation with GST-trap beads, indicating that the peptides stably interacted with the bead fraction. The protease removed GST-tags, yielding purified PDZ domains in solution (Fig. 4.9 lanes 5, 9).

These experiments demonstrate that we successfully synthesized and purified both NHERF1 PDZ domains. We subsequently used these domains to probe for interaction with C-termini from vomeronasal receptors and proteins from vomeronasal sensory neurons.

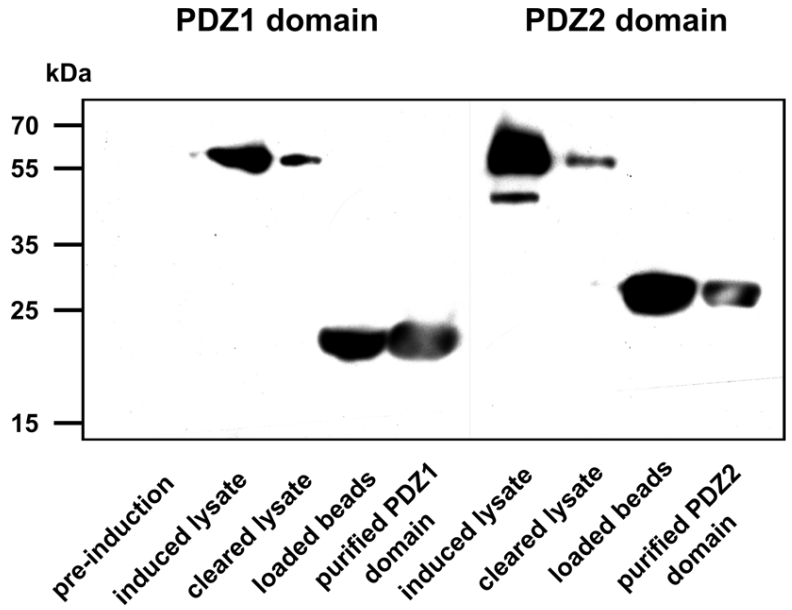

Figure 4.9: Expression of NHERF1 PDZ domains in *E.coli* BL21 cells. NHERF1 PDZ domains were synthesized in *E.coli* BL21 cells using an IPTG-inducible system. The stages of protein expression were monitored by Western Blot detected with HA-tag antibody. Phases shown for both PDZ domains: pre-induction, after induction, cleared lysates, protein-loaded beads and purified protein.

We conducted three independent trials for both PDZ domains. Thereto, we applied 200 ng/µl of purified PDZ domains to the microarray and detected bound PDZ domains with HA-tag antibody via chemiluminescence detection. Fig. 4.10 A shows a representative experiment. We quantified signals from every spot and ranked them according to signal intensities. The background was defined as the arithmetic mean of empty spots on the array. We defined a positive interaction as signal intensity greater than background + 2 times standard deviation of background intensity. This analysis yielded a list of potential interaction partners for both NHERF1 PDZ domains.

We identified 30 positive interactions for PDZ1 domain, and 49 interactions for PDZ2 domain. A comprehensive list for all positive interaction partners for

both PDZ domains of NHERF1 can be found in the appendix in tables 5.2 and 5.3. 77% of PDZ1 domain interaction partners were V1 receptors. V2 receptors made up for 7% of PDZ1 domain hits. The remaining 16% of PDZ1 domain hits were comprised of non-vomeronasal receptor PDZ ligands (Fig. 4.10 B left). 43% of PDZ2 domain hits were V1 receptors. Only 2% of PDZ2 interaction partners were V2 receptors. 55% of PDZ2 domain hits were non-vomeronasal receptor proteins (Fig. 4.10 B right). These results indicate the ability of NHERF1 to interact with vomeronasal receptors.

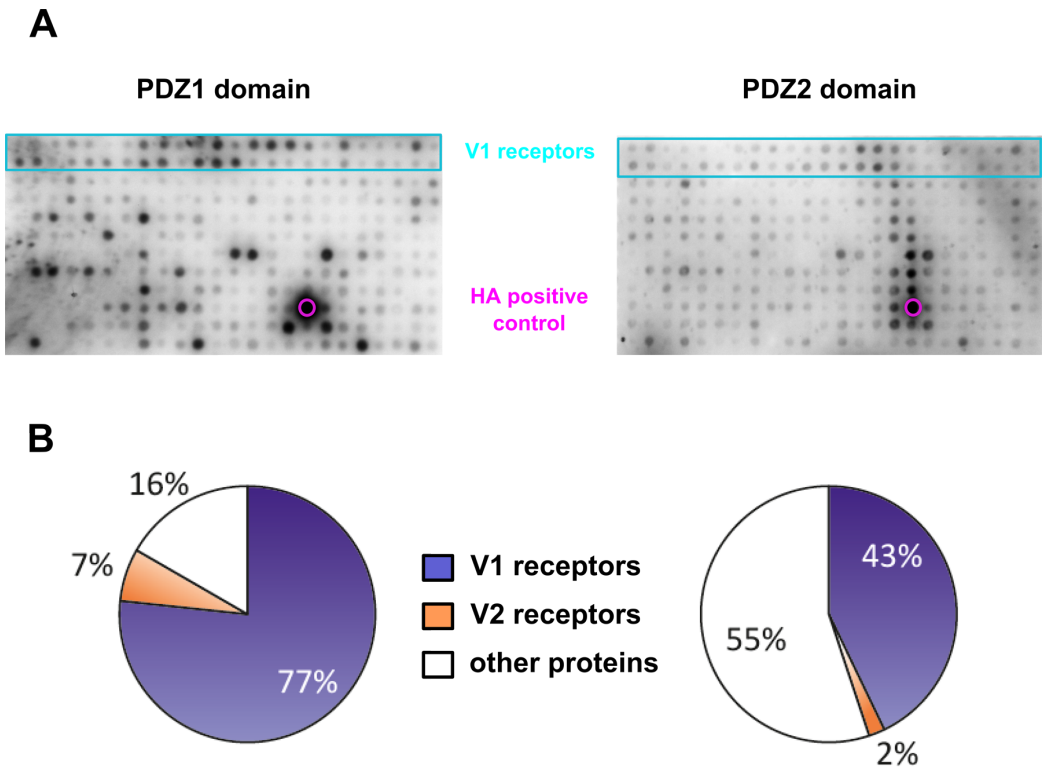

Figure 4.10: Interaction of NHERF1 PDZ domains with vomeronasal proteins. A: PDZ ligand microarrays incubated with NHERF1 PDZ domains and probed for PDZ domain interaction with HRP-coupled antibodies. **B:** Positive interactions for both NHERF1 PDZ domains were classified in three relevant groups, V1 receptors, V2 receptors and other putative PDZ ligands.

15 interaction partners of both domains displayed a Class II PDZ ligand motif, 8 (PDZ1) or 7 (PDZ2) a Class III motif, respectively. Only 4 (PDZ1) or 5 (PDZ2) showed a Class I motif. 5 PDZ1 domain interaction partners did not display a PDZ ligand motif, as did 21 of PDZ2 interaction partners (Fig. 4.11). This analy-

sis demonstrates, NHERF1 favors Class III and Class II PDZ ligands over Class I ligands. In addition, NHERF1 is also able to bind ligands without a PDZ ligand motif.

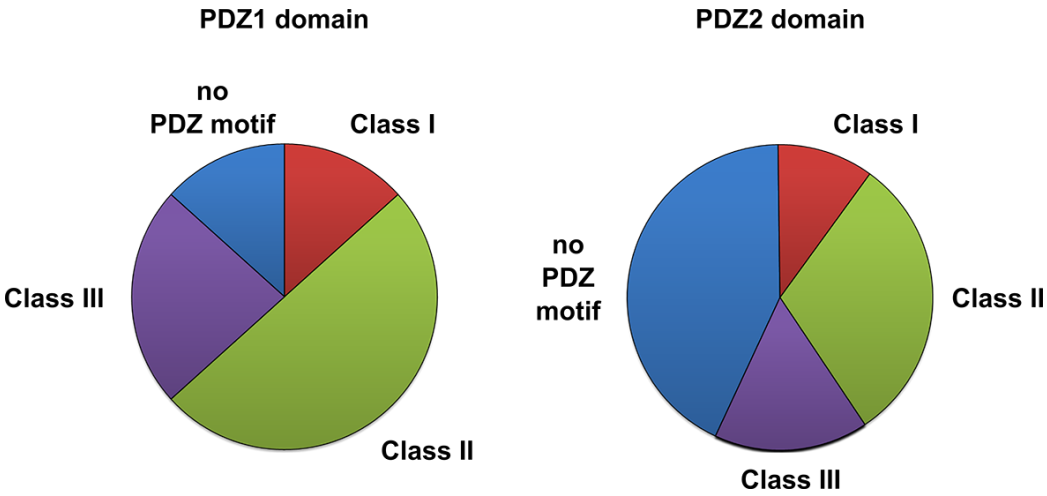

Figure 4.11: Distribution of PDZ ligand motifs of NHERF1 interaction partners. Class I (red), Class II (green), Class III (purple), no PDZ motif (blue).

We also included known interaction partners as positive controls for both PDZ domains in the microarray analysis. CFTR, PTEN and organic anion/cation transporter Slc22a12 interact with NHERF1 PDZ1 domain (Cunningham et al., 2007; Takahashi et al., 2006; Wang et al., 1998). Slc22a12 yielded a positive interaction signal with PDZ1 but not PDZ2 domain in 3 out of 3 experiments. PTEN interacted in 1 out of 3 experiments with both PDZ domains. CFTR did not interact with either domain in any conducted experiment.

β-catenin and NHERF1 are described interaction partners of NHERF1 PDZ2 domain (Wheeler et al., 2011). NHERF1 is capable of intramolecular folding through interaction with its own C-terminus (Morales et al., 2007). Therefore, we also included these two proteins as positive controls for PDZ2 domain. NHERF1 C-terminus was identified in 1 out 3 experiments as interaction partner for PDZ2 domain but never for PDZ1 domain. β-catenin interacted in 2 out 3 independent experiments with PDZ2 domain and we did not observe any interaction with PDZ1 domain.

Moreover, we included proteins with established or supposed roles in vomeronasal signal transduction or modulation in tjis microarray analysis (Francia

et al., 2014). This way, we tested if scaffolding proteins potentially influnce vomeronasal signaling by interaction with established signaling proteins. PLCβ1 and γ1, TrpC2 channel, guanylate cylcase 2d, PDE2A, calmodulin 2, carbonic anhydrase 2 and diacylglycerol lipases α and β were all tested for interaction with NHERF1 PDZ domains. Additionally, G_{α}-proteins s1, i1-3, o1, t1-3, z, q11, q14, q15, and G_{α}-proteins 12 and 13 were probed for interaction, as were PLC enzymes β1,3,4, η1, ϵ1 and γ2. Furthermore, Anoctamin 1, 2, 6 and 10 were spotted on the array. With the exception of PDE2A, none of the aforementioned proteins interacted with PDZ1 domain from NHERF1 in 3 independent experiments.

We found NHERF1 PDZ2 domain interacted with G proteins $G_{\alpha t1\text{-}3}$ (isotypes feature identical C-termini) and $G_{\alpha i3}$. We also observed interactions with PLCη1, PLCγ1 and adenylate cyclases 2, 5 and 6. Furthermore, signal modulating proteins calmodulin 2, DAGβ and PDE2A interacted with PDZ2 domain. Provided that, these proteins are expressed in vomeronasal sensory neurons, NHERF1 could influence their function through PDZ interaction. Thus, NHERF1 could play a part in regulating vomeronasal signal transduction.

We did not find interaction between NHERF1 PDZ domains and TrpC2 channel, Anoctamin 1 or Anoctamin 2. Neither did we find interaction with G proteins $G_{\alpha i2}$ or $G_{\alpha o}$. Taken together, all characterized signaling proteins from the vomeronasal signaling cascade (excluding vomeronasal receptors) had to be considered as non-interacting. These findings argue against a direct organization of the vomeronasal signaling cascade through NHERF1 beyond the level of vomeronasal receptors. The interaction array yielded a list of possible interaction partners from vomeronasal organ for NHERF1. Vomeronasal receptors type 1 were identified as ligands for both NHERF1 PDZ domains. Only few vomeronasal receptors type 2 interacted with NHERF1. An interaction between NHERF1 and further members of the vomeronasal signaling cascade was not found. Still, NHERF1 may influence vomeronasal signal transduction by interacting with vomeronasal receptors.

4.3.3 PDZ ligand microarray successfully identifies new interaction partners

We wanted to confirm the possibility to identify new PDZ interactions with our high-throughput approach. Thus, we used NHERF1 PDZ domains as bait in a pull-down experiment with the C-terminus from vomeronasal receptor Vmn1ra10. This receptor scored highest on our interaction list for both NHERF1 PDZ domains (Tab. 5.2). Vmn1ra10 is a yet undescribed receptor which features a class II PDZ motif in its C-terminus.

We then cloned Vmn1ra10 C-terminus from vomeronasal organ cDNA as GFP fusion protein and expressed Vmn1ra10 C-terminus GFP-fusion in HEK293 cells. We used NHERF1 PDZ domains to pull down Vmn1ra10 C-terminus and verified successful pulldownby probing for GFP-tagged Vmn1ra10 in Western Blot (Fig. 4.12). We detected interaction of Vmn1ra10 C-terminus with both PDZ domains from NHERF1. These results confirmed our microarray findings which identified Vmn1ra10 as NHERF1 interaction partner. Thus, it is possible to detect new PDZ interaction partners with our PDZ ligand microarray approach.

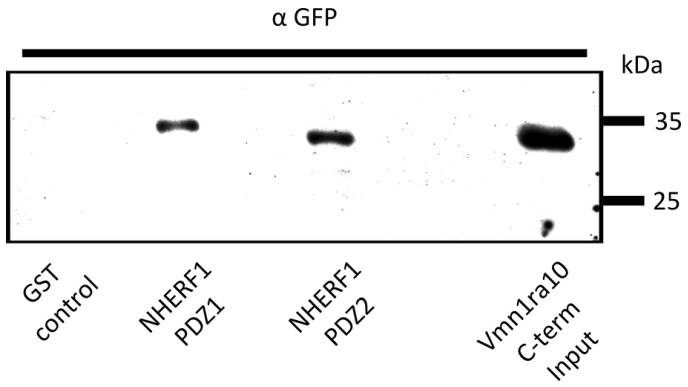

Figure 4.12: Vomeronasal receptor Vmn1ra10 co-immunoprecipitates with NHERF1 PDZ domains. Vomeronasal receptor Vmn1ra10 was probed for direct interaction with PDZ1 and PDZ2 domains from NHERF1. NHERF1 PDZ domains were used to pulldown GFP-tagged C-terminus from Vmn1ra10. Control represents GST-trap beads loaded with GST. Detection of GFP-tagged Vmn1ra10 C-terminus after pulldown and detection of Vmn1ra10 input with GFP antibody. (Data provided by Willem Bintig, Charite Berlin, Neurocure)

4.3.4 NHERF1 is expressed in microvilli of both neuronal subpopulations

Due to the fact that considerably more V1 than V2 receptors interacted with NHERF1, we analyzed if NHERF1 was predominately expressed with V1 receptor-expressing neurons.

Since there were no pan-V1 or pan-V2 antibodies available, we needed an alternative to distinguish between those two cell populations. Cells expressing V1 or V2 receptors can also be distinguished by their expression of $G_{\alpha i2}$ (V1 receptors) or $G_{\alpha o}$ (V2 receptors) (Munger et al., 2009). Therefore, we ensured localization of both G proteins in neuronal microvilli, by staining cryosections of vomeronasal organ for both G proteins together with mature olfactory neuron marker OMP (Fig. 4.13). We identified expression of only one G protein subtype in certain parts of the microvillar layer (Fig. 4.13 E). Consequently, only one certain receptor family should be expressed in these areas. Thus, we were able to discriminate between microvilli of V1 or V2 receptors in vomeronasal cryosections.

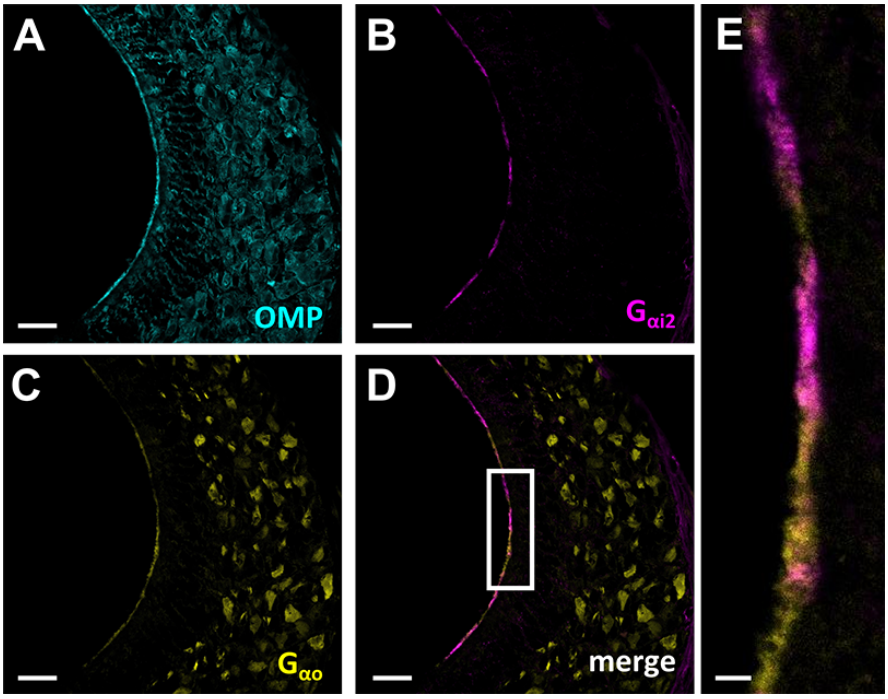

Figure 4.13: $G_{\alpha i2}$ and $G_{\alpha o}$ mark two neuron subpopulations in the vomeronasal organ. Vomeronasal cryosections stained for **A:** OMP. **B:** $G_{\alpha i2}$ and **C:** $G_{\alpha o}$ proteins. **D:** Overlay of both G proteins show parts of the microvillar layer that are stained only for one specific G protein subtype. Box illustrates the magnified area shown in E. **E:** High magnification overlay of $G_{\alpha i2}$ and $G_{\alpha o}$ staining in microvillar layer. Scale bars A-D = 20 µm F = 2.5 µm.

With the possibility to differentiate between V1 and V2 receptor-expressing neurons, we analyzed co-localization of NHERF1 together with $G_{\alpha i2}$ and $G_{\alpha o}$ (Fig. 4.14). Therefore, we stained cryosections of vomeronasal organ for both G proteins together with NHERF1. A specific region of the microvillar layer was selected as region of interest (ROI) (Fig. 4.14 A & C, E & G). We calculated intensities for each pixel in this ROI for all three colors. High intensities for two colors indicated expression of both proteins in the same spatial area and illustrated co-localization. We plotted intensities for both G proteins against each other to ensure specific expression of one G protein subtype in the ROI (Fig. 4.14 B, F). Next, we looked for co-localization with NHERF1 in this specific area (Fig. 4.14 D, H).

We analyzed in ROI on 6 different cryosections from 3 individual animals for both G proteins in this way and did not find a significant difference in NHERF1 expression between V1- or V2-receptor-expressing neurons. In both neuronal

subpopulations NHERF1 did co-localize with corresponding G proteins (Fig. 4.15 yellow bars), while G proteins from the other neuronal subpopulation were absent (Fig. 4.15 magenta / cyan bars). NHERF1 showed 73% $\pm$ 8,6 % overlap with $G_{\alpha i2}$ in V1 receptor-expressing neurons and 80% $\pm$ 7,3 % overlap with $G_{\alpha o}$ in V2 receptor-expressing neurons. Thus, NHERF1 is expressed in microvilli from both sensory neuron subpopulations, although more V1 than V2 receptors might interacted with NHERF1.

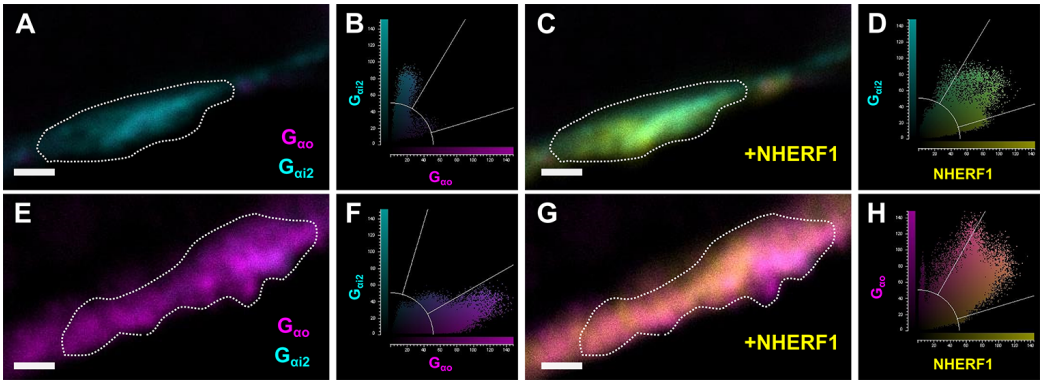

Figure 4.14: NHERF1 is expressed in both vomeronasal neuron subpopulations. NHERF1 expression was analyzed in parts of vomeronasal microvillar layer expressing either $G_{\alpha i2}$ or $G_{\alpha o}$ to distinguish between V1 and V2 receptor-expressing neurons. **A:** Region of interest (white line) used for expression analysis of NHERF1 in V1 receptor neurons. **B:** Co-localization diagram for both G proteins in the ROI. **C:** Expression of NHERF1 and both G proteins in the ROI (white line). **D:** Co-localization diagram for NHERF1 and $G_{\alpha i2}$ (V1 receptors). **D-H:** Same analysis for V2 receptor-expressing neurons labeled with $G_{\alpha o}$.

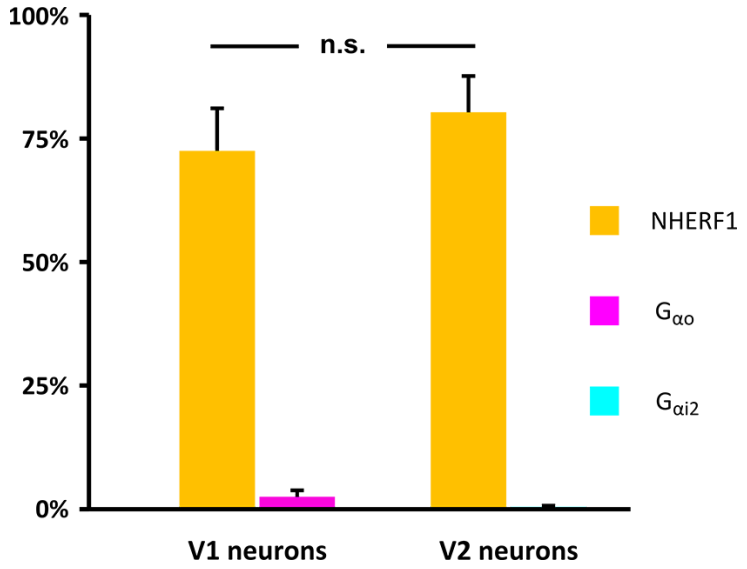

Figure 4.15: Co-expression of NHERF1 with $G_{\alpha i2}$ and $G_{\alpha o}$. vomeronasal microvilli. Co-localization of NHERF1 with either $G_{\alpha i2}$ or $G_{\alpha o}$ was used to analyze expression of NHERF1 in V1 or V2 receptor-expressing microvilli. Student's t-test was used to compare NHERF1 expression in V1- and V2 receptor-expressing neurons, p = 0.51, n = 6.

4.4 DLG1 protein in the vomeronasal organ

Besides scaffolding protein NHERF1, we also found expression of DLG1 (aka SAP97) in the mouse vomeronsal organ (Fig. 4.1 A). DLG1 is a scaffolding protein with three PDZ domains. Like NHERF1, DLG1 is able to interact with G protein-coupled receptors and ion channels to anchor them to the cytoskeleton (He et al., 2006; Sabio et al., 2005; Sans et al., 2001; Wu et al., 1998). Moreover, DLG1 is able to form multimers with other scaffolding proteins (Colledge et al., 2000; Feng et al., 2004; Lee et al., 2002; Oliveria et al., 2003). In addition, DLG1 plays a pivotal role in some receptor trafficking and internalization processes (Gardner et al., 2007; Nooh et al., 2013).

These characteristics make DLG1 an interesting candidate for regulation of vomeronasal signaling processes. The ability to multimerize with other scaffolding proteins enables DLG1 to function as a potential hub in scaffolding complexes. Therefore, we investigated the role of DLG1 in vomeronasal signaling as we did for NHERF1.

4.4.1 DLG1 is expressed in neuronal microvilli and dendrites

We demonstrated expression of DLG1 in the vomeronasal organ via RT-PCR (Fig. 4.1 B) and staining of vomeronsal organ sections identified protein localization in sensory neurons (Fig. 4.3 A). To analyze whether DLG1 localized to the microvillar compartment, we co-stained DLG1 with the mature olfactory neuron marker OMP. Confocal microscopy revealed expression of DLG1 in neuronal microvilli and dendrites but not in supporting cells of the vomeronasal organ (cf. Fig. 4.16 B and C). Therefore, the identification of DLG1 in neuronal microvilli supports the idea of DLG1 playing a role in vomeronasal signal transduction.

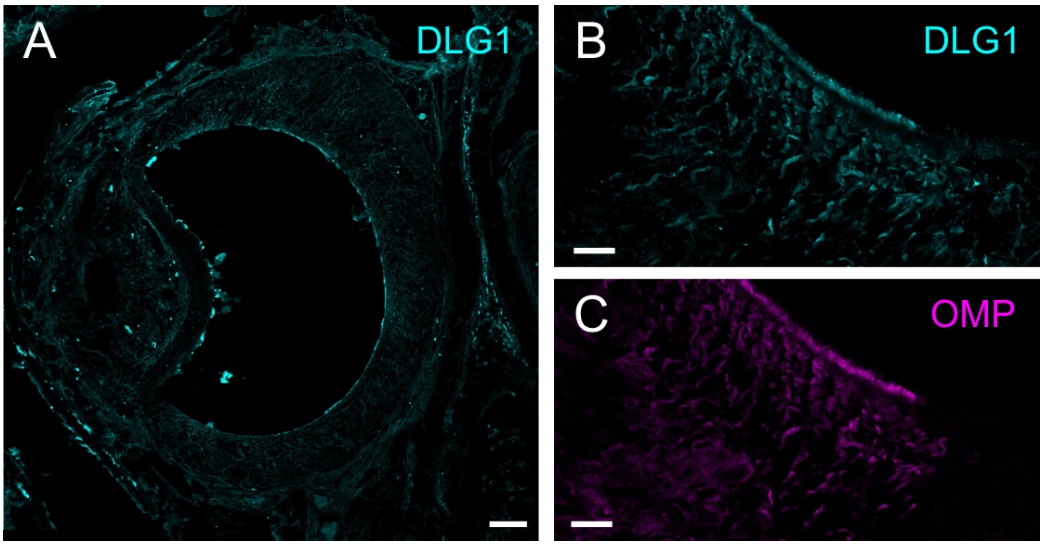

Figure 4.16: DLG1 is expressed in microvilli of vomeronasal sensory neurons. Cryosections of vomeronasal organ were stained for DLG1 protein. **A:** Overview picture of the complete vomeronasal organ. **B, C:** Vomeronasal microvillar layer in detail, showing the transition zone between neuronal and non-neuronal epithelium. Scale bars: A = 50 µm, B, C = 10 µm

4.4.2 Interaction of DLG1 PDZ domains with vomeronasal proteins

Next, we used our custom-made PDZ interaction microarray to analyze whether DLG1 interacts with proteins involved in vomeronasal signaling. Therefore, we cloned DLG1 PDZ domains with added HA-tag as described in Wang et al. (2005) and expressed all three domains as GST fusion in BL21 cells. The GST tag was

used to purify the domains via GST trap beads as described before. We successfully purified all three PDZ domains from bacterial lysates (Fig. 4.17 A, C, E). Thus, DLG1 PDZ domains could be tested in our microarray.

We applied 200 ng/µl of purified PDZ domains the PDZ interaction microarray to probe for interaction (Fig. 4.17 B, D, F). Although we purified all three domains from bacterial lysates, only PDZ2 domain yielded interaction results in our microarray analysis. Neither PDZ1 nor PDZ3 domain did interact with any spotted peptide on the array. Therefore, we were only able to determine a list of potential PDZ2 domain interaction partners from vomeronasal organ.

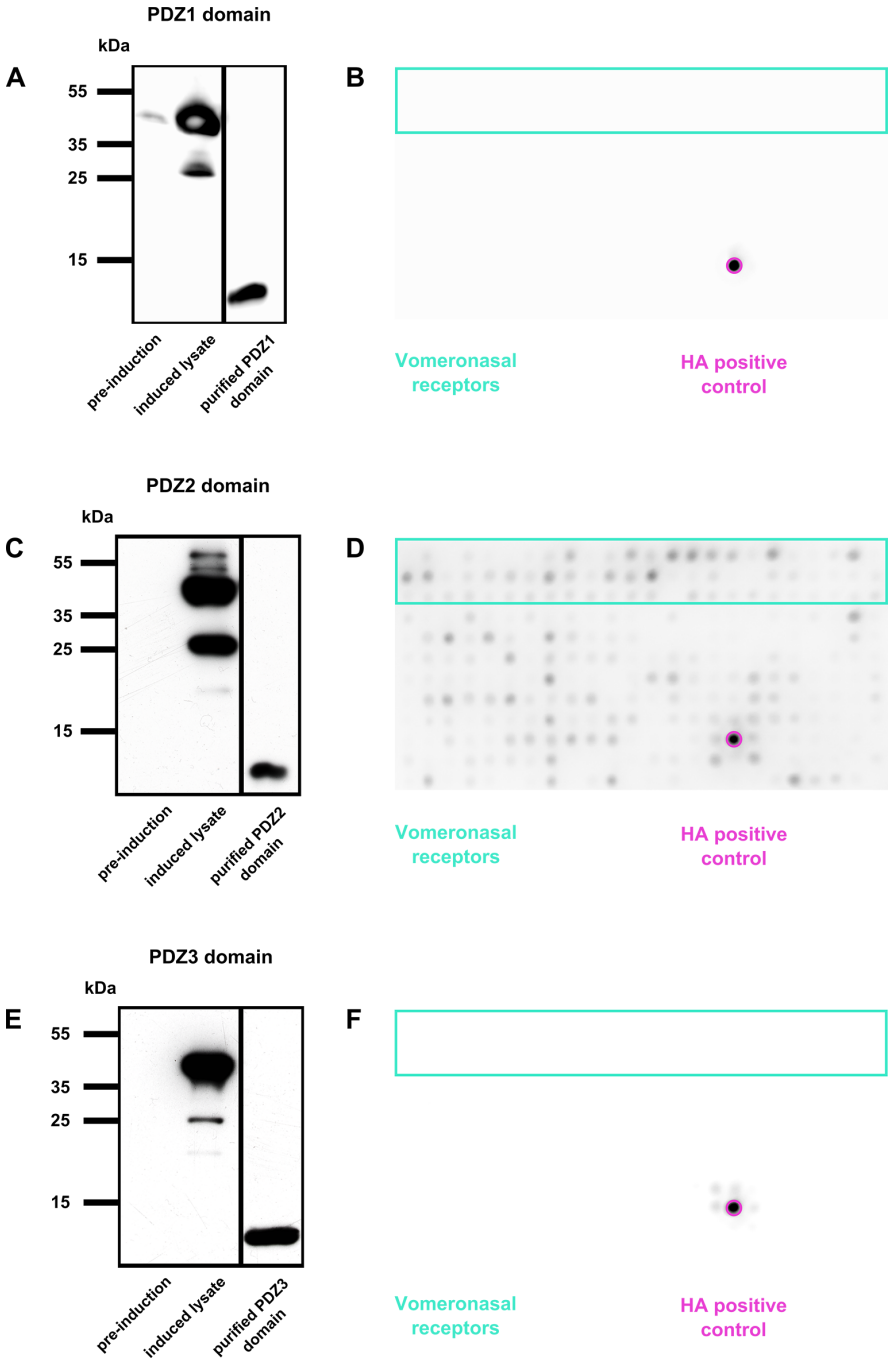

Figure 4.17: Expression and interaction analysis of DLG1 PDZ domains. A, C, E: DLG1 PDZ domains were expressed in *E.coli* BL21 cells using an IPTG-inducable system. The stages of protein expression were monitored by Western Blot, showing pre-induction expression, lysates after induction with IPTG, and purified protein cleaved from GST trap beads for all three PDZ domains. Proteins were detected with HA-tag antibody **B, D, F:** Purified DLG1 PDZ domains were applied to PDZ ligand microarrays to probe for interaction. HA-tag and HRP-coupled antibodies were used to detect bound PDZ domains.

We conducted five independent trials for PDZ2 domain and defined positive hits as chemiluminescence signals larger than background + 2x standard deviation. The background was calculated as median chemiluminescence signal from a row of empty spots on the array. We considered all proteins meeting this criteria in at least 3 independent experiments as interaction partners for DLG1.

We identified 22 interaction partners for DLG1 PDZ2 domain, a complete list for all positive interaction partners can be found in the appendix in tables 5.4 and 5.5. 50% of identified hits were vomeronasal receptors. DLG1 PDZ2 domain predominantly interacted with V1 receptors (9 V1 vs 2 V2). 17 of the 22 identified candidates also interacted with NHERF1. The five unique interaction partners were one V1 receptor, two V2 receptors, potassium large conductance calcium-activated channel Mb4 and PLCβ1 (Tab. 5.4, Tab. 5.5). These results show DLG1 is interacting with vomeronasal receptors and therefore, could influence vomeronasal signaling.

The majority of hits possessed either a Class II (8/22) or a Class III (4/22) PDZ motif. Only 2 out of 22 hits contained a Class I (2/22) PDZ motif. Notably, 8 out of 22 hits did not display a PDZ ligand motif. This indicates DLG1 preferred Class II and Class III PDZ ligands over class I ligands but is also able to interact with non-canonical PDZ ligands.

Moreover, we observed DLG1 PDZ2 domain tended to interact with several proteins known to influence signal transduction (Francia et al., 2014). Each of $G_{\alpha o}$, phosphodiesterase 2A, carbon anhydrase 2 and PLCγ1 were identified 2 out of 3 experiments. Interestingly, also NHERF1 C-terminus was found to interact in 2 independent experiments with PDZ2 domain from DLG1. Therefore, DLG1 could possibly interacts with further signaling proteins and even scaffolding protein NHERF1.

This data provides a list of potential DLG1 interaction partners for the vomeronasal organ. The identified interactions between DLG1 and vomeronasal receptors support our hypothesis of DLG1 influencing vomeronasal signal transduction. In addition, the tendency to interact with scaffolding protein NHERF1 raises the possibility of DLG1 functioning as hub in a signaling complex.

4.5 Several Phospholipase C enzymes are expressed in the vomeronasal organ

In general, vomeronasal signal transduction is believed to work in the following way: Activation of vomeronasal receptors lead to elevation of intracellular calcium and subsequent opening of TrpC2 cation channel. The rise in intracellular calcium is possibly mediated by second messenger molecules IP3 and DAG, which are generated by PLC enzymes (Munger et al., 2009).

The molecular identity of the enzymes involved remain elusive, though. Since we identified PLC enzymes interacting with NHERF1 and DLG1, we were curious about which PLC enzymes are exactly expressed in the vomeronasal organ. Therefore, we examined vomeronasal organ microarray data used before to identify PDZ scaffolding proteins, for expression of PLC enzymes (Fig. 4.18).

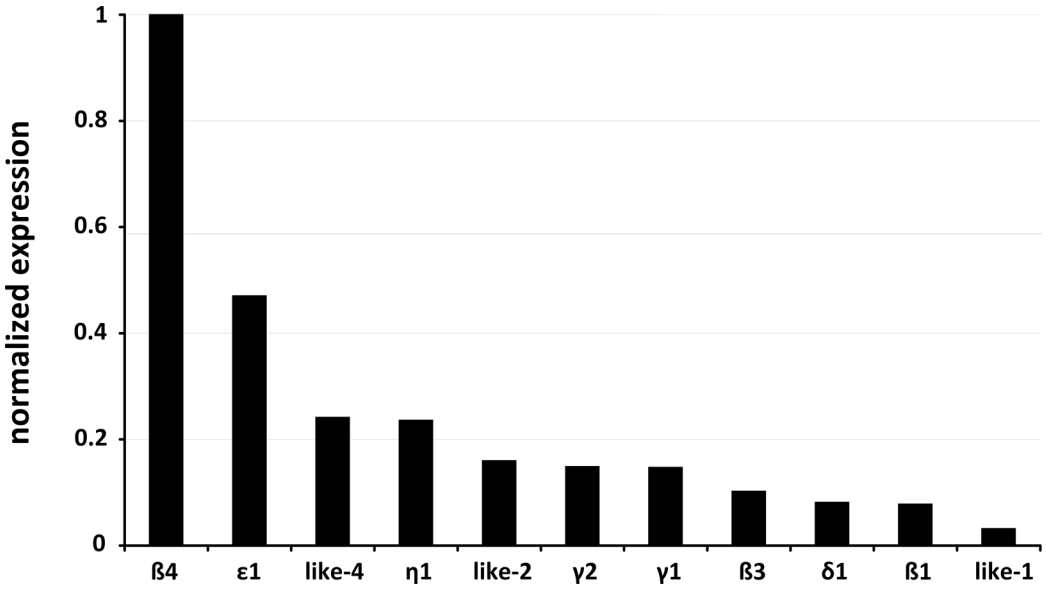

Figure 4.18: Numerous PLC subtypes are expressed in the vomeronasal organ. Expression of PLC subtypes in vomeronasal organ was analyzed on RNA level using data from an mRNA microarray analysis. Results were normalized to the expression level of the most abundant subtype.

We identified PLCη1 as hypothetical candidate for vomeronasal signaling. This PLC isoenzyme features a class II PDZ motif at its C-terminus and we identified PLCη1 as potential NHERF1 interaction partner in our microarray analy-

sis (Tab. 5.3). When G protein-coupled receptors activate other PLC enzymes, PLCη1 enhances their activity through a positive feedback loop (Kim et al., 2011). Since we detected expression of several PLC enzymes in the vomeronasal organ, this concept is conceivable for vomeronasal signaling.

We used RT-PCR to further analyze expression of PLC isotypes we found in the microarray data from vomeronasal organ. We confirmed expression for all isotypes except PLCη1 (Fig. 4.19 A) thus, we hypothesized the observed signal could reflect a false identification of another PLCη subtype. We generated new primer pairs for PLCη1 to rule out simple disfunctionality of the first primers. In addition, we designed primers to identify PLCη2. Also the second PLCη1 primer did not detect PLCη1 expression. Instead, we identified PLCη2 expressed in vomeronasal organ (Fig. 4.19 B). Therefore, PLCη1 microarray signal possibly arose from PLCη2 expression.

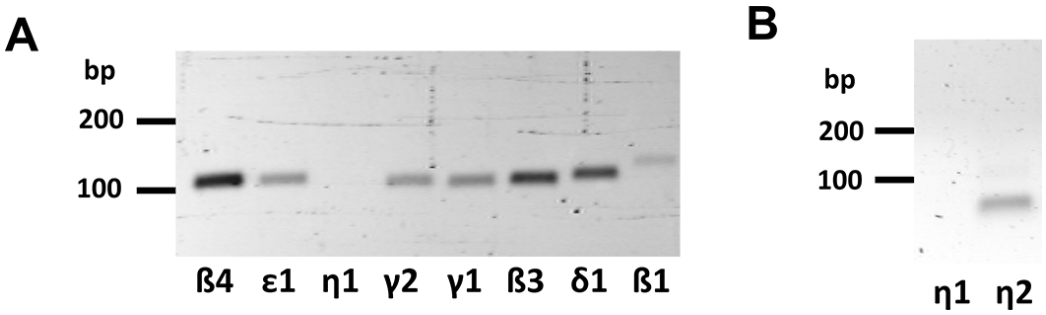

Figure 4.19: RT-PCR analysis of PLC subtypes expressed in the vomeronasal organ. A: Expression of PLC subtypes in vomeronasal organ was verified by RT-PCR using vomeronasal organ cDNA as template. **B:** PLCη2 but not PLCη1 is expressed in vomeronasal organ.

We further focused our analysis on PLCβ enzymes for the following reasons: First, we found the highest expression levels for PLCβ4 in the microarray data (Fig. 4.18). Second, all PLCβ isoforms posses PDZ ligand motif and interact with scaffolding proteins (Kim et al., 2011). Therefore, this PLC isoenzymes could play a part in vomeronasal signaling which is organized through scaffolding proteins. However, three different splice variants of PLCβ4 have been described and only PLCβ4a features a PDZ ligand motif (Adamski et al., 1999; Kim et al., 1998).

Thus, we analyzed expression of PLCβ4 splice variants a, b and c in vomeronasal organ using two splice-variant specific primer pairs (Fig. 4.20). The first

would amplify a 350 bp fragment from PLCβ4a and a 100 bp fragment from PLCβ4b. The second pair would amplify a 110 bp fragment from PLCβ4c. We identified a 350 bp but no 100 bp fragment with the first primer (Fig. 4.20 A). The second primer pair amplified a 110 bp fragment (Fig. 4.20 B). This results showed, PLCβ4a and PLCβ4c, but not PLCβ4b are expressed in the vomeronasal organ. Thus, PDZ ligand PLCβ4a could interact with scaffolding proteins.

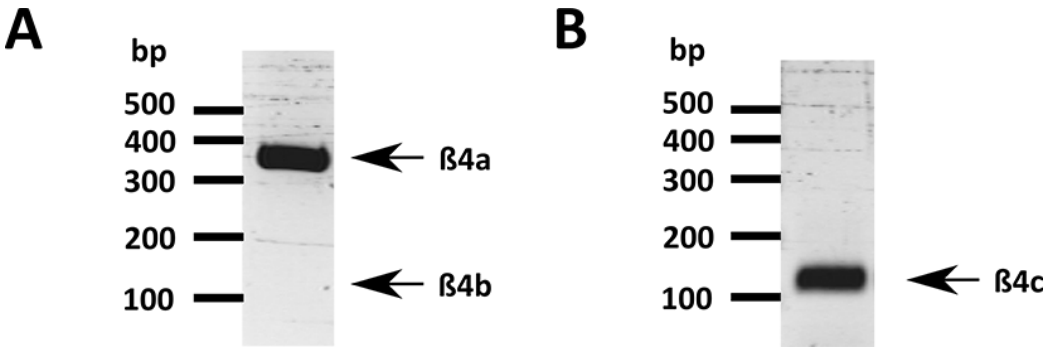

Figure 4.20: PLCβ4a and 4c splice variants are expressed in the vomeronasal organ. Specific primer pairs for different splice variants of PLCβ4 were used to identify variants expressed in the vomeronasal organ. **A:** The first pair amplifies a 350 bp fragment from PLCβ4a and a 100 bp fragment from PLCβ4b. **B:** The second pair amplifies a 110 bp fragment from PLCβ4c.

4.5.1 PLCβ3, but not PLCβ4 is expressed in microvilliar layer of the vomeronasal organ

Our previous investigations on NHERF1 or DLG1 revealed no interaction with PLCβ4. However, PLCβ4 could be regulated by other scaffolding proteins present in the vomeronasal organ (Fig. 4.1). PLCβ4 would need to be expressed in neuronal microvilli to participate in vomeronasal signal transduction. Therefore, we used cryosections from adult vomeronasal organ to localize PLCβ4 protein (Fig. 4.21). We used TrpC2 channel from the vomeronsal signaling cascade to label neuronal microvilli (Liman et al., 1999) and looked for co-localization with PLCβ4.

We found PLCβ4 protein was absent from vomeronasal microvilli but instead was expressed in axons from vomeronasal sensory neurons. This result argues against a significant role of PLCβ4 in vomeronasal signal transduction or interaction with scaffolding proteins in neuronal microvilli.

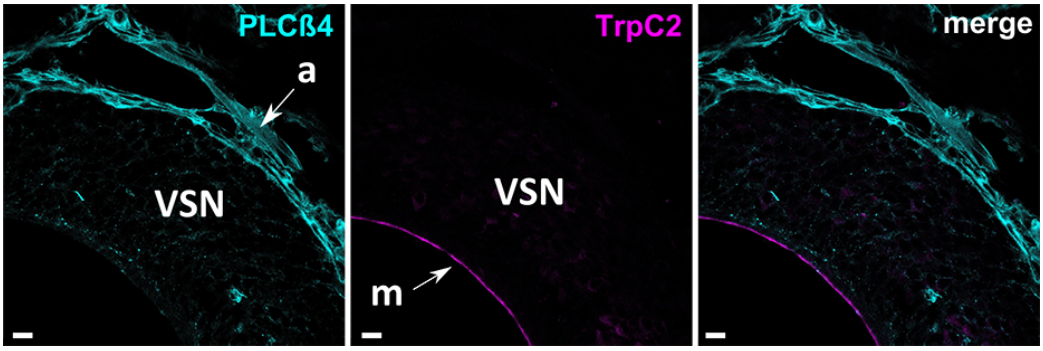

Figure 4.21: PLCβ4 is not expressed in vomeronasal microvilli. cryosections of vomeronasal organ were stained for PLCβ4 protein. Sensory microvilli of VSN were labeled with TrpC2 immunostaining. m = microvillar layer, VSN = vomeronasal sensory neurons, a = vomeronasal neuron axons. Scale bars = 10 µm

We identified expression of another PLCβ enzyme, PLCβ3, in the microarray data. Two splice variants are described and both feature a class I PDZ motif in the C-terminus. Thus, PLCβ3 is a potential PDZ ligand. We explored the localization of PLCβ3 in cryosections of vomeronasal organ and used fluorophore-labled Phalloidin as microvilli marker (Fig. 4.22) (Faulstich et al., 1988). We found PLCβ3 expression was enriched in neuronal microvilli, as indicated by co-localization with Phalloidin. This restricted expression of PLCβ3 might account for a role in signaling processes. Although we did not identify PLCβ3 as NHERF1 or DLG1 interaction partner, the enzyme could interact with other scaffolding proteins in neuronal microvilli.

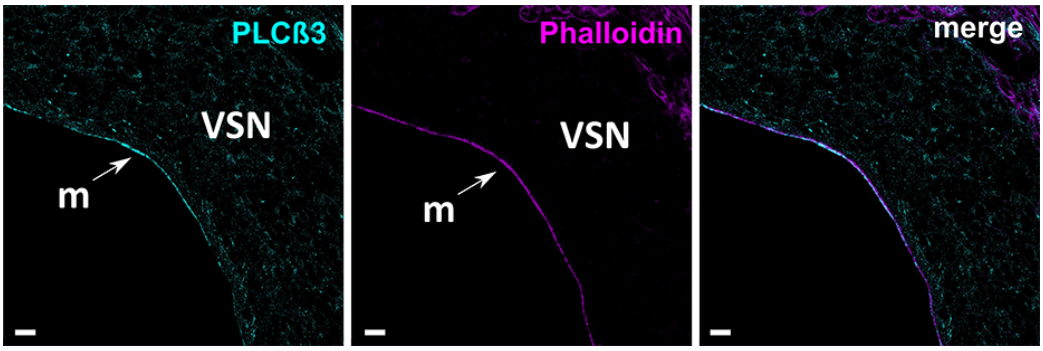

Figure 4.22: PLCβ3 localizes to vomeronasal microvilli. cryosections of vomeronasal organ were stained for PLCβ3 protein. Microvilli were labeled with fluorophore-labled Phalloidin. m = microvillar layer, VSN = vomeronasal sensory neurons. Scale bars 10 µm

4.6 The role of Anoctamins in olfactory systems

Calcium-gated chloride channels have been described as an elementary part of olfactory receptor current in the main olfactory epithelium as in vomeronasal organ (Kim et al., 2011; Kleene, 2008). Anoctamin 2 is the calcium-gated chloride conductance in the main olfactory epithelium (MOE) (Rasche et al., 2010; Stephan et al., 2009). Anoctamins are also present in the vomeronasal organ (Billig et al., 2011; Rasche et al., 2010) and calcium-gated chloride currents take part in vomeronasal signal transduction (Kim et al., 2011). The molecular identity of the calcium-gated chloride conductance remains elusive, though.

We addressed the question, which (additional) Anoctamin proteins are expressed in the main olfactory epithelium and the vomeronasal organ. Therefore, we employed deep sequencing data from vomeronasal organ (*in collaboration with M. Spehr, RWTH Aachen*) and from olfactory epithelium (*now in revision as Kanageswaran et al., 2014*) to screen for Anoctamin expression in both systems (Fig. 4.23).

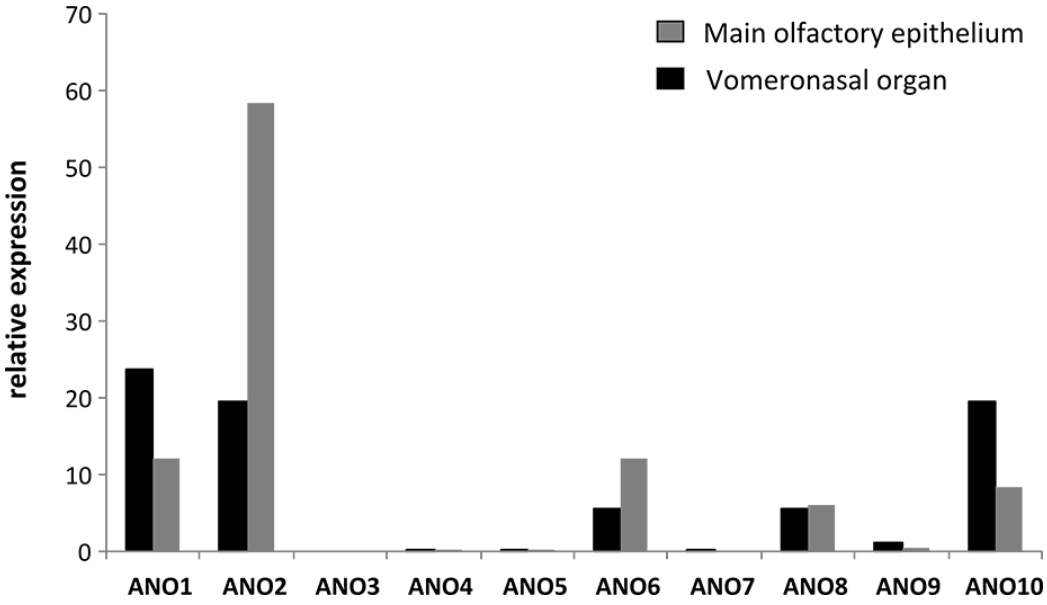

Figure 4.23: ANO1, ANO2 and ANO6 are expressed in the main olfactory epithelium and vomeronasal organ. Deep sequencing data from vomeronasal organ and main olfactory epithelium were analyzed for expression of Anoctamin family members.

We found Anoctamin 2 was the most abundant member in the main olfac-

tory epithelium but was also expressed in the vomeronasal organ, which confirmed data from Rasche et al. (2010). We also found Anoctamin 1, Anoctamin 6, Anoctamin 8 and Anoctamin 10 expression in both systems. It is not certain if Anoctamin 8 and Anoctamin 10 proteins form functional ion channels at the plasma membrane. They do not display membrane localization but remain cytosolic, if expressed in heterologous cell systems . This renders them inappropriate for direct signal transduction processes (Tian et al., 2012). This work explored Anoctamins as part of olfactory signal transduction in the vomeronasal system and the main olfactory epithelium. Therefore, we focused on Anoctamin 1 (ANO1), Anoctamin 2 (ANO2) and Anoctamin 6 (ANO6).

4.6.1 Anoctamin 2 and Anoctamin 6 are expressed in the main olfactory epithelium, but not Anoctamin 1

We used acetylated tubulin (AcTub) as a marker for cilia from olfactory sensory neurons and stained cryosections of adult olfactory epithelium (Wloga & Gaertig, 2010). We probed for co-localization of ANO1, ANO2 and ANO6 with acetylated tubulin and confirmed ciliary expression for ANO2 as described in Billig et al. (2011); Rasche et al. (2010) (Fig. 4.24 A). We also identified ciliary expression of ANO6 (Fig. 4.24 B). ANO1 was not expressed in olfactory cilia, as also reported by Billig et al. (2011) (Fig. 4.24 C). These findings confirm the role of ANO2 in olfactory signal transduction and rule out involvement of ANO1. Additionally, the data raises the possibility of ANO6 taking part in olfactory signal transduction in olfactory cilia.

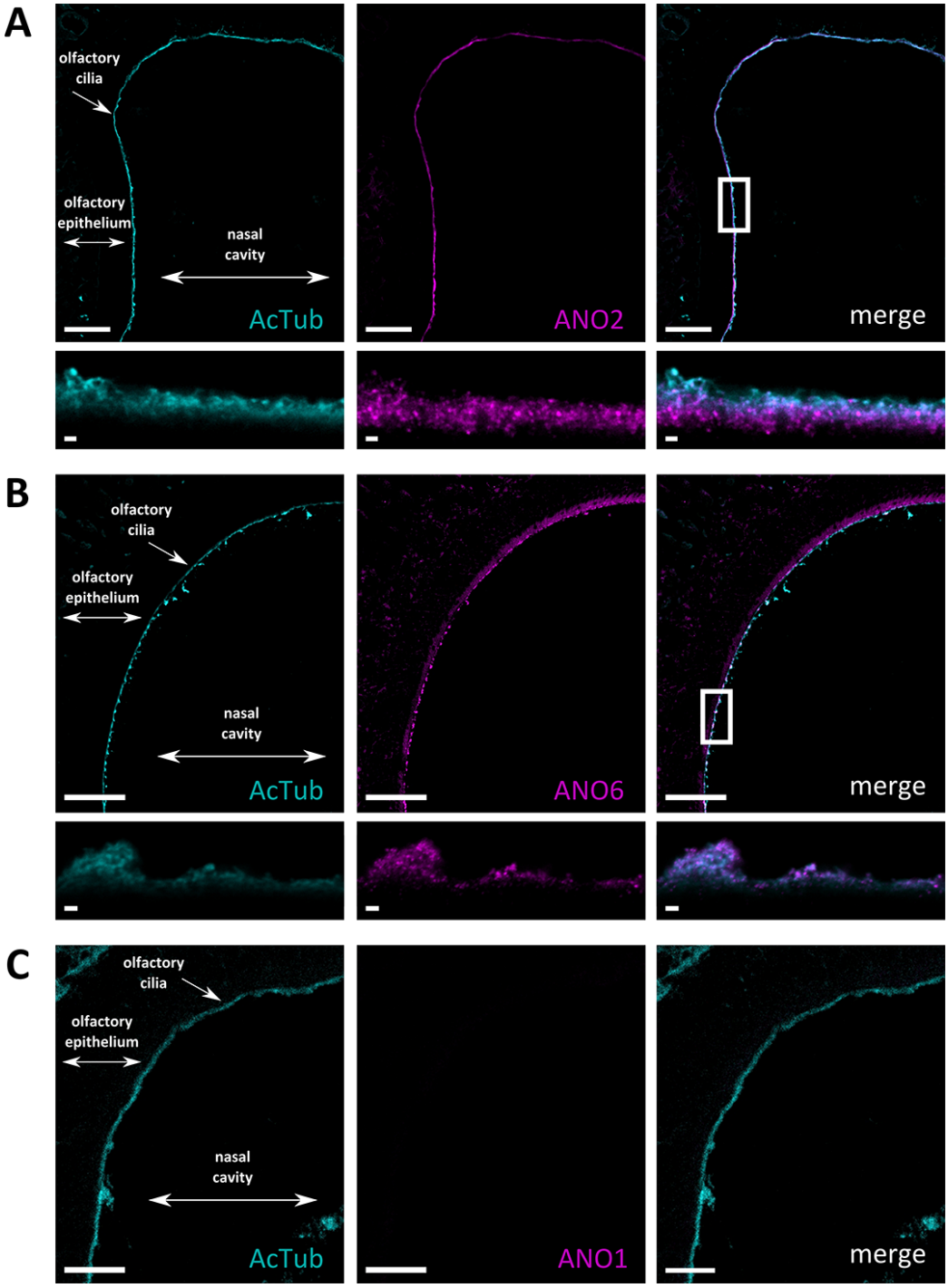

Figure 4.24: ANO2, ANO6 are expressed in olfactory cilia, but not ANO1. Cryosections of the adult olfactory epithelium were stained for **A:** ANO2, **B:** ANO6 and **C:** ANO1 expression. Acetylated tubulin was used as a marker for olfactory cilia. Large overview images illustrate labeled structures of the olfactory epithelium. Box exemplifies the magnified area. Small images show the according ciliary layer in detail. Scale bars: Overview = 75 µm, Detail = 1 µm

4.6.2 Olfactory signaling protein CNG localizes to segregated microdomains in olfactory cilia

We noticed heterogeneous distribution of Anoctamin proteins in olfactory cilia compared to acetylated tubulin staining (Fig. 4.24). That is why we hypothesized about the organization of olfactory signaling proteins in signaling microdomains. There is no optical evidence for signaling microdomains in the olfactory system available, since the size of spatially segregated microdomains is below the resolution limit of conventional light microscopy (Hensel et al., 2013). Therefore, we used dual color STED microscopy, to investigate the subcellular organization of signaling proteins in olfactory cilia in super-resolution. We tested our hypothesis by imaging a well established part of the olfactory signaling cascade, the olfactory CNG channel (Zheng & Zagotta, 2004).

We started with staining cryosections of adult main olfactory epithelium for CNG channel together with acetylated tubulin as ciliary marker (Fig. 4.25). We confirmed localization of CNG channel in olfactory cilia (Fig. 4.25 A). Super-resolution images of the ciliary layer revealed CNG channels were organized in distinct microdomains around the tubulin core (Fig. 4.25 B). Heterogeneous distribution of CNG channels in the ciliary membrane argues for the presence an organizing element. Otherwise, diffusion would distribute CNG channels evenly inside the ciliary membrane. Therefore, microdomain organization of olfactory signaling proteins in olfactory cilia is possible.

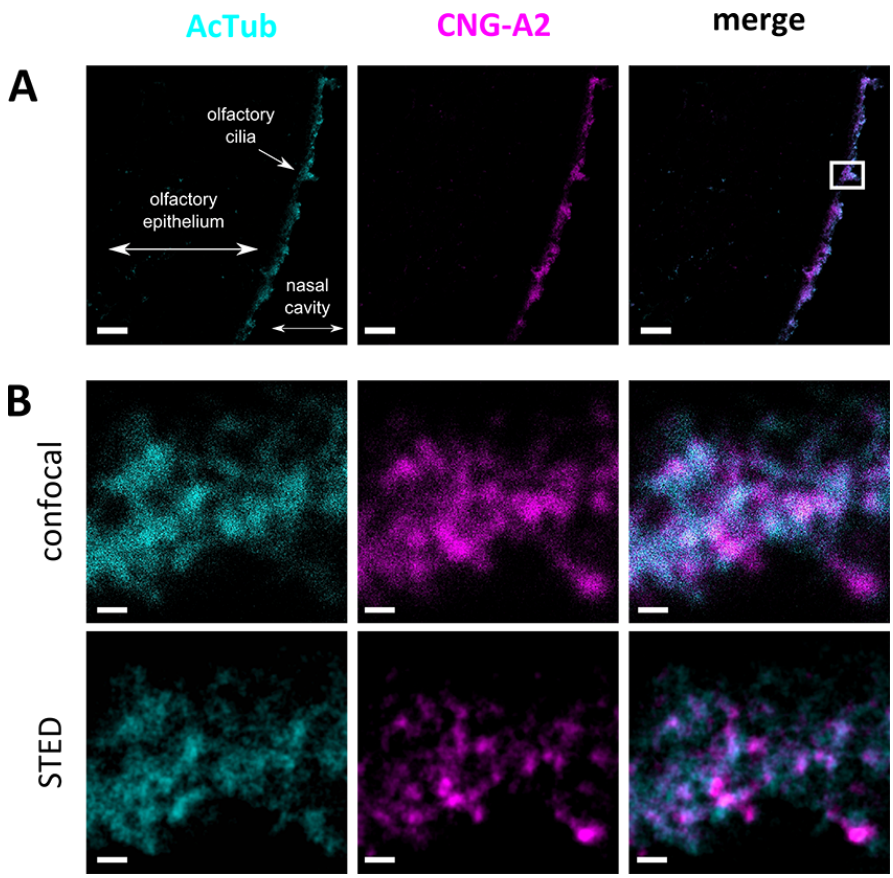

Figure 4.25: CNG channel forms microdomains in olfactory cilia around the tubulin core. A: Cryosections of olfactory epithelium were stained for olfactory CNG channel, using antibodies against the A2 subunit. Acetylated tubulin is used as ciliary marker. Overview pictures illustrate labeled structures and boxed area exemplifies magnification of ciliary layer. **B:** High magnification images of the ciliary layer, showing conventional confocal images (upper row) vs. super-resolution (lower row). Scale bars: A = 5 µm, B = 500 nm

4.6.3 Anoctamins appear in segregated microdomains in olfactory cilia

We next used super-resolution microscopy to analyze the organization of ANO2 and ANO6 in the ciliary layer. We started with analyzing ANO2 organization, since ANO2 is also an established part of the olfactory signaling cascade (Billig et al., 2011). We stained cryosections of olfactory epithelium for ANO2 together with acetylated tubulin and imaged the ciliary layer (Fig. 4.26 A).

ANO2 mimicked the appearance of CNG channel expression. We found ANO2

also organized in segregated microdomains around the tubulin core (Fig. 4.26 A). The same results could be shown for ANO6, as we stained olfactory epithelium sections for ANO6 together with acetylated tubulin (Fig. 4.26 B). Both Anoctamins resembled the organization of CNG channel protein. They formed spatially segregated microdomains around the tubulin core. The organization of ANO6 points out that this calcium-gated chloride channel could also participate in olfactory signal transduction. Therefore, two Anoctamin proteins potentially mediate calcium-gated chloride currents in olfactory cilia.

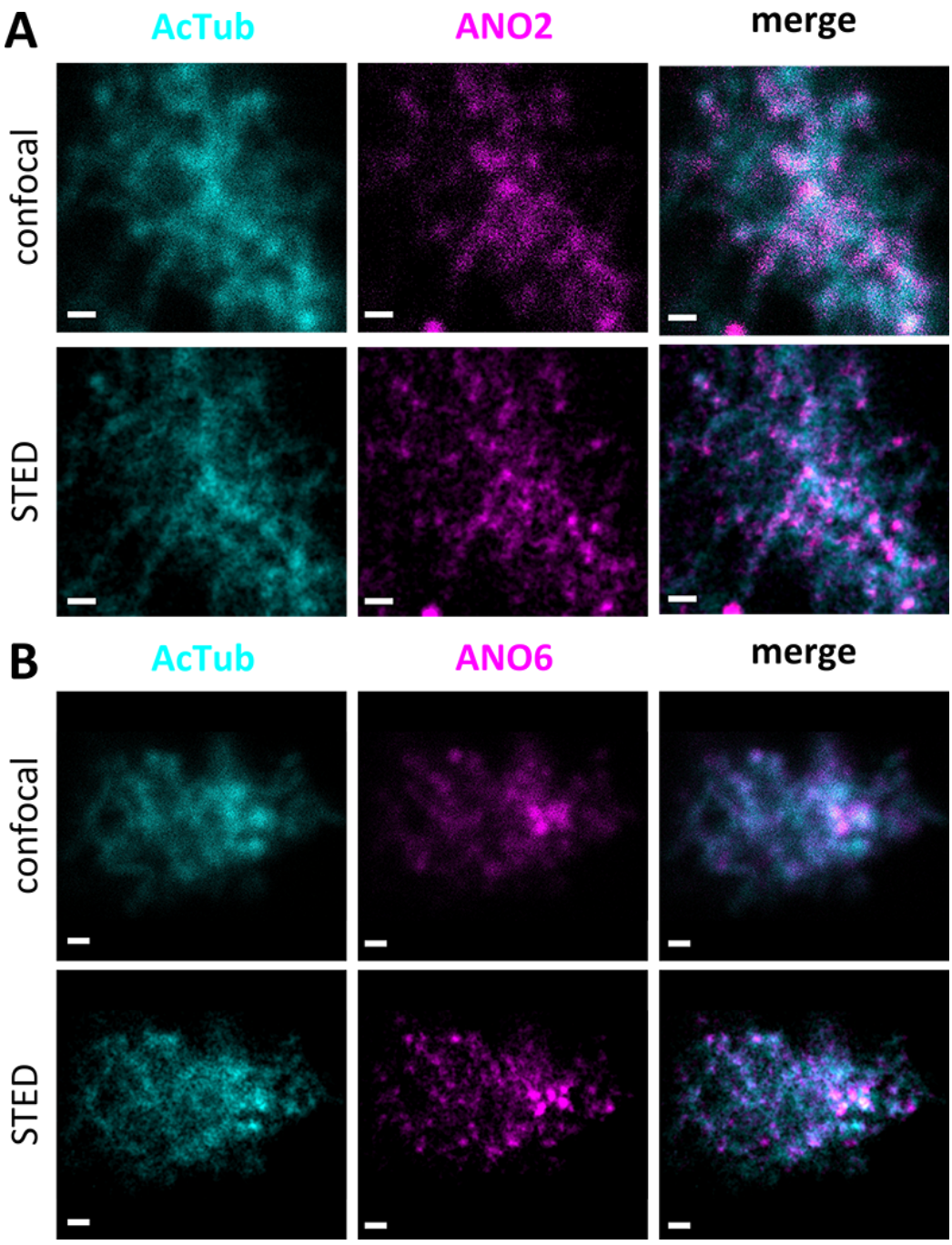

Figure 4.26: ANO2 and ANO6 form segregated microdomains around the tubulin core in olfactory cilia. High magnification images of ciliary layer stained for acetylated tubulin together with **A:** ANO2 and **B:** ANO6. Upper rows show conventional confocal images, lower rows show identical images in super-resolution. Scale bars = 500 nm

Intrigued by the finding of both Anoctamins organized in segregated microdomains, we examined whether ANO2 and ANO6 were present in the same microdomains. We used the dual color STED technique and stained cryosections of olfactory epithelium for ANO2 in combination with ANO6.

Since both Anoctamin antibodies were generated in rabbit, we had to adapt our staining protocol. First, we detected ANO6 as usual with secondary antibody Oregon 488. Afterwards, we blocked remaining rabbit FC regions from ANO6 antibody with anti-rabbit Fab fragments. Next, we applied ANO2 antibody and detected with V500.

We conducted two control experiments with omitted ANO2 or ANO6 antibodies, to ensure no cross-labeling with secondary antibodies occurred. These experiments provided the following findings. First, we demonstrated that saturation of ANO6 FC regions with anti-rabbit FAB fragments was sufficient. No anti-rabbit V500 bound to ANO6 antibodies and showed up in the ANO2-channel (Fig. 4.27 upper left). Second, we guaranteed no leftover anti-rabbit Oregon 488 bound to ANO2 antibodies, as we detected no Oregon 488 signal if ANO6 antibody was omitted (Fig. 4.27 lower right). In this way, we were able to label both Anoctamins without cross-talk from secondary antibodies.

We also showed blocking of ANO6 FC regions did not interfere with ANO2 staining. V500-labeled ANO2 was also detected if sections were incubated with anti-rabbit Fab fragments without ANO6 antibody (Fig. 4.27 lower left). Therefore, unbound Fab fragments did not interfere with subsequent ANO2 detection.

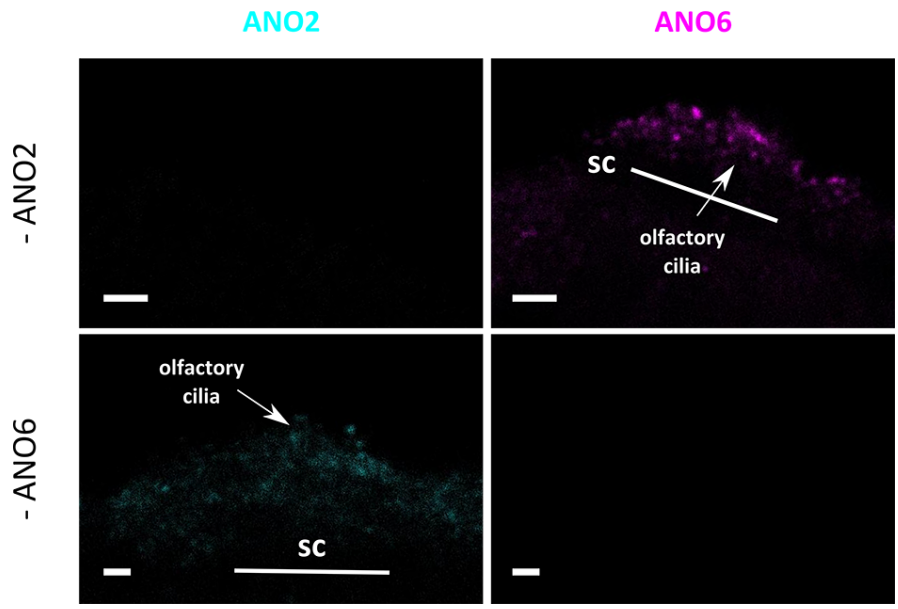

Figure 4.27: Dual color STED controls for staining with primary antibodies from the same host species. Olfactory cilia stained with ANO2 or ANO6 antibodies, both generated in rabbit. Upper row shows omitted ANO2 antibody images. Lower row displays omitted ANO6 antibody images. Image settings were kept identical and used in co-stainings with both antibodies. sc = supporting cell layer - indicated by line. Scale bars = 2µm

After we demonstrated the possibility to label ANO2 and ANO6 antibodies without cross-talk, we imaged the ciliary layer in super-resolution (Fig. 4.28). We found both proteins localized to segregated microdomains in the ciliary layer. Furthermore, we identified several ANO2 and ANO6 microdomains are co-localizing (arrows). Thus, we detected co-expression of ANO2 and ANO6 in the same microdomains, which supports the idea of ANO6 taking part in olfactory signal transduction.

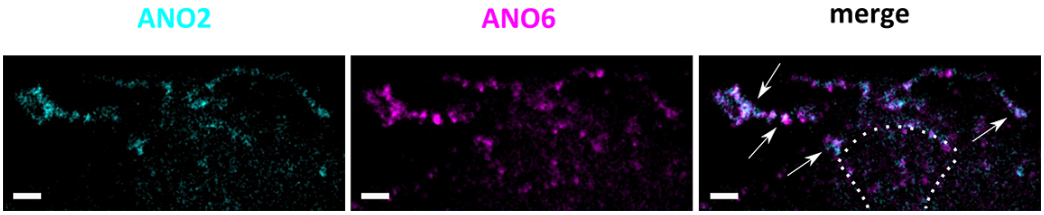

Figure 4.28: ANO2 and ANO6 are expressed in the same microdomains in olfactory cilia. STED images of olfactory cilia stained for ANO2 and ANO6 in cryosections. Dotted line indicates dendritic knob of a single olfactory sensory neuron. Arrows point to co-localization of ANO2 and ANO6 in the same microdomains. Scale bars: = 1µm

We demonstrated both Anoctmins were co-localized in the same microdomains. That led us to hypothesize about a possible direct interaction of ANO2 and ANO6. Sheridan et al. (2011) has shown that ANO1 is forming homo-dimers and Tien et al. (2013) has mapped the dimerization domain for ANO1 inside the N-terminus. Thus, we deemed hetero-dimer formation between ANO2 and ANO6 possible. But if ANO2 and ANO6 interact with each other, wouldn't we expect full co-localization even in super-resolution?

We sought to answer this question by co-staining two different subunits of the same protein and compare these findings to ANO2-ANO6 co-staining. The olfactory CNG channel consists of four individual subunits, two CNG-A2 subunits, one CNG-B1 and one CNG-A4 subunit. These four subunits form one functional channel inside the ciliary membrane and are in direct physical contact with each other (Trudeau & Zagotta, 2003).

Therefore, we stained cryosections of olfactory epithelium for CNG-A2 together with CNG-A4 and imaged the ciliary layer (Fig. 4.29). We found labeling of the two subunits did not completely co-localize in super-resolution. Like ANO2 and ANO6 co-staining, staining for both CNG channel subunits displayed partially overlapping areas. This result argues against a complete co-localization in super-resolution images even for proteins in physical contact with each other. Thus, the possibility of ANO2 and ANO6 forming one complex in olfactory microdomains may be correct.

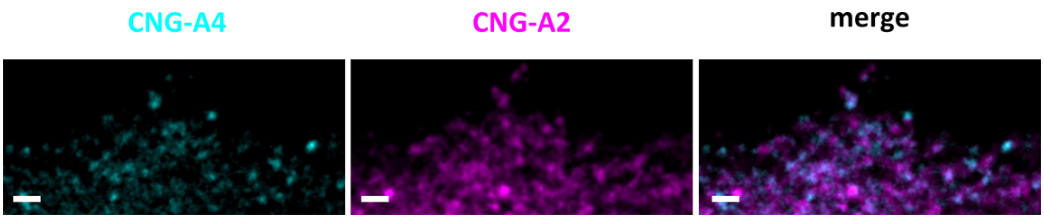

Figure 4.29: Subunits A4 and A2 of olfactory CNG channel do not overlap completly in super-resolution images. STED images of olfactory cilia stained for olfactory CNG channel subunits A4 and A2 in cryosections. Scale bars = 1µm

We identified three different proteins from olfactory cilia were organized in spatially segregated microdomains around the tubulin core. Two of these proteins appeared to be localized to the same microdomains. That is why, we further analyzed the characteristic of the identified microdomains. We counted

the number of microdomains for ANO2, ANO6 and CNG-A2 in a defined area of ciliary layer. Three individual animals for each protein were analyzed (Fig. 4.30 A). We analyzed 78 single counting for ANO2, 57 for ANO6 and 73 for CNG-A2. Every single count comprised an area of 5 μm^2 ciliary layer. The complete area was summed up from these counting to a total area of 285 μm^2. We found 4.99 $\pm$ 0.12 ANO2, 2.71 $\pm$ 0.09 ANO6 and 2.88 $\pm$ 0.07 CNG-A2 microdomains per μm^2. This analysis showed that significantly more ANO2 microdomains are present in olfacotry cilia.

Next, we measured the mean diameter of microdomains from ANO2, ANO6 and CNG-A2. We analyzed around 200 microdomains for each protein in three individual animals. We recognized all three proteins aggregate into clusters of the same size (Fig. 4.30 B). The mean diameter of ANO2 domains was 127 nm $\pm$ 36 nm. ANO6 were measured with 132 nm $\pm$ 34 nm and and CNG-A2 domains with 111 nm $\pm$ 33 nm.

In this analysis with three different antibodies we demonstrated comparable characteristics for microdomains in olfactory cilia. In combination with co-localization of ANO2 and ANO6, this data provides further evidence for a possible role of ANO6 in olfactory signal transduction. Although the amount of ANO2 and ANO6 microdomains differed significantly, their size was identical. Therefore, multiple ANO2 microdomains could also include ANO6.

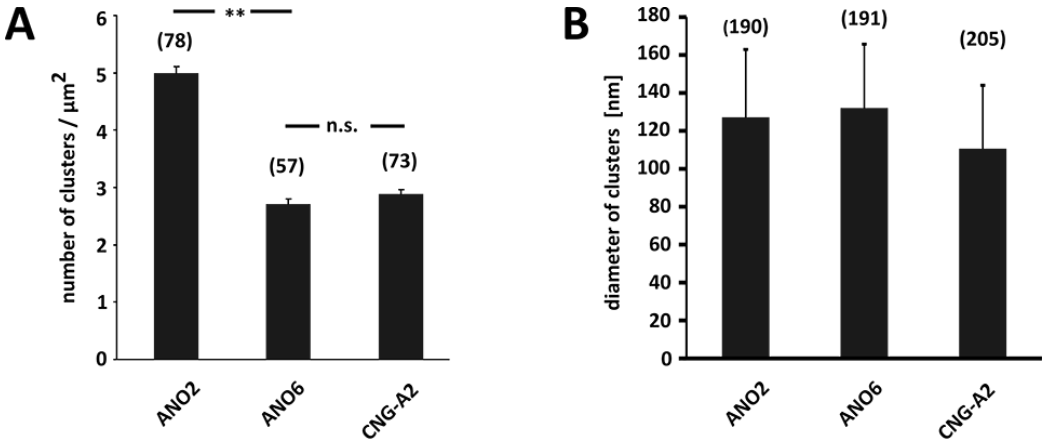

Figure 4.30: ANO2, ANO6 and CNG-A2 microdomains are comparable in frequency and size. A: Average amount of clusters found in 1 µm^2 of ciliary layer. Error bars represent SEM. Three individual animals were analyzed. Total number of single counting displayed in brackets. Student's t-test was used to compare ANO2 vs. ANO6, p = 0,003 and ANO6 vs. CNG-A2 p = 0.66 **B:** Mean diameter of clusters from ANO2, ANO6 and CNG-A2. Error bars represent SD. Three individual animals were analyzed. Total number of measured clusters for each protein in brackets. Student's t-test was used to compare Anoctamins and CNG-A2 cluster diameters, ANO2 vs. ANO6, p = 0.82, ANO2 vs. CNG-A2, p = 0.37, ANO6 vs. CNG-A2, p = 0.27.

4.6.4 Anoctamin 1 and Anoctamin 2 are expressed in the vomeronasal organ, but not Anoctamin 6

We found two of the three expressed Anoctamins from main olfactory epithelium localized to olfactory cilia and we detected ANO1, ANO2 and ANO6 expression also in vomeronasal organ on RNA level (Fig. 4.23). The relevance of a calcium-gated chloride conductance for efficient vomeronasal signaling is documented (Kim et al., 2011). Therefore, we wanted to know if any of these Anoctamins could possibly mediate the calcium-gated chloride currents in vomeronasal signal transduction. Thus, we analyzed the localization of ANO1, ANO2 and ANO6 proteins also in vomeronasal organ cryosections.

We labeled vomeronasal neurons with mature olfactory neuron marker OMP and looked for co-localization of Anoctamin proteins in neuronal microvilli (Fig. 4.31). We found ANO1 and ANO2, but not ANO6 expression in neuronal microvilli (Fig. 4.31). Since ANO2 is the major component of chloride conductance in the main olfacotry epithelium, these findings indicated a potential role for ANO2 and / or ANO1 also in vomeronasal signaling. Furthermore, the results ruled

out participation of ANO6 in vomeronasal signaling, since it is not expressed in neuronal microvilli.

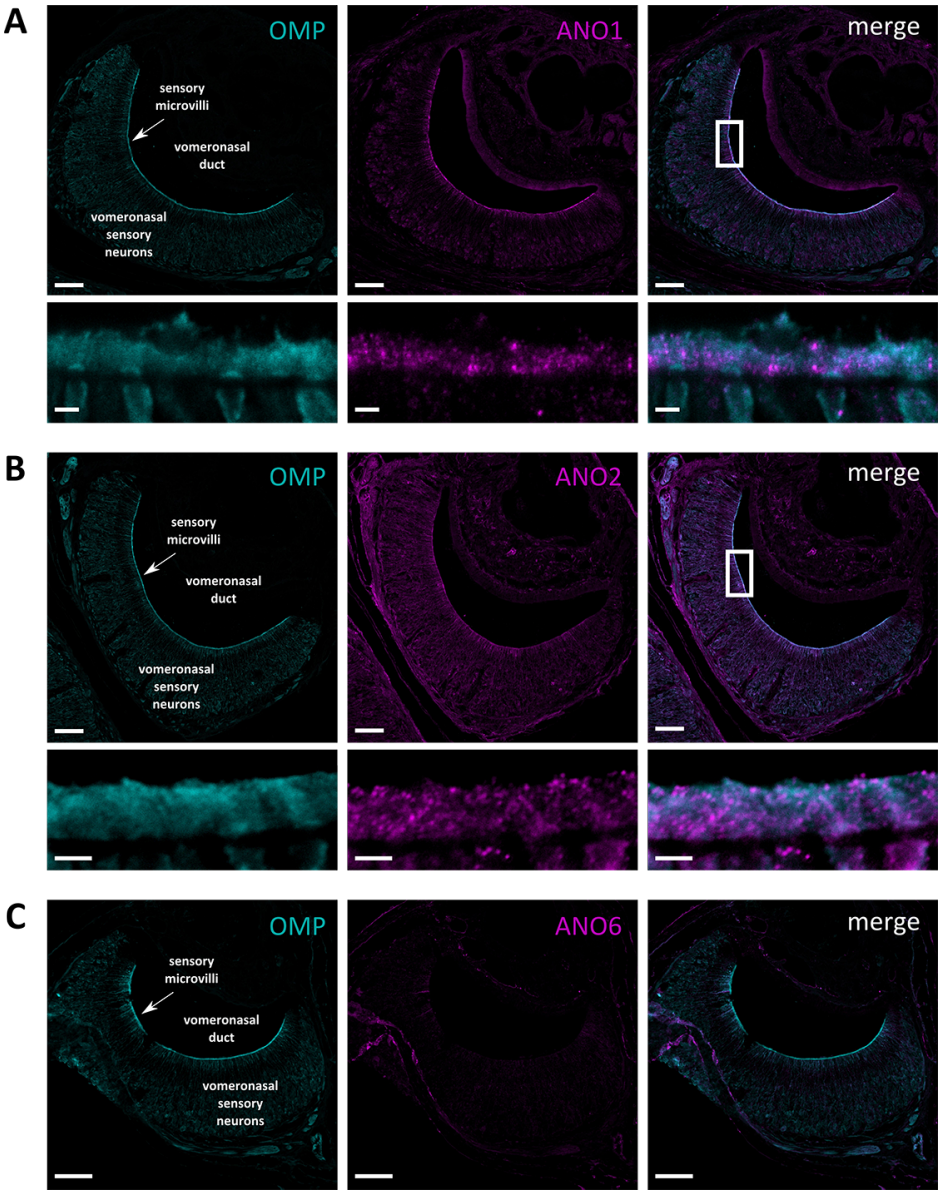

Figure 4.31: ANO1 and ANO2 are expressed in neuronal microvilli, but not ANO6. Cryosections of the vomeronasal organ were stained for **A:** ANO1, **B:** ANO2 and **C:** ANO6. OMP was used as a marker for vomeronasal neurons. Large overview images with labeled structures illustrate orientation, small images show the according microvillar layer in detail. Scale bars: Overviews = 75 µm, Detail = 1 µm

4.6.5 Anoctamins localize to segregated microdomains in neuronal microvilli

We found olfactory signaling proteins CNG and ANO2 were expressed in spatially segregated microdomains in olfactory cilia (Fig. 4.25, 4.26). Moreover, vomeronsal signaling protein $G_{\alpha i2}$ was also expressed in segregated domains in neuronal microvilli (Fig. 4.7). That is why, we hypothesized, if ANO1 or ANO2 participate in vomeronasal signal transduction both proteins may also be organized in segregated microdomains in neuronal microvilli. Therefore, we analyzed subcellular organization of ANO1 and ANO2 and investigated for co-localization within $G_{\alpha i2}$ microdomains.

We stained cryosections of adult vomeronasal organ for $G_{\alpha i2}$ together with ANO1 or ANO2 and imaged the microvillar layer (Fig. 4.32). Super-resolution microscopy revealed expression of both Anoctamins was focused in segregated microdomains (Fig. 4.32). Furthermore, these microdomains partially co-localized with $G_{\alpha i2}$ microdomains (arrows). This showed, Anoctamins in the vomeronasal organ display an expression pattern comparable to other signaling proteins and the results resembled findings from the main olfactory epithelium. In addition, single Anoctamin microdomains co-localized with signaling protein $G_{\alpha i2}$. Therefore, microdomain organization of Anoctamin proteins and co-localization with $G_{\alpha i2}$ support a possible role of ANO1 and ANO2 in vomeronasal signaling.

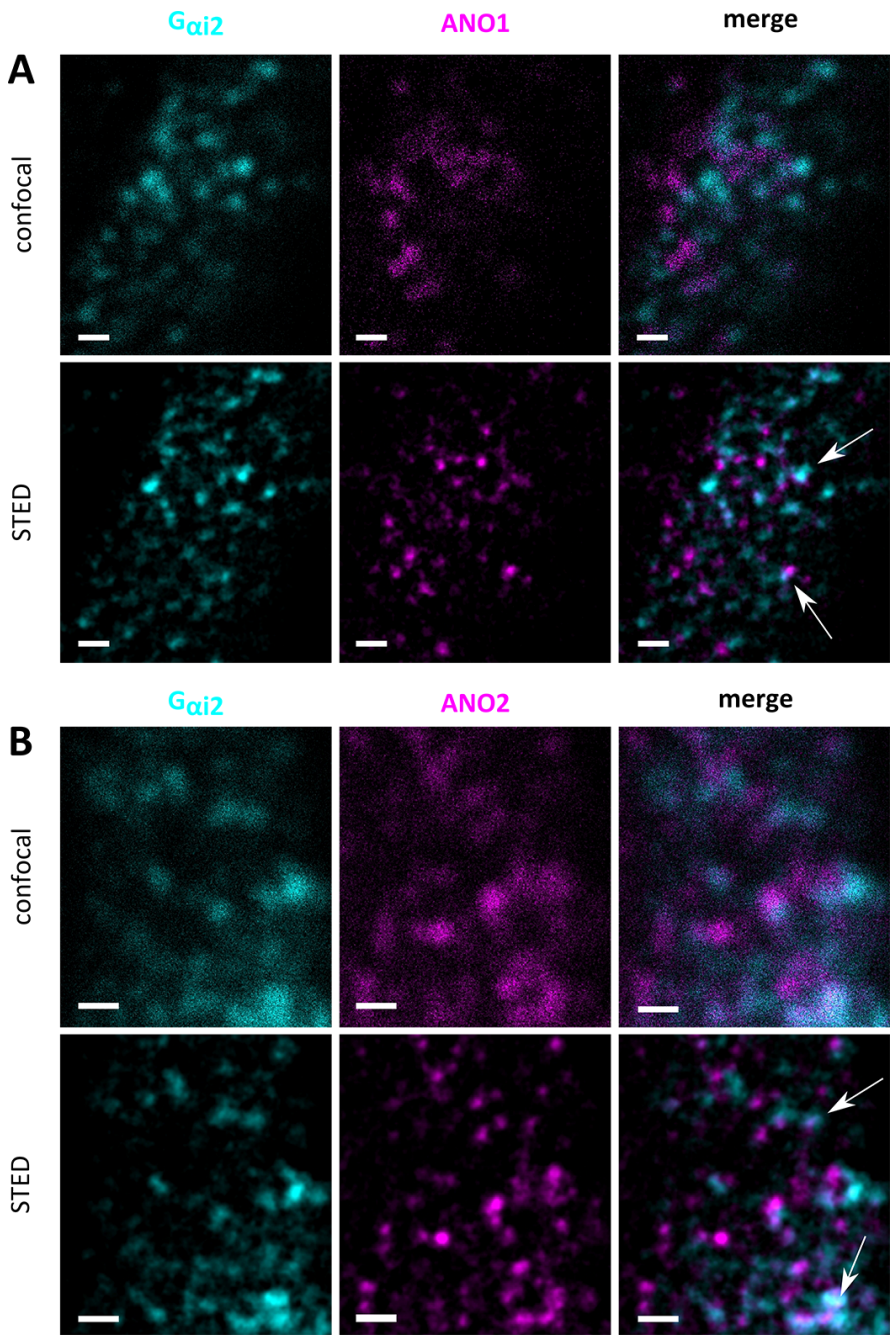

Figure 4.32: ANO1 and ANO2 form segregated microdomains with $G_{\alpha i2}$ in neuronal microvilli. High magnification images of microvillar layer stained for signaling protein $G_{\alpha i2}$ together with (**A**) ANO1 and (**B**) ANO2. Upper rows show conventional confocal images, lowers row the same images in super-resolution. Arrows point at co-localization of both proteins. Scale bars: = 500 nm

4.7 Electrophysiological effects of Anoctamin co-expression

We identified ANO2 expression with either ANO6 or ANO1 in olfactory cilia or the neuronal microvilli, respectively (Fig. 4.24, 4.31). In addition, we demonstrated expression of Anoctamins in spatially segregated microdomains in both olfactory systems (Fig. 4.26, 4.32). Furthermore, we showed ANO2 and ANO6 are co-localized in the same microdomains (Fig. 4.28).

Both ANO1 and ANO2 are described as *bona fide* calcium-gated chloride channels (Kunzelmann et al., 2011; Schroeder et al., 2008). However, the functions of ANO6 are currently under debate (Kunzelmann et al., 2014). Nonetheless, the fact that ANO6 expression gives rise to a chloride channel conductance is supported through several studies (Grubb et al., 2013; Kmit et al., 2013; Martins et al., 2011). Therefore, all three Anoctamins, ANO1 and ANO2 in the vomeronasal organ and ANO2 and ANO6 in the main olfactory epithelium possibly contribute to olfactory signal transduction in their respective system.

We engaged in a collaboration with M. Spehr‘s lab from RWTH Aachen to analyze the physiological relevance of co-expressing two Anoctamins in the same cell compartment, since they are specialized in olfactory electrophysiology. Daniela Drose and Tobias Ackels from RWTH Aachen characterized the electrophysiological properties of co-expressed Anoctamins in HEK293 cells and provided the presented data and figures.

4.7.1 Co-expression of different Anoctamins alters current densities

We verified calcium-gated chloride conductance of ANO1 and ANO2 and showed calcium-gated chloride currents elicited upon ANO6 expression. Thereby, we demonstrated that the expression system is suitable to analyze the effect of co-expressing of two Anoctamins. (Drose, 2013). We further addressed the question whether co-expression of Anoctamin combinations found in the olfactory systems (ANO1 + ANO2 in vomeronasal organ, ANO2 + ANO6 in main olfactory

epithelium) has any effect on calcium-gated chloride currents. We co-transfected HEK293 cells with vectors coding for ANO1 and ANO2 and characterized the measured currents (Fig. 4.33).

The channels were activated by a rise in intracellular calcium through stimulation with ATP. In whole-cell voltage-clamp recordings at constant holding potential (V_{hold} = -80 mV), we observed robust negative currents in response to ATP (Fig. 4.33 B). We performed voltage ramp recordings from -100 mV to +100 mV at 500 ms duration with different extracellular solutions. The current reversed under symmetrical chloride concentrations around 0 mV. Substitution of external chloride with gluconate shifted the reversal potential in a positive direction. Application of the well-described chloride channel blocker niflumic acid (NFA) (Kirkup et al., 1996) severely attenuated the measured current (Fig. 4.33 C). We further performed calcium imaging to determine EC_{50} value for intracellular calcium necessary to activate the chloride channel. Therefore, we stimulated cells with different ATP concentrations and monitored intracellular calcium levels. In a corresponding set of experiments, we measured chloride currents to create a dose-response relationship between intracellular calcium concentration and relative elicited currents (Fig. 4.33 D). The average current densities were calculated at -80 mV and +80 mV, to quantify measured currents (Fig. 4.33 E) (Tab 4.1).

Table 4.1: ANO2 + ANO1 current densities

Condition	**-80 mV [pA/pF]**	**+80 mV [pA/pF]**
Symmetric Cl^-	-30.28 $\pm$ 6.96	19.89 $\pm$ 6.95
Reduced Cl^-	-37.85 $\pm$ 6.87	0.74 $\pm$ 3.10
NFA	1.51 $\pm$ 0.31	-2.68 $\pm$ 0.57

ANO1 + ANO2 transfections elicited calcium-gated chloride currents comparable to singular expression of both Anoctamins, albeit with intermediate current densities (Fig. 4.33 C, D) & (Drose, 2013). Therefore, the combination of

ANO1 and ANO2 could function as calcium-gated chloride channel in vomeronasal signaling.

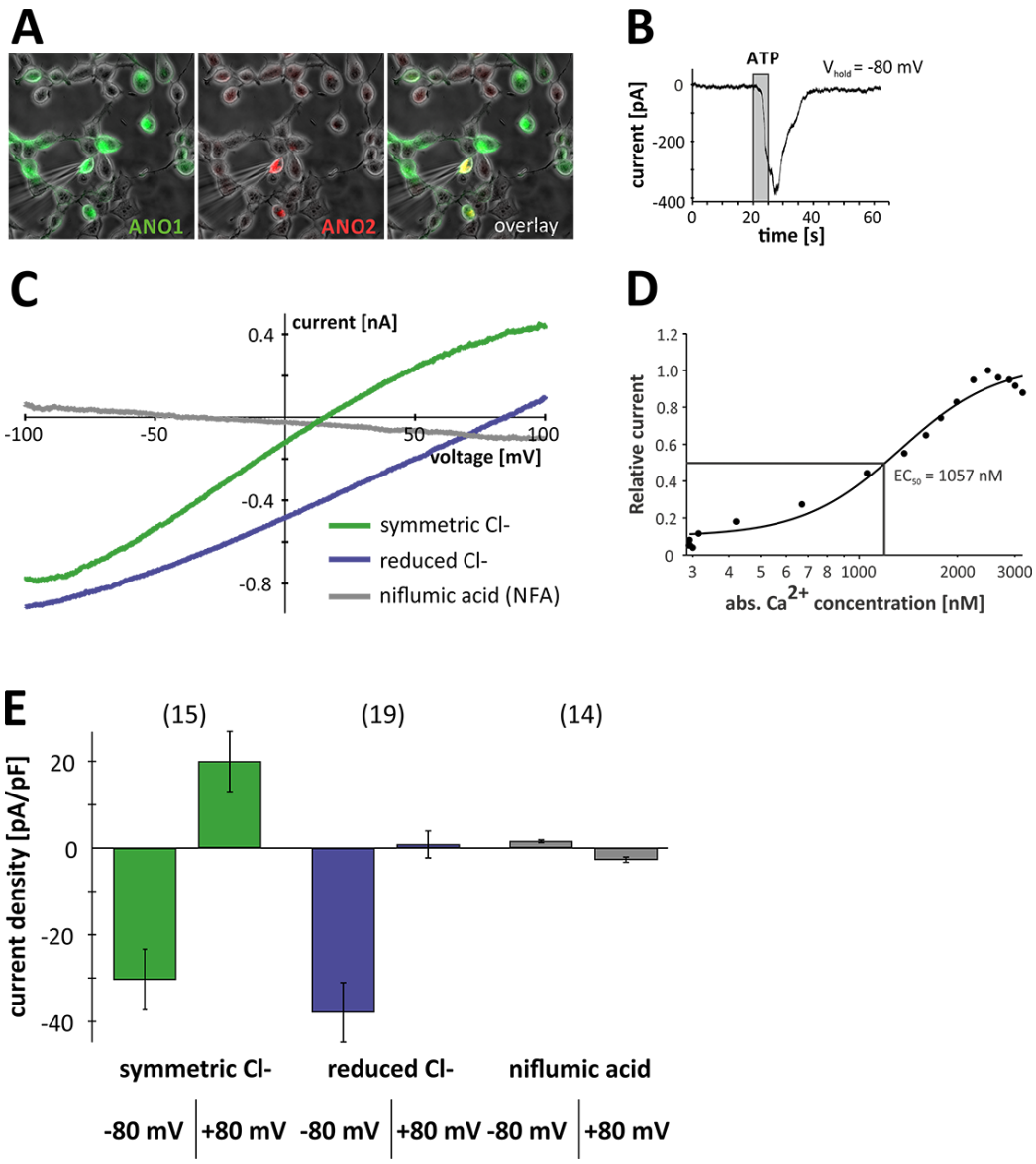

Figure 4.33: Co-expression of ANO1 and ANO2 result in intermediate phenotype. **A:**,Fluorescence-labeled ANO1 and ANO2 constructs were expressed in HEK293 cells. **B:** Current measured upon ATP stimulation. **C:** I-V diagram with currents measured under symmetrical chloride conditions, reduced extracellular chloride conditions and with chloride channel blocker NFA. **D:** Dose-response diagram for calcium activation of ANO1 - ANO2 co-expression. **E:** Current densities for three tested conditions stimulated with 10 µM ATP. (Data provided by D. Drose and T. Ackels, RWTH Aachen)

Co-expressing ANO2 together with ANO6 exhibited a more striking effect (Fig. 4.34). We found a strong alteration in current densities (Fig. 4.34 E) (Tab 4.2). These were significantly higher than for singular expression of either ANO2 or ANO6 (Fig. 4.34 F). EC_{50} value, current kinetics and reversal potential shift upon chloride substitution showed no differences to ANO2 or ANO6 singular expression (Fig. 4.34 C,D) & (Drose, 2013).

Table 4.2: ANO2 + ANO6 current densities

Condition	**-80 mV [pA/pF]**	**+80 mV [pA/pF]**
Symmetric Cl^-	-82.86 $\pm$ 20.3	98.34 $\pm$ 20.3
Reduced Cl^-	-65.78 $\pm$ 17.7	0.76 $\pm$ 4.8
NFA	-0.14 $\pm$ 0.5	-1.13 $\pm$ 0.8

These results show, co-expression of ANO2 with either ANO1 or ANO6 had direct influence on Anoctamin chloride currents. Combination of ANO1 and ANO2 led to an intermediate phenotype, with current densities in between both singular expressions and co-expression of ANO2 with ANO6 led to a potentiating effect in current densities. They peaked in currents twice as large than ANO6 and 10-fold larger than ANO2 singular expression (Fig. 4.34 F). These alterations of current densities implicated that co-expression of two different Anoctamins in the same compartment could have physiological relevance. We identified co-expression of ANO2 and ANO6 in the same microdomains in olfactory cilia. Thus, the observed potentiating effect could affect olfactory signaling.

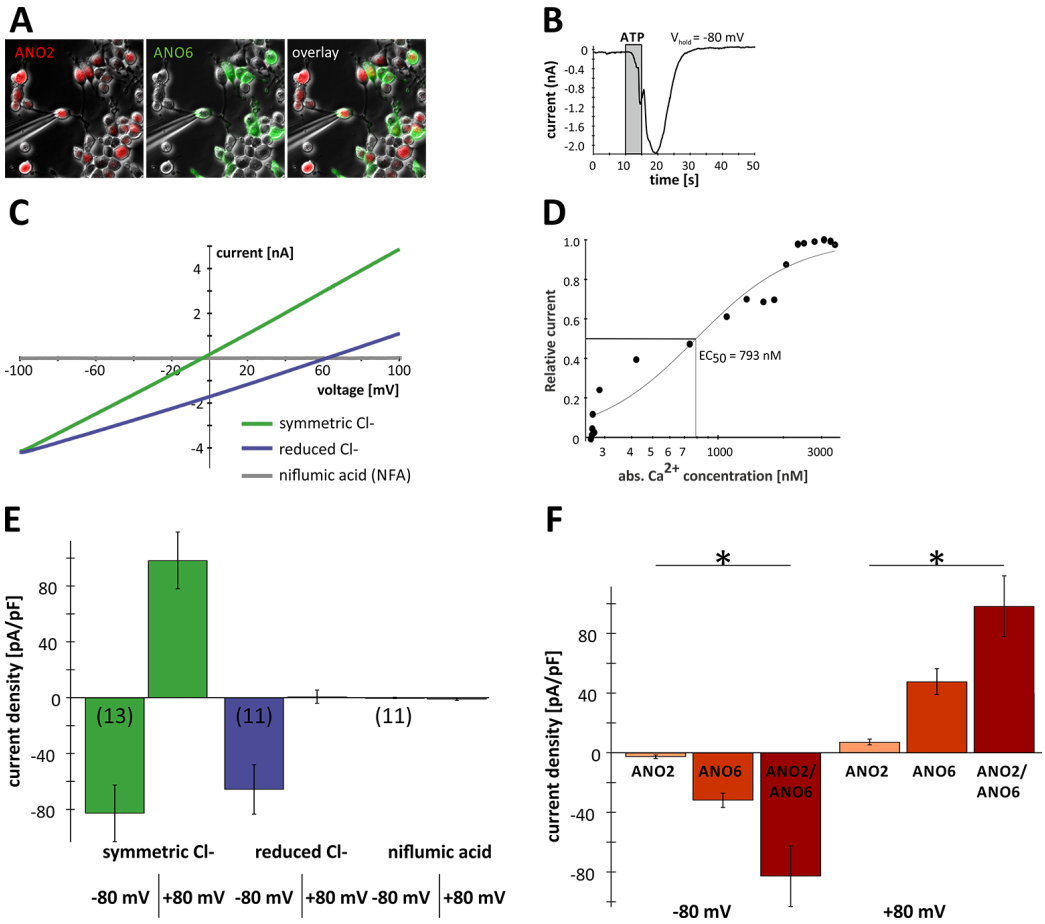

Figure 4.34: Co-expression of ANO2 and ANO6 potentiates chloride current. **A:** Fluorescence-labeled ANO2 and ANO6 constructs were expressed in HEK293 cells. **B:** Current measured upon ATP stimulation. **C:** I-V diagram with currents measured under symmetrical chloride conditions, reduced extracellular chloride conditions and with chloride channel blocker NFA. **D:** Dose-response diagram for calcium activation of ANO2 - ANO6 co-expression. **E:** Current densities for three tested conditions stimulated with 10 µM ATP. **F:** Comparison between current densities of ANO2, ANO6 and ANO2 ANO6 co-expression. (Data provided by D. Drose and T. Ackels, RWTH Aachen)

4.8 Multimerization of Anoctamin proteins

The observed effects on Anoctamin current strength could not be explained by simple co-expression of two different Anoctamin proteins in the same cell. Sheridan et al. (2011) demonstrated ANO1 homodimerization and Tien et al. (2013) identified the ANO1 dimerization domain. We now hypothesized that the ob-

served current modulation results from direct interaction of two different Anoctamins.

4.8.1 Anoctamin proteins form homo-dimers *in vitro*

We examined direct protein-protein interaction between Anoctamin proteins using a bioluminescence resonance energy transfer (BRET) assay (Bacart et al., 2008). We co-expressed ANO1, ANO2 and ANO6 with C-terminal *Renilla* luciferase or GFP fusion in HEK293 cells. At the beginning, we made sure that tagged Anoctamin constructs and untagged control constructs were localized to the plasma membrane by expressing these constructs in HEK293 cells (Fig. 4.35). Luciferase- (Luc) or GFP-tag did not interfere with plasma membrane localization of Anoctamins. Thus, all Anoctamin constructs were suitable to prob for direct protein-protein interaction.

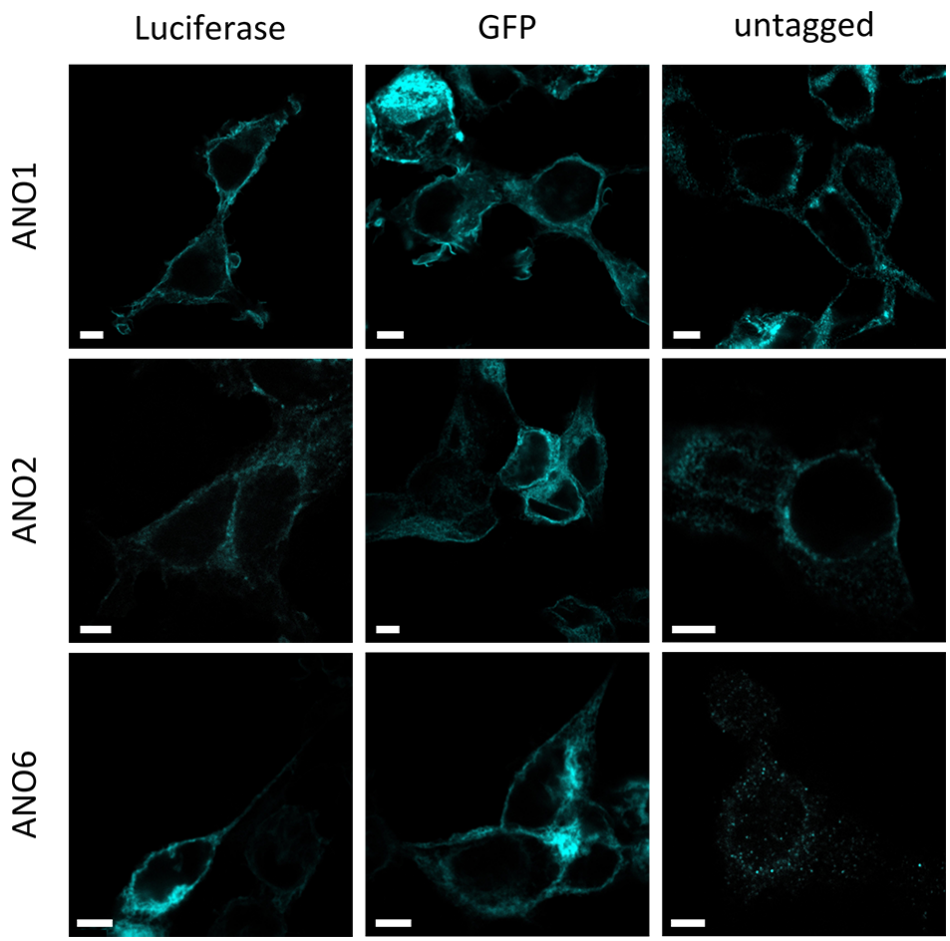

Figure 4.35: Anoctamin constructs for BRET assay localize to the plasma membrane. *Renilla* luciferase-, GFP-tagged and untagged Anoctamins were expressed in HEK293 cells. Cells were fixed and probed for protein expression with specific antibodies against luciferase, GFP or Anoctamin specific antibodies and visualized using fluorophore-coupled secondary antibodies. Scale bars = 5 µm

Next, we co-expressed Luc and GFP tagged ANO1, ANO2 and ANO6 in HEK293 cells and probed for homomeric interaction. We measured bioluminescence and fluorescence signals (stimulated through resonance energy transfer) to determine BRET signals. BRET signals are defined as fluorescence signals divided by bioluminescence signals. Since Luc-only transfection should not give rise to a specific BRET signal, we defined BRET values of these transfections as background. We normalized each measurement to BRET signals of these transfections by setting the values of Luc-only transfection to 1. This way we were able to compare independent experiments.

The signal intensities of GFP and luciferase transfected cells (Ano1 = 2,16 $\pm$ 0,33, Ano2 = 1,39 $\pm$ 0,05, Ano6 = 2,72 $\pm$ 0,35) were compared to control-transfected cells (Fig. 4.36 A). Controls were transfected with luciferase construct and untagged Anoctamin as substitute for GFP-tagged construct (Ano1 ctrl = 1,36 $\pm$ 0,16, Ano2 ctrl = 1,1 $\pm$ 0.08, Ano6 ctrl = 0,97 $\pm$ 0,06). All three tested Anoctamins showed a significant increase in BRET signal thus, ANO1, ANO2 and ANO6 possibly form homodimers.

BRET signals can arise just from molecular crowding of proteins in the plasma membrane (Bacart et al., 2008). We raised the donor vs. acceptor ratios and monitored BRET values to control for this possibility. Signals based on molecular crowding rise linearly with increase of acceptor molecules. Specific protein-protein interaction is unaffected by a rise of acceptor molecules, since after a certain ratio, all donor molecules are paired with acceptor molecules. All three tested Anoctamins displayed saturation of signal strength when acceptor concentrations were increased (Fig. 4.36 B). These results provide evidence for a specific and direct homomeric interaction of ANO1, ANO2 and ANO6. Thus, Anoctamin channels may consist of several Anoctamin subunits.

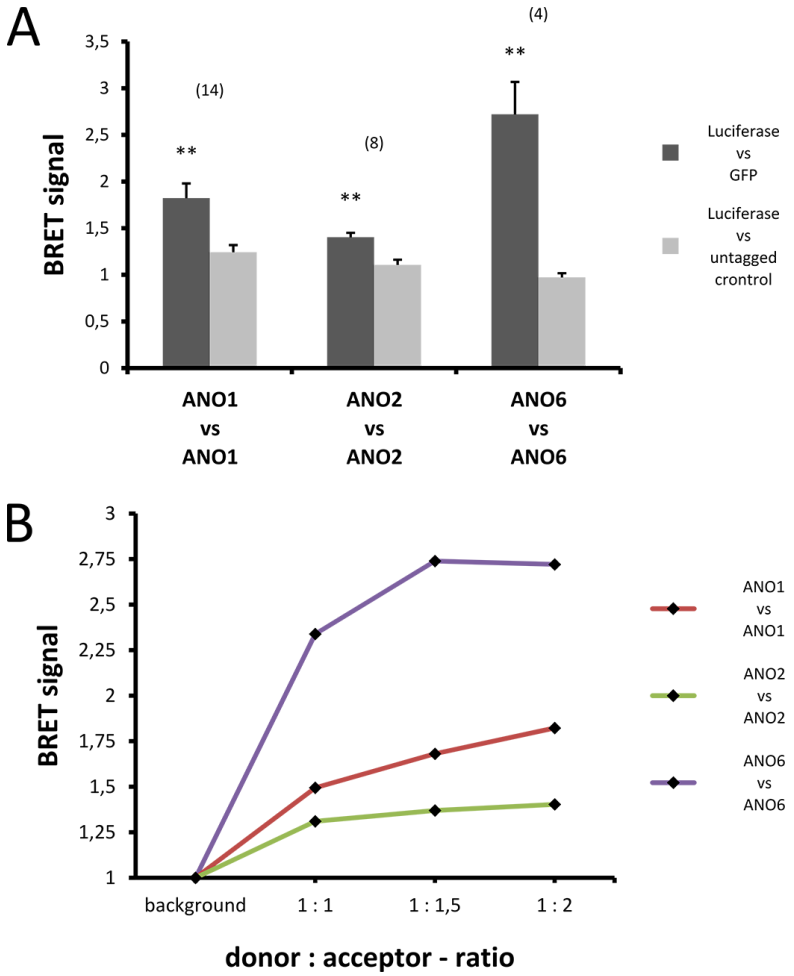

Figure 4.36: Anoctamin proteins from homomers *in vitro*. *Renilla* luciferase-, GFP-tagged Anoctamin constructs were expressed in HEK cells and probed for bioluminescence resonance energy transfer. **A:** BRET signals of ANO1, ANO2 and ANO6 vs. untagged control constructs. Number in brackets indicate set of experiments (n). Students t-test was used to compare GFP vs. ctrl transfecitons. p-values: ANO1 = 0.004, ANO2 = 0.005, ANO6 = 0.003 **B:** Rising BRET signals with increased donor:acceptor ratio.

We further noticed a persistent homomeric interaction of ANO1, ANO2 and ANO6 by Western Blot analysis. We expressed GFP-tagged Anoctamins in HEK293 cells, purified membrane fractions and subjected these fraction to Western Blot analysis, after a rigorous denaturation protocol (10 min 95°C, 4% (w/v) SDS, 100 mM DTT). We detected monomeric proteins of all ANO1, ANO2 and ANO6 but also presumably dimeric versions (Fig. 4.37). This results also supports the idea of Anoctamin channels consisting of at least two Anoctamin subunits.

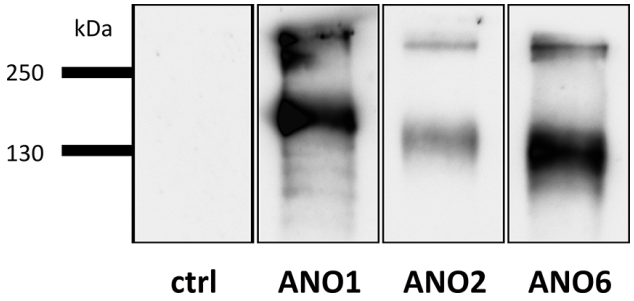

Figure 4.37: Anoctamin dimers form *in vitro*. GFP-tagged ANO1, ANO2 and ANO6 were expressed in HEK293 cells. Ctrl = untransfected cells. Proteins were isolated, separated by SDS-PAGE and probed for Anoctamin expression in Western Blot analysis with specific antibody against GFP.

4.8.2 Anoctamin proteins directly interact with each other

ANO1, ANO2 and ANO6 appeared to form homo-dimers in BRET assay and Western Blot (Fig. 4.36, 4.37) and co-expression of different Anoctamins altered current strength (Fig. 4.33, 4.34). Thus, we went on to probe all three Anoctamins also for heteromeric interaction. We co-expressed ANO1 and ANO2 in HEK293 cells, which yielded a significant BRET signal compared to controls (Ano1 vs. Ano2 = 1,93 $\pm$ 0,17, ctrl = 1,18 $\pm$ 0,06). We additionally found interaction of ANO6 with ANO1 (Ano1 vs. Ano6 = 2,08 $\pm$ 0,22, ctrl = 1,13 $\pm$ 0,03) and ANO2 (Ano2 vs. Ano6 = 1,76 $\pm$ 0,07, ctrl = 1,17 $\pm$ 0,03) (Fig. 4.38 A). Therefore, Anoctamins also seemed to form heterodimers.

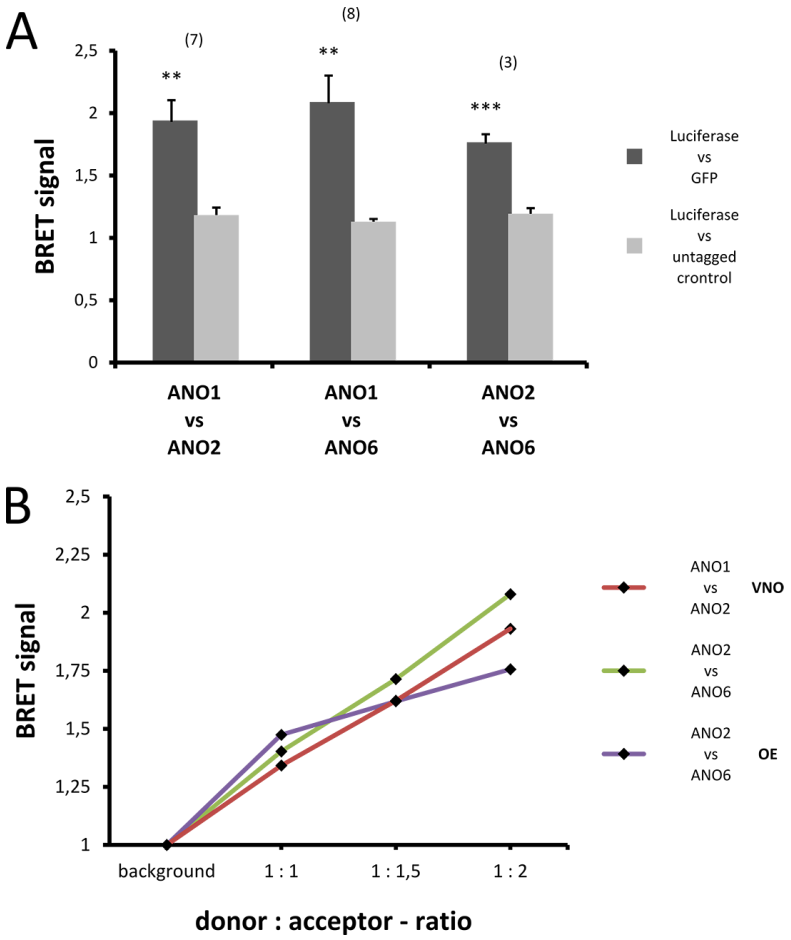

Figure 4.38: Anoctamin proteins form heteromers with each other. Anoctamin proteins were co-expressed in HEK cells and probed for heteromeric interaction via BRET assay. **A:** Bar diagram shows BRET signal for tested Anoctamin combinations vs. untagged control Anoctamins. Number in brackets indicate set of experiments (n). Students t-test was used to compare GFP vs. ctrl transfections. p-values: ANO1 vs. ANO2 = 0.002, ANO1 vs. ANO6 = 0.002, ANO2 vs. ANO6 = 0.0003 **B:** Line diagram displays rising BRET signal upon elevation of donor:acceptor ratio for tested combinations.

Although we detected significant BRET signals for all three tested combinations, signals with ANO1 constructs did not reach saturation when donor : acceptor ratio was increased (Fig. 4.38 B). This result put the specificity of measured interactions into question. However, electrophysiological measurements proved an effect of co-expressing two different Anoctamins (Fig. 4.34). Moreover, Tien et al. (2013) recently demonstrated interaction between ANO1 and ANO2 and also described a crucial residue at position 169 for ANO1 dimeriza-

tion. Mutating this alanine to proline abolishes dimerization (Tien et al., 2013).

We designed mutated ANO1 A169P constructs as negative controls and tested them for protein-protein interaction in our BRET assay. First, we made sure the mutated constructs were expressed in our cell system (Fig. 4.39). Mutating alanine at position 169 in ANO1 to proline did not interfere with plasma membrane localization of the protein. Thus, mutated ANO1 constructs could be subjected to BRET analysis.

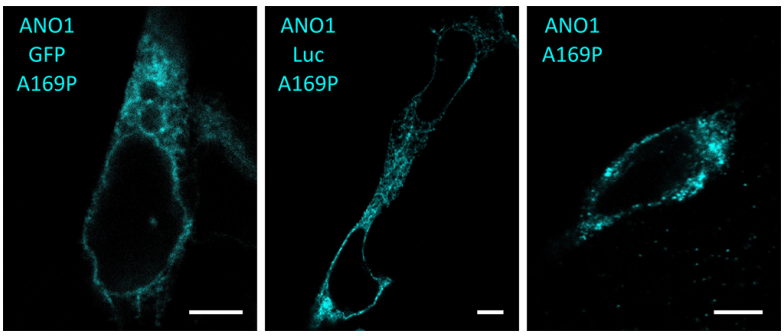

Figure 4.39: A169P mutation in ANO1 does not alter surface expression. Mutated ANO1 constructs were expressed in HEK293 cells, stained with antibodies against luciferase tag or ANO1 and fluorescent-coupled secondary antibodies. Fluorescence of secondary antibodies or GFP fluorescence were imaged with a conofocal microscope to detect ANO1 expression. Scale bars = 5 µm

We co-expressed mutated ANO1 with wildtype ANO1 in HEK293 cells and probed for BRET signals (Fig. 4.40). Mutating GFP-tagged ANO1 effectively abolished BRET signals for ANO1 homomers at all tested donor : acceptor ratios. We did not observe significant differences in signal strength between mutated ANO1-GFP (purple line) and untagged wildtype ANO1 (blue line) (Fig. 4.40 A).

Next, we analyzed the effect of mutating ANO1-Luc construct at the same position and tested BRET interaction with wildtype ANO1-GFP or untagged construct. Again, we detected no significant difference in signal strength between the mutated construct (purple line) and untagged wildtype construct (blue line) (Fig. 4.40 B). This results show, substituting alanine at position 169 with proline is sufficient in either BRET construct to abolish homomeric interaction of ANO1.

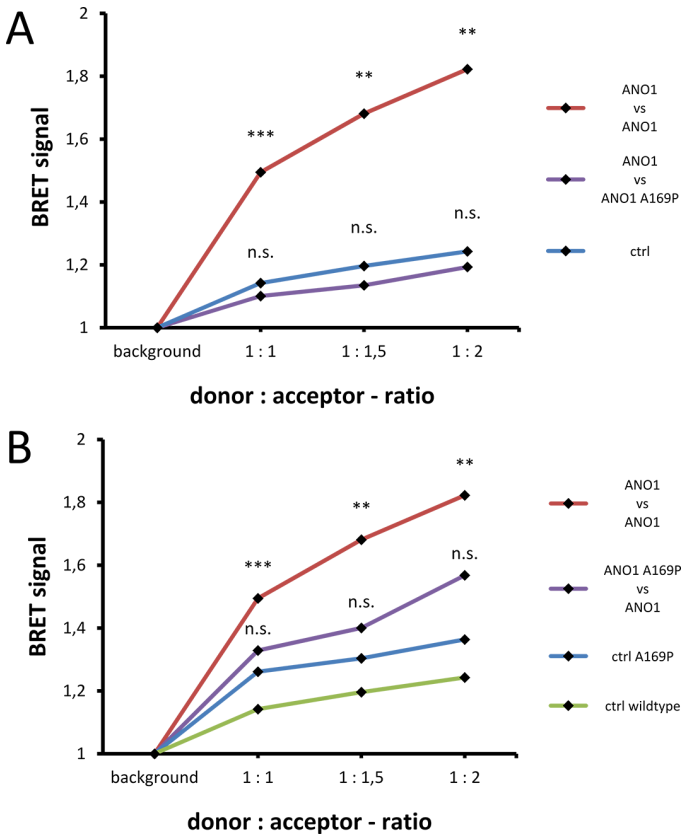

Figure 4.40: A169P mutation in Ano1 abolishes homomeric interaction. A: A169P mutation was introduced into ANO1-GFP construct and tested for interaction with wildtype ANO1-Luc via BRET assay. Students t-test was used to compare WT and mutated construct vs. ctrl transfecitons. p-values for WT, ctrl in brackets: 1:1 = 0.0002 (0.66), 1:1.5 = 0.002 (0.34), 1:2 = 0.004 (0.32). **B:** Mutation in ANO1-Luc construct tested with wildtype ANO1-GFP. Untagged ANO1 wildtype constructs were used as negative control. Students t-test was used to compare WT and mutated construct vs. ctrl transfections. p-values for WT, ctrl in brackets: 1:1 = 0.0002 (0.11), 1:1.5 = 0.002 (0.09), 1:2 = 0.004 (0.16).

We next expressed ANO1-A169P-GFP construct in HEK293 cells and performed Western Blot analysis on membrane-enriched fractions. Thereby, we noticed dimeric protein formation was reduced in mutated ANO1 (Fig. 4.41). This result demonstrated two things. On one hand again, mutation A169P in ANO1 is sufficient to abolish protein dimerization. On the other hand, this result supported the hypothesis that the observed bands in Fig. 4.37 really consisted of Anoctamin dimers.

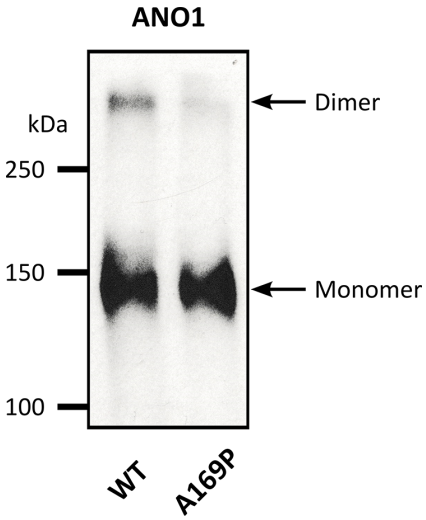

Figure 4.41: ANO1-A169P does not form dimers. Western Blot analysis after denaturating SDS-PAGE of ANO1 wildtype vs. ANO1-A169P. Both constructs were expressed GFP-tagged in HEK293 cells and membrane fraction was enriched. Proteins were detected via GFP-antibody.

With the possibility to negate ANO1 interaction, we addressed the question whether heteromeric interactions between ANO1 and ANO2 or ANO6 are also influenced by this mutation. If the observed interactions between ANO1 and other Anoctamins were specific (Fig. 4.38), we would expect a decline in BRET signal intensities to levels indistinguishable from untagged controls.

We expressed ANO2 or ANO6 together with mutated ANO1 in HEK293 cells and probed for BRET interaction. We found BRET signals of mutated Anoctamin (purple lines) were not distinguishable from untagged controls (blue lines) and significantly lower compared to wildtype ANO1 (red lines) (Fig. 4.42)

The linear trend in wildtype ANO1 titration curves argued for a non-specific interaction between ANO1 and ANO2 / ANO6 (Fig. 4.42 red lines). However, mutation of critical residue 169 in ANO1 was enough to reduce BRET signal intensities to control levels. Since muted ANO1 GFP construct was transported to the plasma membrane (Fig. 4.39), a signal due to molecular crowding would not have been influenced by the mutation. One exception was noted by an equal ratio between ANO2-Luc and ANO1-GFP A169P but all other donor-acceptor ratios showed no significant differences between mutation and control (Fig. 4.42 A, purple line). These results demonstrate mutation of A169P in ANO1 is enough to abrogate homo- and heteromeric interactions with Anoctamin pro-

teins. Furthermore, these controls support specificity of ANO1 heteromerization with ANO2 and ANO6.

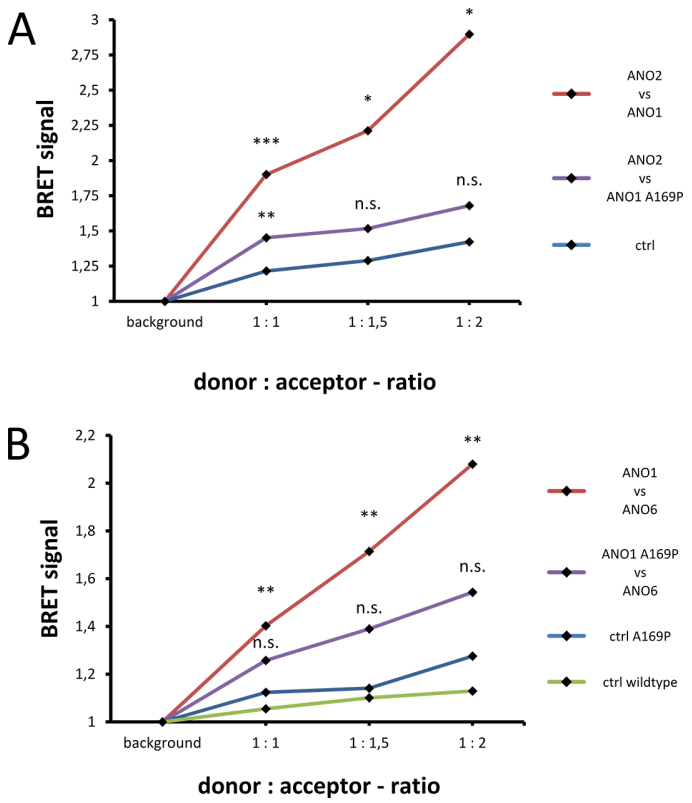

Figure 4.42: A169P mutation in ANO1 abolishes interaction with other Anoctamins. A: ANO2-Luc construct was tested with tagged ANO1-GFP, with mutated ANO1-GFP A169P and with untagged wildtype ANO1. Students t-test was used to compare WT and mutated construct vs. ctrl transfections. p-values for WT, ctrl in brackets: 1:1 = 0.0007 (0.03), 1:1.5 = 0.03 (0.07), 1:2 = 0.04 (0.05). **B:** Wildtype and mutated ANO1-Luc constructs were tested for BRET interaction with ANO6-GFP or untagged ANO6 control constructs. Students t-test was used to compare WT and mutated construct vs. ctrl transfections. p-values for WT, ctrl in brackets: 1:1 = 0.006 (0.11), 1:1.5 = 0.003 (0.08), 1:2 = 0.002 (0.25).

4.8.3 Anoctamin dimers are present in olfactory tissue

Intrigued by the idea, that co-expression of different Anoctamins modulates calcium-gated chloride currents through forming hetero-dimers, we probed for Anoctamin dimers in olfactory tissues. Anoctamin dimers withstood rigorous denaturation treatment during SDS-PAGE sample preparation (Fig. 4.37). Thus, we probed lysate of main olfactory epithelium for ANO2 / ANO6 expression (Fig.

4.43 A) and lysate from vomeronasal organ for ANO1 / ANO2 expression, respectively (Fig. 4.43 B).

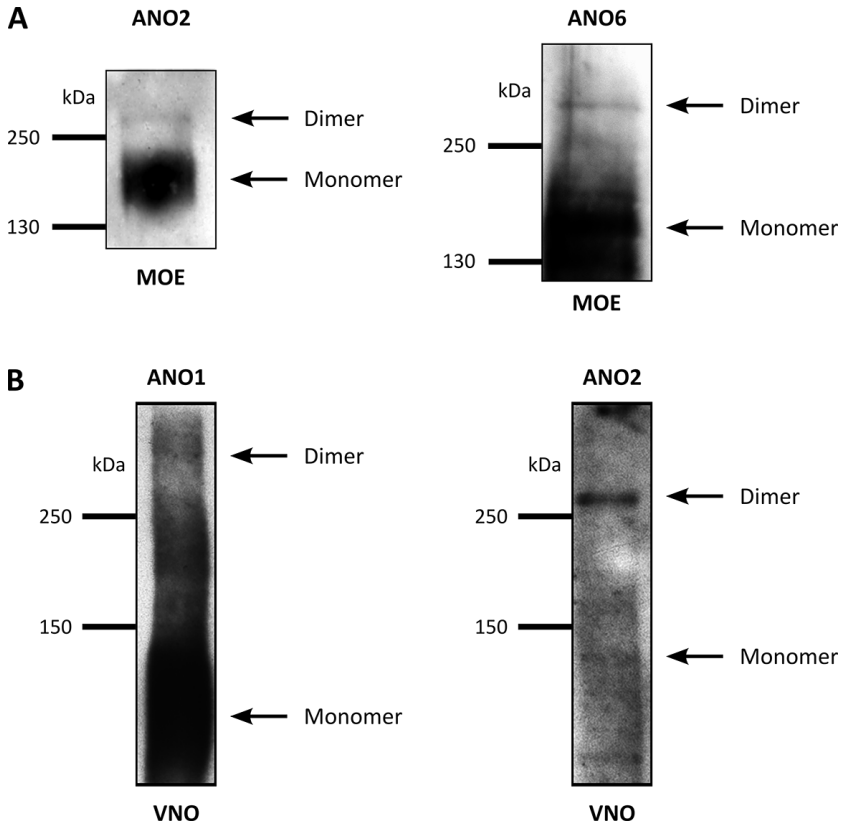

Figure 4.43: Anoctamin dimers are present in main olfactory epithelium and vomeronasal organ. Proteins from olfactory tissues were analyzed by Western Blot and probed for Anoctamin proteins with specific antibodies. **A:** Main olfactory epithelium was probed for ANO2 and ANO6 expression. **B:** Vomeronasal organ was probed for ANO1 and ANO2 expression.

We found a predominant signal for monomeric versions of Anoctamins in olfactory tissues. Nonetheless, we also detected dimeric proteins for ANO2 and ANO6 in the main olfactory epithelium and for ANO1 and ANO2 in the vomeronasal organ. Since all Anoctamin proteins are about the same molecular size, we could not distinguish between homo-or heter-dimers with this method. The presence of Anoctamin dimers however, supports the hypothesis of Anoctamin proteins forming functional channels from multiple Anoctamin subunits to participate in olfactory signal transduction.

5 Discussion

5.1 A potential role for scaffolding proteins in vomeronasal signal transduction

Scaffolding proteins mediate numerous signaling processes through protein-protein interactions (Good et al., 2011). They form functional microunits for enzymatic reactions or signaling events. Scaffolding proteins combine interacting proteins in a spatially defined area (Zeke et al., 2009), for example in the postsynaptic density of excitatory synapses. This mesh of scaffolding proteins below the postsynaptic membrane regulates receptor localization at the postsynaptic membrane, receptor internalization, presentation of the cell-cell adhesion molecules and downstream receptor signaling. Thus, scaffolding proteins are essential for synapse function (Feng & Zhang, 2009).

Sensory systems are less well studied, although they use comparably sophisticated signaling mechanisms to transmit stimuli from the periphery (Huber, 2001). A scaffolding complex similar to the postsynaptic density is not described in sensory systems. INAD complex from *Drosphila* photoreceptors is the best understood scaffolding complex in sensory systems, today. INAD recruits all involved signaling proteins into one macro-molecular complex to form a signaling microdomain (Montell, 2012). Furthermore, INAD forms supra-molecular complexes of several INAD scaffolding complexes through PDZ-PDZ domain interaction (Xu et al., 1998). This way, INAD forms a complete signaling network in a sensory system.

In this study, we present data supporting the existence of similar signaling networks in olfactory signal transduction. We show optical and biochemical evidence for the formation of signaling microdomains in the olfactory system through PDZ domain scaffolding proteins. The existence of so called "olfactosomes" was already proposed in the early 2000‘s (Huber, 2001; L’Etoile & Bargmann, 2000). Dooley et al. (2009) and Baumgart et al. (2014) investigated the role of PDZ scaffolding protein MUPP1 in the main olfactory epithelium.

This scaffolding protein is comprised of 13 PDZ domains + one L27 domain, and shares high sequence similarity with INAD (Ullmer et al., 1998). MUPP1 is expressed in cilia of olfactory sensory neurons and interacts with olfactory receptors and downstream signaling proteins. Additionally, MUPP1 influences activation kinetics and response termination in olfactory sensory neurons through PDZ ligand binding. The organization of vomeronasal signaling, however, is unknown. We aimed to provide further knowledge about organization of olfactory signaling by investigating scaffolding proteins in the vomeronasal organ.

We analyzed RNA from vomeronasal organ with two different methods and identified expression of several scaffolding proteins (Fig. 4.1). We reasoned that scaffolding proteins participating in signal transduction need to be expressed in the microvilli, as it has been shown that other signaling proteins localize therein (Halpern & Martinez-Marcos, 2003). Therefore, we localized scaffolding proteins newly identified by our screen in cryosections of adult vomeronasal epithelium (Fig. 4.3). Ahnak, Gipc1 and Lin7c did not localize specifically to the microvillar compartment, which argues against direct participation of these proteins in signal transduction. In contrast, we identified expression of DLG1 and NHERF1 in the microvillar layer (Fig. 4.4). Hence, these two are the first identified scaffolding proteins potentially organizing vomeronasal signal transduction.

5.2 NHERF1 - a scaffolding protein for organizing vomeronasal signal transduciton

NHERF1, a PDZ scaffolding protein with two PDZ domains, recruits G protein-coupled receptors and ion channels into macro-molecular complexes (Naren et al., 2003). Furthermore, NHERF1 is involved in G protein-coupled receptor trafficking (Bauch et al., 2014) and mediates phospholipase C signaling through G protein-coupled receptors (Capuano et al., 2007). Since vomeronasal signaling is based on G protein-coupled receptors activating a phospholipase C (Munger et al., 2009), we identified with NHERF1 a promising candidate to regulate vomeronasal signal transduction. The capacity of NHERF1 to interact with

other scaffolding proteins (LaLonde et al., 2010; Lau & Hall, 2001) or to form homo-dimers (Fouassier et al., 2000) could enable NHERF1 to form signaling networks.

The vomeronasal organ continues to develop postnatally until mice reach sexual maturity (Horowitz et al., 1999). Thus, we compared expression of NHERF1 in vomeronasal organ between adult (P90) and juvenile (P8) mice. We demonstrated NHERF1 expression increasing in parallel with expression of vomeronasal signaling proteins $G_{\alpha o}$ and TrpC2 during functional maturation of the vomeronasal organ (Fig. 4.2). This indicates a role of NHERF1 in vomeronasal signaling.

The microvillar layer of the vomeronasal sensory epithelium is comprised of two types of microvilli, neuronal microvilli and microvilli from the supporting cells (Menco et al., 2001). Since we observed NHERF1 expression in the complete vomeronasal microvillar layer (Fig. 4.3), we aimed to discern if expression was limited to the supporting cell microvilli or if NHERF1 is also expressed in neuronal microvilli. Via examining dissociated neurons from vomeronasal epithelium, we demonstrated NHERF1 expression in neuronal microvilli (Fig. 4.5, 4.6), which bespeaks NHERF1 influencing vomeronasal signaling.

Expression of NHERF1 in polarized cells was observed in many epithelia (Ingraffea et al., 2002; Morales et al., 2004), which is in agreement with expression of NHERF1 in microvilli of vomeronasal supporting cells. NHERF1 is also crucial for microvillar formation (Garbett et al., 2010). That is also a possible NHERF1 function in either neurons and supporting cells.

5.2.1 NHERF1 potentially mediates microdomain assembly in neuronal microvilli

We analyzed the subcellular organization of NHERF1 in neuronal microvilli with super-resolution microscopy and demonstrated that NHERF1 is expressed in spatially segregated microdomains (Fig. 4.6). Since NHERF1 is a cytosolic protein (Reczek et al., 1997), focused expression indicates binding of NHERF1 to the cytoskeleton or another organizing element. Otherwise, diffusion would have distributed NHERF1 homogeneously inside the microvilli lumen. NHERF1 inter-

acts with actin-binding proteins Ezrin, Radixin and Moesin through its C-terminal ERM domain (Reczek et al., 1997). This interaction transfers NHERF1 into an active state and promotes PDZ ligand binding (Morales et al., 2007). Thus, cytoskeleton anchoring increases the possibility of NHERF1 forming signaling microdomains through PDZ interaction.

In order to form signaling microdomains NHERF1 would most likely interact with signaling proteins or with other scaffolding proteins, which recruit signaling proteins into a complex. We analyzed subcellular organization of vomeronasal signaling proteins TrpC2 and $G_{\alpha i2}$ in neuronal microvilli to investigate microdomain formation. We used dual color STED microscopy to image both signaling proteins in super-resolution (Fig. 4.7 B). This analysis yielded several results. We found TrpC2 and $G_{\alpha i2}$ being organized in putative microdomains. To our knowledge, this is the first demonstration of vomeronasal signaling proteins being organized in distinct domains. Signaling protein $G_{\alpha i2}$ displayed a subcellular distribution similar to NHERF1 while TrpC2 channel did not. TrpC2 expression was less focused throughout the microvilli membrane. Moreover, we demonstrated, TrpC2 and $G_{\alpha i2}$ did not entirely co-localize in super-resolution, although they are expressed in the same cell compartment and part of the same signaling cascade. In addition, we showed microdomains of NHERF1 and $G_{\alpha i2}$ did co-localize in neuronal microvilli (Fig. 4.7 C). The subcellular organization of $G_{\alpha i2}$ indicates formation of signaling microdomains in vomeronasal signal transduction. Co-localization of NHERF1 and $G_{\alpha i2}$ domains demonstrates NHERF1‘s potential role in organizing such domains. Thereby, we newly identified a scaffolding protein presumably involved in vomeronasal signaling.

5.2.2 NHERF1 interacts with vomeronasal receptors

Since NHERF1 is a scaffolding protein with two PDZ domains, we looked for vomeronasal receptors as potential PDZ ligands. Most PDZ interactions are determined through the PDZ ligand‘s C-terminal sequence. Songyang et al. (1997) defined three binding classes on the basis of sequence motifs. We scanned annotated vomeronasal receptors for these motifs and identified 19% of V1 receptors and 38% of V2 receptors feature a PDZ ligand motif (Fig. 4.8). Thus, signaling in

the vomeronasal organ could well be organized by PDZ scaffolding proteins as it has been described for the main olfactory epithelium (Baumgart et al., 2014).

We designed a PDZ interaction microarray with C-terminal peptides to investigate interaction of NHERF1 PDZ domains with vomeronasal signaling proteins. Our high-throughput approach identified 25 out of 42 V1 receptors and 3 out of 30 V2 receptors as potential NHERF1 interaction partners (Fig. 4.10). We further verified one of these interactions by co-immunoprecipitation - vomeronasal receptor Vmn1ra10 immunoprecipitates with both PDZ domains of NHERF1 (Fig. 4.12). Interestingly, both PDZ domains appear to interact primarily with V1 receptors. However, V1 receptor PDZ ligands contain almost exclusively class II or class III motifs (28/30), while only about half of the V2 receptors feature such motifs (20/43). We identified mostly class II and class III PDZ ligands as binding partners for both PDZ domains which could explain this result. We compared NHERF1 expression in V1 and V2 receptor-expressing neurons and found that NHERF1 was expressed in equal amounts in both neuron subpopulations (Fig. 4.15). This result argues against a V1 specific role. However, the presence of NHERF1 in microvilli of both neuron subpopulations indicates the essential role of NHERF1 for microvilli formation also in vomeronasal sensory neurons (Garbett et al., 2010).

NHERF1 could organize vomeronasal signal transduction in signaling microdomains through binding and anchoring vomeronasal receptors. However, NHERF1 did not interact with any described vomeronasal signaling proteins apart from vomeronasal receptors (Tab. 5.3). Signaling proteins though, could be recruited by additional scaffolding proteins into a signaling complex. We found expression of several scaffolding proteins in the vomeronasal organ (Fig. 4.1) thus, members of the vomeronasal signaling cascade could be integrated into a supra-molecular scaffolding complex by interacting with additional scaffolding proteins. Three types of interaction have been described for NHERF1: NHERF1 could either bind another scaffolding protein as PDZ ligand (LaLonde et al., 2010) or acts as a PDZ ligand itself (Morales et al., 2007) or interaction between PDZ domains of NHERF1 and an additional PDZ scaffolding protein is possible (Fouassier et al., 2000). The ability to interact with the cytoskeleton enables NHERF1 to function as anchor for a putative signaling complex. Therefore,

NHERF1 could be part of a signaling network in neuronal microvilli.

Many G protein-coupled receptors are internalized upon ligand binding (von Zastrow, 2001). This mechanism has also been described for olfactory receptors in in the main olfactory epithelium of rodents and fish (Mashukova et al., 2006; Rankin et al., 1999). A comparable mechanism for vomeronasal receptors has not been shown, but NHERF1 could also mediate receptor recycling. Internalization and recycling of receptors is promoted by PDZ scaffolding proteins (Heydorn et al., 2004; Lauffer et al., 2009). NHERF1 takes part in recycling of G protein-coupled $\beta 2$ adrenergic receptor after ligand binding (Cao et al., 1999). In contrast to other G protein-coupled receptors, $\beta 2$ adrenergic receptor is not degraded after ligand-induced internalization but recycled to the plasma membrane (Tsao & Zastrow, 2000). This recycling process is potentially mediated through interaction with NHERF1 (Gage et al., 2005). Mashukova et al. (2006) observed a similar mechanism for internalization of olfactory receptors where these receptors were not targeted for degradation but rapidly recycled to the plasma membrane. It is tempting to speculate NHERF1 recycles vomeronasal receptors through a comparable mechanism which is supported by results from Garbett & Bretscher (2012) who observed fast turnover of NHERF1 in microvilli and presumed PDZ ligand trafficking or recycling as a possible cause. Since NHERF1 binds vomeronasal receptors (Fig. 4.10) and mediates G protein-coupled receptor trafficking, it could recycle receptors after activation.

5.2.3 NHERF1 interacts with potential vomeronasal signaling proteins

We further identified novel interaction partners of NHERF1 in our interaction microarray (Tab. 5.3). Some candidates could play a role in vomeronasal signaling, such as PLCη1 or PLCγ1. Neither one has been considered as vomeronasal signaling protein yet, but PLC enzymes partake in vomeronasal signaling (Munger et al., 2009). We did not detect expression of PLCη1 in vomeronasal organ (Fig. 4.19), but identified PLCγ1 in a mRNA microarray analysis (Fig. 4.18). The latter is also known to activate TrpC2 channel, another protein from the vomeronasal signaling cascade (Tong et al., 2004). Thus, PLCγ1 is an interesting

candidate for vomeronasal signal transduction.

Besides PLC enzymes, we showed interaction of calmodulin 2 with NHERF1 PDZ domains. Calmodulin is known to regulate Anoctamin 1 (Jung et al., 2013), a calcium-gated chloride channel we detected in vomeronasal neuronal microvilli (Fig. 4.31 A). Additionally, Calmodulin 2 is part of the adaptation cycle in vomeronasal sensory neurons (Spehr et al., 2009). Thus, it can affect signal transduction proteins in a significant way. Therefore, NHERF1 could add calmodulin 2 as a signal-regulating protein to a hypothetical signaling complex.

We also found interaction between NHERF1 and G proteins $G_{\alpha t1\text{-}3}$ and $G_{\alpha i3}$. G proteins $G_{\alpha t1}$ mediate signal transduction in rod photoreceptor cells and $G_{\alpha t2}$ in cone photoreceptor cells (Umino et al., 2008). $G_{\alpha t3}$ is responsible for G protein-coupled signaling in taste cells (Wong et al., 1996). Expression of $G_{\alpha t}$ proteins has not been studied in vomeronasal organ. G protein $G_{\alpha i3}$ is known to play a role in primary cilium migration, but no data is available regarding olfactory signaling (Ezan et al., 2013). The closely related isotype $G_{\alpha i2}$ was described as G protein associated with V1 vomeronasal receptors (Berghard et al., 1996). Given that $G_{\alpha i2}$ shares 85% sequence identity with $G_{\alpha i3}$, one might speculate $G_{\alpha i3}$ could also mediate signaling in vomeronasal neurons.

We did not observe direct interaction between NHERF1 and $G_{\alpha i2}$. However, we confirmed expression of $G_{\alpha i2}$ in neuronal microvilli and super-resolution microscopy revealed subcellular distribution of $G_{\alpha i2}$ in segregated clusters (Fig. 4.7 B). This finding supports the idea of a vomeronasal signaling cascade organized in signaling microdomains. We also showed co-localization of NHERF1 with $G_{\alpha i2}$ microdomains (Fig. 4.7 C). This indicates that NHERF1 could participate in organizing these signaling complexes, since NHERF1 promotes signaling of G protein-coupled receptors via $G_{\alpha i}$ proteins (Huang, 2004).

We here show for the first time that NHERF1 directly interacts with vomeronasal receptors, PLC and possibly $G_{\alpha i}$ enzymes in vomeronasal neurons. Moreover, NHERF1 is able to anchor these proteins and additional scaffolding proteins to the cytoskeleton. Furthermore, we demonstrate NHERF1 being expressed in microdomains where it co-localizes with signaling proteins. We therefore conclude that vomeronasal signal transduction may be organized in signaling microdromains with NHERF1 contributing to their orgnization

5.3 DLG1 - a scaffolding protein interacting with vomeronasal receptors

We found DLG1, another PDZ domain scaffolding protein, expressed in the microvillar layer of the vomeronasal organ (Fig. 4.16). Co-localization studies with mature olfactory neuron marker OMP demonstrated that DLG1 expression is restricted to vomeronasal sensory neurons. We did not detect any DLG1 expression in non-neuronal parts of the epithelium. Due to these findings we considered DLG1 to be a candidate for organizing vomeronasal signaling through interaction with vomeronasal receptors, signaling proteins or other scaffolding proteins. DLG1 is best known for organizing AMPA receptor trafficking in excitatory synapses (Sans et al., 2001). Moreover, DLG1 regulates trafficking and recycling of G protein-coupled receptors through PDZ interactions (Gardner et al., 2007; Nooh et al., 2013). Therefore, DLG1 may exert a similar role in vomoronasal receptor trafficking.

We identified 9 V1 and 2 V2 vomeronasal receptors as potential interaction partners for DLG1 PDZ2 domain (Tab. 5.4). We also found PLC enzymes PLCγ1 and PLCβ1 interacting with DLG1 (Tab. 5.5). Since both are expressed in vomeronasal organ, they could participate in vomeronasal signal transduction. We were not able to identify additional proteins from the vomeronasal signaling cascade as interaction partners. Since DLG1 is well known to form scaffolding complexes including other scaffolding proteins, it is worth mentioning that NHERF1 C-terminus bound to DLG PDZ2 domain in two experiments. The L27 domain allows protein-protein interaction with other MAGUK proteins (Feng et al., 2004) or with another DLG1 protein (Nakagawa et al., 2004). These complexes are further recruited to the plasma membrane (Valentine & Haggie, 2011). Moreover, PDZ-PDZ domain interaction occur in over 30% of mammalian PDZ proteins (Chang et al., 2011). Therefore, DLG1 could organize signaling complexes in vomeronasal sensory neurons through interaction with other scaffolding proteins and traffic them to the plasma membrane.

Although we successfully purified all three DLG1 PDZ domains from bacterial cell lysates, only PDZ2 domain interacted with PDZ ligands in our microar-

ray analysis (Fig. 4.17). We designed PDZ domain proteins as described before (Wang et al., 2005). Wang et al. (2005) analyzed the interaction of DLG1 PDZ domains with NMDA receptor subunit NR2B. They studied *in vitro* association of NR2B C-terminal peptides with DLG1 PDZ domains and identified interaction with PDZ1 and PDZ2 domain but notably they did not find any interaction with PDZ3 domain. PDZ interaction often depends on more than simple association of PDZ ligand with the core domain (Wang et al., 2010). However, for our interaction assay only the core domains were used, which may limit the identification of interaction partners for PDZ1 and PDZ3 domains and explain lack of interactions in our assay. Furthermore, the core domains only cover 90 amino acids of the entire 927 amino acid DLG1 protein. Thus, it is possible that in our expression system these domains are not folded as in the full length protein. Several PDZ domains do not fold correctly in bacterial expression systems, especially when only core domains are expressed (Wang et al., 2010). Misfolding of PDZ1 and PDZ3 domains could prevent any PDZ interactions in our assay. This effect is less likely to occur for our experiments with NHERF1 PDZ domains. Since we used two halves of the NHERF1 protein, each featuring one PDZ respectively as described in Huang (2004). These protein fragments contained more amino acids than the PDZ core domains.

We demonstrated that DLG1 is localized in neuronal microvilli and its PDZ2 domain interacted with vomeronasal receptors and PLC enzymes. Thus, we identified a second scaffolding protein putatively influencing vomeronasal signaling. Since we were only able analyze interactions through PDZ2 domain, two further PDZ domains could possibly bind interaction partners involved in vomeronasal signaling. Interestingly, DLG1 tended to interact with NHERF1 and possesses multiple ways for interaction with other scaffolding proteins. Therefore, DLG1 possibly plays a role in organizing vomeronasal signaling through interaction with signaling proteins and other scaffolding proteins.

5.4 Quality of PDZ microarray data

Using microarrays to identify PDZ domain interaction partners is a high-throughput approach. This methods provides certain benefits: We were able to test domains of interest against a large number of selected PDZ ligands. This approach led to the identification of vomeronasal receptors as interaction partners of NHERF1 and DLG1 and yielded lists of numerous potential interaction partners. However, a high-throughput analysis has certain restraints: The results need further validation to rule out false positive or false negative hits. We incorporated Sl22a12, CFTR, PTEN and β-catenin as controls for NHERF1 in the microarray analysis. However, Sl22a12 transporter was the only positive control for NHERF1 PDZ1 domain interaction which was successfully identified in our assay. We were not able to reproduce interaction with CFTR or PTEN. Likewise, PDZ2 domain ligand β-catenin only interacted in 2 out 3 experiments with the PDZ domain. Nonetheless, the assay correctly identified vomeronasal receptor V1ra10 as NHERF1 interaction partner, which was verified by pull-down (Fig. 4.12). Taken together, these results illustrate that it is possible to identify PDZ ligand binding via the applied PDZ microarray. However, it also demonstrates that an artificial approach mimics the *in vivo* situation only to some extent and subsequent validation is necessary to draw final conclusions.

5.5 PLCβ3 is a candidate for vomeronasal signaling

Phospholipase C enzymes take part in vomeronasal signaling by producing second messenger DAG which presumably activates TrpC2 (Zufall et al., 2005). The partaking PLC enzymes however, have not been identified (Francia et al., 2014). Thus, we investigated microarray RNA data from vomeronasal organ and found several PLC enzymes expressed (Fig. 4.18). We first focused on PLCη1 as it has been shown that PLCη1 enhances activity of other PLC enzymes subsequent to G protein-coupled receptor activation (Kim et al., 2011). Since multiple PLC enzymes are present in the vomeronasal organ, engagement of several PLC en-

zymes as described by Kim et al. (2011) could likely happen.

We identified PLCη1 in RNA microarray screening from vomeronasal organ (Fig. 4.18), but could not verify expression via RT-PCR (Fig. 4.19). Since, RNA microarray studies are high-throughput approaches which are limited in their specificity, the identified PLCη1 hit could be caused by expression of another PLCη subtype. We investigated expression of PLCη2 in vomeronasal epithelium as both enzymes share sequence similarity. Although initially undetected by the microarray RNA screen, we confirmed expression of PLCη2 by RT-PCR. However, since PLCη2 does not enhance PLC activity (Kim et al., 2011) a mechanism of PLCη enhancing another PLC is unlikely to occur in vomeronasal signal transduction.

Moreover, we investigated the expression of PLCβ enzymes in the vomeronasal organ, since PLCβ subtypes are PDZ ligands interacting with PDZ scaffolding proteins (Kim et al., 2011). Thus, they could be part of a vomeronasal signaling complex. We identified expression of PLCβ1, 3 and 4 (Fig. 4.18). Three different splice variants of PLCβ4 are known, but only PLCβ4a is a PDZ ligand (Adamski et al., 1999; Kim et al., 1998). We demonstrated PLCβ4a expression in vomeronasal organ (Fig. 4.20) and localized PLCβ4 expression to axons of vomeronasal sensory neurons (Fig. 4.21). These results argue against a role in vomeronasal signaling, since signal transduction takes place in neuronal microvilli. PLCβ3 however, localized to neuronal microvilli, as we demonstrated with Phalloidin co-stainings (Fig. 4.22). Therefore, PLCβ3 is an enzyme which could take part in vomeronasal signaling and could bind to PDZ scaffolding proteins in signaling complexes. Taken together, we could rule out the participation of PLCη1 and PLCβ4 enzymes in vomeronasal signal transduction and identify PLCβ3 as promising candidate.

5.6 Signaling proteins in olfactory neurons are organized in microdomains

In 2010 our group identified ANO2 a calcium-gated chloride channel specifically expressed in cilia of olfactory sensory neurons (Rasche et al., 2010). Subsequent

knockout studies demonstrated, ANO2 being the major constituent of calcium-gated chloride channels in olfactory sensory neurons (Billig et al., 2011). Apart from ANO2, protein expression of ANO1 and ANO6 has been found in the olfactory epithelium (Kuhlmann et al., 2014; Rasche et al., 2010) Here, we confirmed expression of ANO1, ANO2 and ANO6 by deep RNA sequencing (Fig. 4.23). ANO1 is also calcium-gated chloride channel (Caputo et al., 2008). The function of ANO6 is currently under debate (Kunzelmann et al., 2014). Several studies identified ANO6 as calcium-gated chloride channel (Kmit et al., 2013; Martins et al., 2011), but other groups reported calciumgated cation channel activity (Suzuki et al., 2013; Yang et al., 2012) or a participation in volume-activated chloride currents (Juul et al., 2014). Moreover, ANO6 is involved in phospholipid scrambling (Suzuki et al., 2013, 2010), a function which appears to be independent of ion channel function (Kmit et al., 2013). Nothing is known about the roles of ANO1 and ANO6 in the olfactory system. Hence, we analyzed expression of these Anoctamins in the olfactory epithelium.

We confirmed ANO2 expression in olfactory cilia (Fig. 4.24 A). In addition, we newly identified ANO6 expression in olfactory cilia (Fig. 4.24 B). ANO1 did not localize to the ciliary layer (Fig. 4.24 C), which is in agreement with observations from Billig et al. (2011). Moreover, we noticed a focused distribution of Anoctamins compared to the uniform tubulin stainings along olfactory cilia. Scaffolding proteins influence signaling in olfactory sensory neurons and presumably recruit olfactory receptors and signaling proteins into signaling microdomains (Baumgart et al., 2014; Dooley et al., 2009). Thus, we hypothesized that focused staining of Anoctamin proteins reflected microdomain formation of signaling proteins. We analyzed the subcellular distribution of the CNG channel in olfactory cilia which is part of the olfactory signaling cascade (Kleene, 2008). Using super-resolution microscopy, we demonstrated for the first time that CNG channel forms segregated domains in olfactory cilia (Fig. 4.25). Since diffusion would distribute the protein evenly in the ciliary membrane CNG channel expression in microdomains indicates complex formation or anchoring to static components such as the cytoskeleton. The olfactory CNG channel features no PDZ ligand motif but subunits A2 and A4 interact with olfactory scaffolding protein MUPP1 (Baumgart et al., 2014). Therefore, our findings emphasize that sig-

naling proteins in olfactory cilia are potentially organized in signaling microdomains mediated by scaffolding proteins like MUPP1.

5.6.1 ANO2 and ANO6 possibly mediate signal transduction in olfactory sensory neurons

We continued our analysis of olfactory signaling proteins with ANO2. As for the CNG channel, super-resolution microscopy revealed that ANO2 is localized to segregated microdomains in olfactory cilia (Fig. 4.26 A). In addition to subunits of CNG channel and olfactory receptors, Baumgart et al. (2014) showed interaction of ANO2, $G_{\alpha olf}$ and adenylate cyclase III with MUPP1. Therefore, segregated ANO2 and CNG channel clusters could indeed reflect individual signaling complexes comprised of the complete signaling cascade. We here provide first optical evidence for signaling microdomain formation in olfactory cilia.

We noticed that localization of newly identified ANO6 appeared similar to ANO2 in olfactory cilia (Fig. 4.24). Therefore, we also analyzed subcellular organization of ANO6. Super-resolution microscopy demonstrated that ANO6 also forms segregated domains in olfactory cilia (Fig. 4.26 B). These domains co-localized with ANO2 microdomains (Fig. 4.28). In addition, the size of olfactory microdomains was similar for ANO6, ANO2 and the CNG channel (Fig. 4.30 B). The number of ANO6 clusters in the ciliary layer was identical to the number CNG channel clusters (Fig. 4.30 A). Since MUPP1 recruits ANO2 and CNG channel into one complex (Baumgart et al., 2014), it is likely that all three proteins are present in the same microdomain. ANO6 is a calcium-gated chloride channel and appears in olfactory microdomains which potentially enables ANO6 to participate in olfactory signal transduction.

5.6.2 ANO2 and ANO1 may be the calcium-gated chloride conductance of vomeronasal sensory neurons

Besides the main olfactory epithelium, we confirmed ANO1, ANO2 and ANO6 expression in the vomeronasal organ on RNA level (Fig. 4.23). Expression of ANO2 (Rasche et al., 2010) and ANO1 (Billig et al., 2011) has been described be-

fore, but their localization and physiological relevance remained elusive. Since all three Anoctamins were described as calcium-gated chloride channels (Tian et al., 2012) and the general relevance of chloride currents for vomeronasal signal transduction has been shown before (Kim et al., 2011), we analyzed the localization of these Anoctamins in vomeronasal organ. We identified expression of ANO1 and ANO2 in neuronal microvilli, but not ANO6 (Fig. 4.31). Thus, like in the main olfactory epithelium, ANO2 is co-expressed with another Anoctamin in the vomeronasal organ.

If Anoctamins take part in vomeronasal signaling, we hypothesized that they are most likely organized in signaling microdomains. MUPP1 could mediate microdomain formation in the main olfactory epithelium by binding all components of the signaling cascade (Baumgart et al., 2014). In this work, we present evidence for signaling microdomain formation also in the vomeronasal organ. We identified several scaffolding proteins expressed in the vomeronasal organ. In addition, we demonstrated expression of NHERF1 and DLG1 in neuronal microvilli and showed interaction with signaling cascade constituents, such as vomeronasal receptors. We showed that NHERF1 and signaling protein $G_{\alpha i2}$ co-localize in microdomains in neuronal microvilli. Taken together, we assume vomeronasal signal transduction is also organized in signaling microdomains. Thus, we analyzed subcellular distribution of ANO1 and ANO2 together with vomeronasal signaling protein $G_{\alpha i2}$. Both Anoctamins appeared to be organized in microdomains and partially co-localized with $G_{\alpha i2}$ (Fig. 4.32). Therefore, we conclude that both Anoctamins potentially take part in vomeronasal signaling and signaling proteins also appear organized in signaling microdomains.

5.7 Co-expression of Anoctamins alters current strength

We wondered if co-expression of Anoctamins in the same cell compartment has physiological relevance. To address this question, we co-expressed ANO2 with either ANO1 or ANO6 in HEK293 cells and characterized the properties of chloride currents. Both combinations yielded calcium-gated chloride currents.

Co-expression of ANO2 with ANO1 yielded current densities in between both singular expressions and resulted in an intermediate phenotype (Fig. 4.33). Electrophysiological properties of the channel, like EC_{50} value for calcium activation, niflumic acid sensitivity and chloride conductance were on par with singular expressions of either channel (Drose, 2013). After showing that both Anoctamins are localized to microdomains together with signal transduction protein $G_{\alpha i2}$, we here demonstrated ANO1 and ANO2 co-expression is able to mediate calcium-gated chloride conductance. Together with data from co-localization studies, this could imply a role of both Anoctamins in vomeronasal signaling.

Co-expression of ANO2 with ANO6, as found in olfactory cilia, resulted in a potentiation of current densities (Fig. 4.34). Although physiological properties of the channels remained the same when co-expressed, the current densities were two fold larger than ANO6 and ten fold lager than ANO2 expressed alone. Since we found both Anoctamins present in the same microdomains, this effect likely happens in olfactory signal transduction. Native calcium-gated chloride currents in the olfactory system have been characterized in isolated olfactory sensory neurons (Reisert, 2003) and compared with *in vitro* ANO2 currents. ANO2 elicits currents which resemble native olfactory chloride currents fairly well, but e.g. only with different current densities and current rundown characteristics (Ponissery Saidu et al., 2013; Stephan et al., 2009). Ponissery Saidu et al. (2013) gives the expression of different ANO2 splice variants in olfactory sensory neurons as reason for this discrepancy. As Anoctamin proteins supposedly dimerize (Sheridan et al., 2011; Tien et al., 2013), they speculated that native olfactory chloride channels are heteromers comprised of different ANO2 splice variants.

However, this model did not fully recapitulate native channels *in vitro* (Ponissery Saidu et al., 2013). In addition, due to different technical approaches (suction pipette technique vs. excised patches) elctrophysiological measurements for native olfactory chloride channels and recombinatly expressed ANO2 are hardly comparable. Since we found ANO6, another Anoctamin protein, to be localized with ANO2 in the same microdomains, we propose that differences between native olfactory chloride currents and ANO2 currents could also result

from interaction with ANO6 in olfactory cilia.

5.7.1 Physiological relevance of Anoctamin oligomerization

The potentiation of current densities upon co-expression of ANO2 and ANO6 implies a form of physiological modulation of the chloride channel. In order to investigate this hypothesis, we used BRET measurements to analyze potential physical interaction between Anoctamin proteins and showed ANO1, ANO2 and ANO6 form homo- and hetero-dimers (Fig. 4.36, 4.38). Homodimeric interaction was strong enough to withstand even SDS-PAGE denaturation (Fig. 4.37), which was also observed for ANO6 by Suzuki et al. (2010). Hetero-dimer formation is presumably as resistant, since both dimerization forms are mediated through the same mechanism. We demonstrated that mutation of critical alanine residue at position 169 is enough to abolish homo- and heterodimerization of ANO1 (Fig. 4.40, 4.42, 4.41). This is in agreement with results from Tien et al. (2013).

In contrast to Tien et al. (2013), we also found heteromeric interaction of ANO6 (Fig. 4.38). Our BRET analysis demonstrated interaction between ANO2 and ANO6 which was supported by our electrophysiological measurements. We also found interaction between ANO1 and ANO6 via BRET analysis (Fig. 4.38). This interaction was abrogated by mutating a critical residue A169 from ANO1 dimerization domain (Fig. 4.42). Different methological approaches might explain the differing findings between our study and Tien et al. (2013), the latter used co-immunoprecipitation to probe for Anoctamin interaction. Heterodimerization of Anoctamin proteins may explain modulation of chloride currents we recorded upon co-expression of ANO2 with either ANO1 or ANO6 in HEK293 cells.

Furthermore, we looked at multimerization of Anoctamins in olfactory tissue. We found evidence for complex formation of ANO1 / ANO2 in vomeronasal organ and ANO2 / ANO6 main olfactory epithelium via Western blot (Fig. 4.43). Their presence indicate dimer formation *in vivo* in both olfactory subsystems. It remains to be investigated whether these dimers are homo- or heterodimers, respectively. Moreover, ANO2 and ANO6 co-localized in super-resolution microscopy (Fig. 4.28). In summary, we demonstrated Anoctamin heterodimer

formation is possible in olfactory systems and the interaction has physiological implications for calcium-gated chloride currents.

5.8 Conclusion

Vomeronasal scaffolding proteins NHERF1 and DLG1 could organize vomeronasal signaling. We demonstrated the expression of PDZ scaffolding proteins in the vomeronasal organ and showed that several vomeronasal receptors are PDZ ligands. Thus, we conclude vomeronasal receptors may be organized through PDZ interaction. We showed that PDZ scaffolding proteins NHERF1 and DLG1 are located to microvilli of vomeronasal sensory neurons and interact with vomeronasal receptors. Moreover, these scaffolding proteins interacted with potential signaling proteins from the vomeronasal signaling cascade. Thus, we conclude that NHERF1 and DLG1 may organize vomeronasal signaling through recruiting signaling proteins into functional complexes. NHERF1 could recruit V1 receptors and additional scaffolding proteins into one complex in different ways. This complex could than be tethered to the cytoskeleton by NHERF1. Additional scaffolding proteins could interact with other constituents of the vomeronasal signaling cascade and recruit them into the complex (Fig. 5.1 A-C). Another possible NHERF1 function in vomeronasal sensory neurons is to initiate recycling of receptors after ligand binding (Fig. 5.1 D).

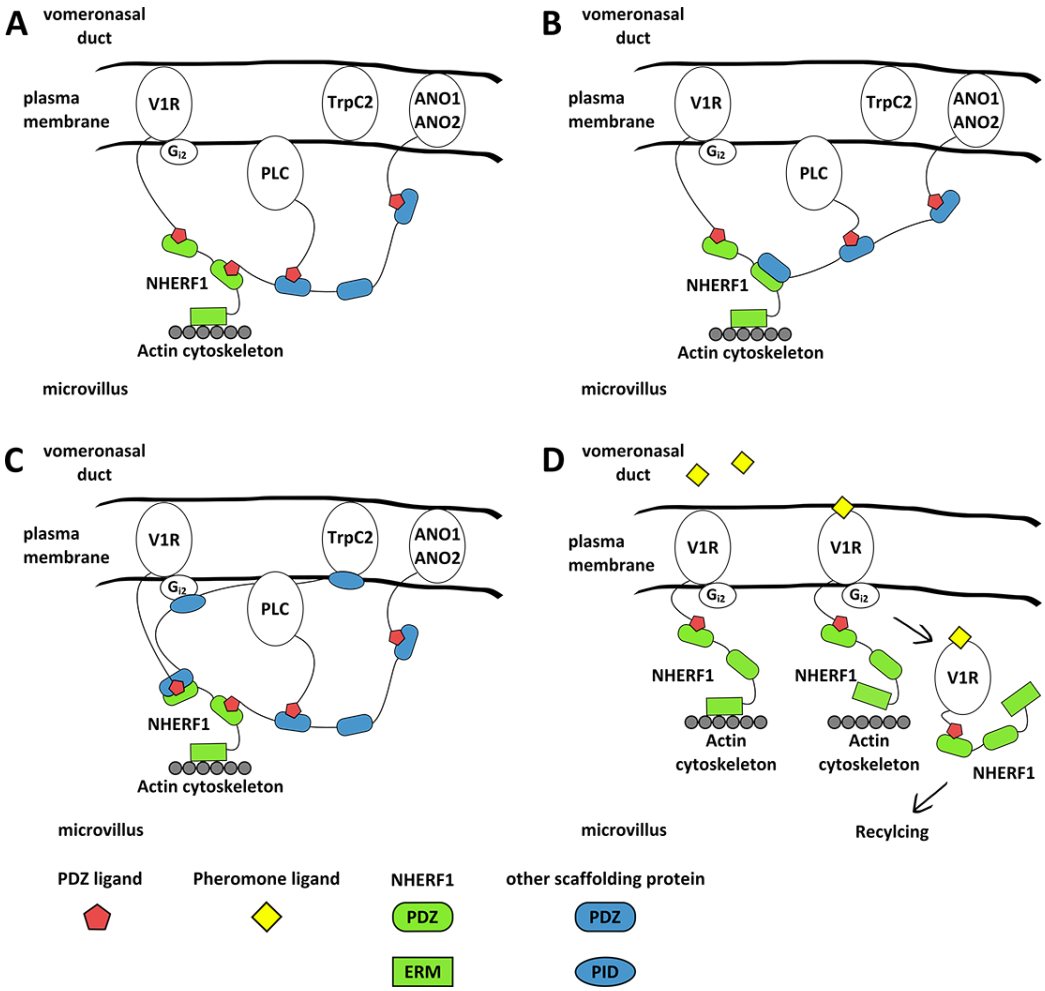

Figure 5.1: Possible models for NHERF1 signaling microdomains. **A:** NHERF1 binding V1 receptors and other scaffolding proteins as PDZ ligands to tether scaffolding complex to cytoskeleton. **B:** NHERF1 engages in PDZ-PDZ domain interaction with other scaffolding proteins to form signaling complexes. **C:** NHERF1 engaging in PDZ-PDZ domain connections to form scaffolding complexes with scaffolding proteins featuring other protein interacting domains. This interaction domains could recruit non-PDZ ligand signaling proteins into signaling complexes **D:** V1 receptors tethered to the cytoskeleton by NHERF1 are recycled to the cell body upon ligand binding. ERM = Ezrin/Radixin/Moesin binding domain, PID = protein interaction domain.

Vomeronasal signaling proteins are organized in segregated microdomains, possibly through interaction with PDZ scaffolding proteins. We further showed that NHERF1 and $G_{\alpha i2}$ co-localize and are organized in segregated microdomains in neuronal microvilli. In addition, we demonstrated co-localization of these microdomains. Thus, we assume vomeronasal signal transduction could be or-

ganized in signaling microdomains and moreover, NHERF1 could play a crucial role in this organization. We further demonstrated that signaling proteins CNG channel and ANO2 are organized in segregated microdomains in cilia of olfactory sensory neurons from the main olfactory epithelium. Since scaffolding proteins in the main olfactory epithelium are known to bind signaling proteins, we assume they organize signal transduction in signaling microdomains.

ANO1 and ANO2 could be part of the vomeronasal signaling cascade. We also showed ANO1 and ANO2 expression in microvilli of vomeronasal sensory neurons. Furthermore, we demonstrated both Anoctamins form segregated microdomains which partially co-localize with signaling protein $G_{\alpha i2}$. We provided evidence for heterodimerization between ANO1 and ANO2 and showed that co-expressed proteins function as calcium-gated chloride channels. Since calcium-gated chloride channels play a substantial role in vomeronasal signaling and our data suggest segregated domains in neuronal microvilli represent signaling microdomains, we assume ANO1 and ANO2 dimers could fulfill this role in vomeronasal signaling.

ANO6 possibly influences signal transduction in olfactory sensory neurons via direct interaction with ANO2. We newly identified expression of ANO6 in olfactory cilia and showed that ANO6 is expressed in segregated microdomains which co-localize with signaling protein ANO2. In addition, we demonstrated direct heterodimerization between ANO2 and ANO6 and showed that presumably this interaction potentiates chloride currents *in vitro*. Moreover, we found ANO2 and ANO6 dimers in olfactory tissue. Thus, we propose calcium-gated chloride currents in main olfactory epithelium could be mediated by a heterodimeric channel of several Anoctamins.

5.9 Perspectives

In this study, we identified a multitude of potential NHERF1 and DLG1 interaction partners expressed in the vomeronasal organ. As we demonstrated inter-

action of both scaffolding proteins with vomeronasal receptors, this work provides a basis to identify further proteins with specific roles in vomeronasal signaling. However, the results from high-throughput approach need to be verified using additional methods.

We provided data for possible role of NHERF1 and DLG1 in the vomeronasal organ, but their contribution to vomeronasal signaling remains unclear and further experiments are needed to analyze the influence of these proteins on vomeronasal signaling. Baumgart et al. (2014) investigate the functional impact of PDZ scaffolding protein MUPP1 on signal transduction in the main olfactory epithelium. They used a patch pipette to infuse short peptides which competed with PDZ ligands for MUPP1 and thereby disrupted PDZ interaction in acute slices. A similar approach would be possible in acute vomeronasal slices with peptides competing for NHERF1 or DLG1 PDZ domains. Furthermore, two mouse lines deficient for NHERF1 are available, but no olfactory phenotype has been described (Morales et al., 2004; Shenolikar et al., 2002). Deficiency of DLG1 is embryonic lethal (Caruana & Bernstein, 2001). Morphological analysis could provide insight into the role of NHERF1 in vomeronasal organ. If microvillar morphology of deficient mice is similar to wildtype mice, an electrophysiological characterization of vomeronasal signals in knockout animals could allow a better understanding of NHERF1s‘ role in the vomeronasal organ. Since mature olfactory neurons specifically express olfactory marker protein OMP, a conditional knockout for NHERF1 or DLG1 could also be established.

DLG1 and NHERF1 both are able to interact with additional scaffolding proteins through several mechanisms. Based on our work, it would be interesting to analyze if additional scaffolding proteins are expressed in neuronal microvilli and if they interact with DLG1 or NHERF1. These experiments could elucidate if olfactory signaling relies on a signaling network similar to *Drosophila* INAD or the postsynaptic density.

This work provides a basis for further investigations of Anoctamin proteins in the olfactory system. Future investigations may aim to elucidate the contribution of Anoctamins to the olfactory current. Initially, Reisert (2003) estimated the majority of olfactory receptor current was carried by chloride. Billig et al.

(2011) provided genetic proof that ANO2 is essential for olfactory chloride currents. However, Billig et al. (2011) also concluded chloride currents are dispensable for olfaction, since they did not find an olfactory phenotype in ANO2 knockout mice. We here identified the presence of ANO6 in olfactory cilia where it could possibly take part in olfactory signaling. However, since ANO6 also plays a role in phospholipid scrambling or volume-sensitive chloride currents (Kunzelmann et al., 2014) it is necessary to verify its contribution to the olfactory current. We also presented evidence for hetero- and homodimrization of Anoctamins and implied physiological relevance for heterodimerization. Based on our findings, it is now possible to proceed with determining the exact composition of Anoctamin channels in olfactory subsystems and their contribution to olfactory signaling.

Abstract

Over 1.000 olfactory receptors and more than 100 vomeronasal receptors translate a tremendous amount of information into electrical signals in sensory neurons. These receptors are part of complex signaling cascades localized in specialized cell compartments. The elements of these cascades are quite well understood, but their spatial arrangement inside the signaling compartments remains elusive.

The existence of signaling microdomains in the olfactory systems, so called olfactosomes, has been already proposed in the early 2000's. It has been recently demonstrated that MUPP1 recruits members of the signaling cascade from olfactory sensory neurons into a functional complex. In this thesis, we investigated organization of signaling proteins and provide first optical evidence for the formation of signaling microdomains in cilia of olfactory sensory neurons and microvilli of vomeronasal sensory neurons.

The investigations comprised three aspects. (1) We identified potential PDZ domain containing scaffolding proteins which could organize the signal transduction cascade in the vomeronasal organ, and identified NHERF1 and DLG1 as potential organizers of vomeronasal signal transduction. NHERF1 and DLG1 were found to be expressed in the vomeronasal organ, localized in microvilli of vomeronasal sensory neurons, and demonstrated to interact with vomeronasal receptors in an *in vitro* interaction assay. (2) We analyzed the spatial organization of signaling proteins in the main olfactory epithelium and the vomeronasal organ using super-resolution microscopy. We demonstrated that signaling proteins in both neuron types are organized in spatially segregated microdomains. This observation includes Anoctamins, NHERF1 and the G protein $G_{\alpha i2}$. (3) We investigated direct interaction between Anoctamin proteins to elucidate their

function as calcium-gated chloride channels in olfactory signal transduction.

Anoctamin 2 was recently identified as the major component of calcium-gated chloride conductance in olfactory sensory neurons. Vomeronasal sensory neurons also rely on calcium-gated chloride channels for signal transduction, their identity, however, remains elusive. We identified Anoctamin 1 and Anoctamin 2 expression microvilli of vomeronasal sensory neurons, and demonstrate co-localization with the signaling protein $G_{\alpha i2}$. We also identified Anoctamin 6 in cilia of olfactory sensory neurons. Anoctamin 6 is also organized in segregated microdomains, co-localizing with Anoctamin 2. Furthermore, we demonstrated direct interaction of Anoctamin 2 with Anoctamin 6 and Anoctamin 1, and this interaction has direct effects on the chloride currents mediated by recombinantly expressed Anoctamin proteins. Co-expression of different Anoctamins could therefore have physiological relevance for olfactory signaling.

Zusammenfassung

Über 1.000 olfaktorische Rezeptoren und mehr als 100 vomeronasale Rezeptoren übersetzen eine enorme Informationsmenge in elektrische Signale in sensorischen Neuronen. Diese Rezeptoren sind Teil komplexer Signalkaskaden, welche sich in spezialisierten Zellkompartimenten abspielen. Die einzelnen Elemente dieser Kaskaden sind inzwischen relativ gut untersucht, ihre räumliche Organisation innerhalb der zellulären Signalkompartimente ist jedoch weiterhin unverstanden.

Die Existenz von Signalmikrodomänen, sogenannter „Olfaktosome“, ist bereits zu Beginn der 2000er Jahre vermutet worden. Kürzlich wurde gezeigt, dass MUPP1 Mitglieder der Signalkaskade in olfaktorischen Neuronen in einem funktionellen Komplex zusammenführt. In dieser Arbeit haben wir die Organisation olfaktorischer Signalproteine analysiert und liefern erste optische Hinweise, für die Formierung von Signalmikrodomänen in den Zilien olfaktorischer Neurone und den Mikrovilli der vomeronasalen Neurone.

Unsere Untersuchung gliederte sich in drei Teilbereiche. (1) Wir haben potentielle Gerüstproteine mit PDZ Domänen identifiziert, die an der vomeronasalen Signaltransduktion beteiligt sein könnten. Dabei haben wir NHERF1 und DLG1 als potentielle Organisatoren der vomeronasalen Signaltransduktion identifiziert. Wir fanden NHERF1 und DLG1 im vomeronasal Organ exprimiert. Dort waren beide Proteine in den Mikrovilli der vomeronasalen Neurone lokalisiert. Mit Hilfe eines *in vitro* Assay demonstrierten wir die Interaktion von NHERF1 und DLG1 mit vomeronasalen Rezeptoren. (2) Wir haben die räumliche Organisation der Signalproteine im olfaktorischen Epithel und im vomeronasal Organ mithilfe von super-resolution Mikroskopie analysiert. Wir haben gezeigt, dass in beiden Neuronentypen die Signalproteine in räumlich getrennten Mikrodomänen organisiert sind. Diese Beobachtung schließt Anoctamine, NHERF1 und das G-Protein Gi2 ein. (3) Wir haben die direkte funktionelle Interaktion zwischen einzelnen Anoctamin-Proteinen untersucht und deren Rolle als Kalzium aktivierte Chlorid-Kanäle für die olfaktorische Signaltransduktion analisert.

Kürzlich wurde Anoctamin 2 als wichtige Komponente des Kalzium aktivierten Chlorid-Stroms in olfaktorischen Neuronen identifiziert. Vomeronasale Neurone benutzen ebenfalls Kalzium aktivierte Chlorid-Ströme zur Signaltransduktion. Die Iden-

tität der beteiligten Protein ist jedoch unbekannt. Wir haben Anoctamin 1 und Anoctamin 2 in den Mikrovilli der vomeronasalen Neurone identifiziert und zeigen, dass beide mit dem Signalprotein Gi2 kolokalisiert sind. Außerdem konnten wir Anoctamin 6 in Zilien der olfaktorischen Neurone identifizieren. Dort liegt Anoctamin 6 in räumlich getrennten Mikrodomänen vor, die ebenfalls Anoctamin 2 enthalten. Weiterhin haben wir gezeigt, dass Anoctamin 2 mit Anoctamin 1 und Anoctamin 6 interagiert und, dass diese Interaktion direkten Einfluss auf die Kalzium aktivierten Chlorid-Ströme hat, wenn Anoctamine rekombinant exprimiert werden. Koexpression verschiedener Anoctamine in Signalkompartimenten der olfaktorischen Systeme könnte dementsprechend Auswirkungen auf die olfaktorische Signaltransduktion haben.

Bibliography

Adamski, F. M., Timms, K. M., & Shieh, B.-H. (1999). A unique isoform of phospholipase cÎš4 highly expressed in the cerebellum and eye. *Biochimica et Biophysica Acta (BBA) - Gene Structure and Expression*, *1444*(1), 55–60.

Ardura, J. A. & Friedman, P. A. (2011). Regulation of g protein-coupled receptor function by Na+/H+ exchange regulatory factors. *Pharmacological Reviews*, *63*(4), 882–900.

Bacart, J., Corbel, C., Jockers, R., Bach, S., & Couturier, C. (2008). The BRET technology and its application to screening assays. *Biotechnology Journal*, *3*(3), 311–324.

Bakalyar, H. A. & Reed, R. R. (1990). Identification of a specialized adenylyl cyclase that may mediate odorant detection. *Science (New York, N.Y.)*, *250*(4986), 1403–1406. PMID: 2255909.

Bauch, C., Koliwer, J., Buck, F., HÃűnck, H.-H., & Kreienkamp, H.-J. (2014). Subcellular sorting of the g-protein coupled mouse somatostatin receptor 5 by a network of PDZ-Domain containing proteins. *PLoS ONE*, *9*(2), e88529.

Baumgart, S., Jansen, F., Bintig, W., Kalbe, B., Herrmann, C., Klumpers, F., KÃűster, S. D., Scholz, P., Rasche, S., Dooley, R., Metzler-Nolte, N., Spehr, M., Hatt, H., & Neuhaus, E. M. (2014). Scaffolding by MUPP1 regulates odorant-mediated signaling in olfactory sensory neurons. *Journal of cell science*. PMID: 24652834.

Berghard, A., Buck, L. B., & Liman, E. R. (1996). Evidence for distinct signaling mechanisms in two mammalian olfactory sense organs. *Proceedings of the National Academy of Sciences*, *93*(6), 2365–2369. PMID: 8637879.

Bhattacharyya, R. P., RemÃľnyi, A., Yeh, B. J., & Lim, W. A. (2006). Domains, motifs, and scaffolds: The role of modular interactions in the evolution and wiring of cell signaling circuits. *Annual Review of Biochemistry*, *75*(1), 655–680.

Billig, G. M., PÃąl, B., Fidzinski, P., & Jentsch, T. J. (2011). Ca2+-activated cl- currents are dispensable for olfaction. *Nature Neuroscience*, *14*(6), 763–769.

Brann, J. H. & Firestein, S. (2010). Regeneration of new neurons is preserved in aged vomeronasal epithelia. *The Journal of Neuroscience*, *30*(46), 15686–15694. PMID: 21084624.

Breer, H., Fleischer, J., & Strotmann, J. (2006). Signaling in the chemosensory systems. *Cellular and Molecular Life Sciences CMLS*, *63*(13), 1465–1475.

Buck, L. & Axel, R. (1991). A novel multigene family may encode odorant receptors: A molecular basis for odor recognition. *Cell*, *65*(1), 175–187.

Bushdid, C., Magnasco, M. O., Vosshall, L. B., & Keller, A. (2014). Humans can discriminate more than 1 trillion olfactory stimuli. *Science*, *343*(6177), 1370–1372.

Cao, T. T., Deacon, H. W., Reczek, D., Bretscher, A., & von Zastrow, M. (1999). A kinase-regulated PDZ-domain interaction controls endocytic sorting of the Îš2-adrenergic receptor. *Nature*, *401*(6750), 286–290.

Capuano, P., Bacic, D., Roos, M., Gisler, S. M., Stange, G., Biber, J., Kaissling, B., Weinman, E. J., Shenolikar, S., Wagner, C. A., & Murer, H. (2007). Defective coupling of apical PTH receptors to phospholipase c prevents internalization of the na+-phosphate cotransporter NaPi-IIa in nherf1-deficient mice. *American Journal of Physiology - Cell Physiology*, *292*(2).

Caputo, A., Caci, E., Ferrera, L., Pedemonte, N., Barsanti, C., Sondo, E., Pfeffer, U., Ravazzolo, R., Zegarra-Moran, O., & Galietta, L. J. V. (2008). TMEM16A, a membrane protein associated with calcium-dependent chloride channel activity. *Science*, *322*(5901), 590–594.

Caruana, G. & Bernstein, A. (2001). Craniofacial dysmorphogenesis including cleft palate in mice with an insertional mutation in the discs large gene. *Molecular and Cellular Biology*, *21*(5), 1475–1483.

Chamero, P., Leinders-Zufall, T., & Zufall, F. (2012). From genes to social communication: molecular sensing by the vomeronasal organ. *Trends in Neurosciences*, *35*(10), 597–606.

Chang, B. H., Gujral, T. S., Karp, E. S., BuKhalid, R., Grantcharova, V. P., & MacBeath, G. (2011). A systematic family-wide investigation reveals that âĹij30% of mammalian PDZ domains engage in PDZ-PDZ interactions. *Chemistry & Biology*, *18*(9), 1143–1152.

Chess, A., Simon, I., Cedar, H., & Axel, R. (1994). Allelic inactivation regulates olfactory receptor gene expression. *Cell*, *78*(5), 823–834.

Cho, S. J., Jeon, J. H., Chun, D. I., Yeo, S. W., & Kim, I.-B. (2014). Anoctamin 1 expression in the mouse auditory brainstem. *Cell and Tissue Research*.

Colledge, M., Dean, R. A., Scott, G. K., Langeberg, L. K., Huganir, R. L., & Scott, J. D. (2000). Targeting of PKA to glutamate receptors through a MAGUK-AKAP complex. *Neuron*, *27*(1), 107–119.

Coppola, D. M., Budde, J., & Millar, L. (1993). The vomeronasal duct has a protracted postnatal development in the mouse. *Journal of Morphology*, *218*(1), 59âĂŞ64.

Cunningham, R., Brazie, M., Kanumuru, S., E, X., Biswas, R., Wang, F., Steplock, D., Wade, J. B., Anzai, N., Endou, H., Shenolikar, S., & Weinman, E. J. (2007). Sodium-hydrogen exchanger regulatory factor-1 interacts with mouse urate transporter 1 to regulate renal proximal tubule uric acid transport. *Journal of the American Society of Nephrology*, *18*(5), 1419–1425. PMID: 17409311.

Dam, V. S., Boedtkjer, D. M. B., Nyvad, J., Aalkjaer, C., & Matchkov, V. (2013). TMEM16A knockdown abrogates two different ca2+-activated clâĹŠ currents and contractility of smooth muscle in rat mesenteric small arteries. *PflÃijgers Archiv - European Journal of Physiology*.

Dielenberg, R. A. & McGregor, I. S. (2001). Defensive behavior in rats towards predatory odors: a review. *Neuroscience & Biobehavioral Reviews*, *25*(7âĂŞ8), 597–609.

Dooley, R., Baumgart, S., Rasche, S., Hatt, H., & Neuhaus, E. M. (2009). Olfactory receptor signaling is regulated by the post-synaptic density 95, drosophila discs large, zona-occludens 1 (PDZ) scaffold multi-PDZ domain protein 1. *FEBS Journal*, *276*(24), 7279âĂŞ7290.

Drose, D. (2013). Physiologische charakterisierung rekombinanter chemosensorischer signalproteine. *Masterarbeit, FakultÃďt fÃijr Mathematik, Informatik und Naturwissenschaften, Institut fÃijr Biologie II, LuF Chemosensorik, RWTH Aachen*.

Dulac, C. & Torello, A. T. (2003). Molecular detection of pheromone signals in mammals: from genes to behaviour. *Nature Reviews Neuroscience*, *4*(7), 551–562.

Ediger, T. R., Kraus, W. L., Weinman, E. J., & Katzenellenbogen, B. S. (1999). Estrogen receptor regulation of the Na+/H+ exchange regulatory factor. *Endocrinology*, *140*(7), 2976–2982.

Eisthen, H. L. (1992). Phylogeny of the vomeronasal system and of receptor cell types in the olfactory and vomeronasal epithelia of vertebrates. *Microscopy research and technique*, *23*(1), 1–21. PMID: 1392068.

Elsaesser, R. & Paysan, J. (2007). The sense of smell, its signalling pathways, and the dichotomy of cilia and microvilli in olfactory sensory cells. *BMC Neuroscience*, *8*(Suppl 3), S1. PMID: 17903277.

Ezan, J., Lasvaux, L., Gezer, A., Novakovic, A., May-Simera, H., Belotti, E., Lhoumeau, A.-C., Birnbaumer, L., Beer-Hammer, S., Borg, J.-P., Le Bivic, A., NÃijrnberg, B., Sans, N., & Montcouquiol, M. (2013). Primary cilium migration depends on g-protein signalling control of subapical cytoskeleton. *Nature Cell Biology*, *15*(9), 1107–1115.

Fath, K. R. & Burgess, D. R. (1995). Microvillus assembly: Not actin alone. *Current Biology*, *5*(6), 591–593.

Faulstich, H., Zobeley, S., Rinnerthaler, G., & Small, J. V. (1988). Fluorescent phallotoxins as probes for filamentous actin. *Journal of muscle research and cell motility*, *9*(5), 370–383. PMID: 3063723.

Feng, W., Long, J.-F., Fan, J.-S., Suetake, T., & Zhang, M. (2004). The tetrameric l27 domain complex as an organization platform for supramolecular assemblies. *Nature Structural & Molecular Biology*, *11*(5), 475–480.

Feng, W. & Zhang, M. (2009). Organization and dynamics of PDZ-domain-related supramodules in the postsynaptic density. *Nature Reviews Neuroscience*, *10*(2), 87–99.

Fouassier, L., Yun, C. C., Fitz, J. G., & Doctor, R. B. (2000). Evidence for ezrin-radixin-moesin-binding phosphoprotein 50 (EBP50) self-association through PDZ-PDZ interactions. *Journal of Biological Chemistry*, *275*(32), 25039–25045.

Francia, S., Pifferi, S., Menini, A., & Tirindelli, R. (2014). Vomeronasal receptors and signal transduction in the vomeronasal organ of mammals. In C. Mucignat-Caretta (Ed.), *Neurobiology of Chemical Communication*, Frontiers in Neuroscience. Boca Raton (FL): CRC Press. PMID: 24830038.

Fuelle, H. J., Vassar, R., Foster, D. C., Yang, R. B., Axel, R., & Garbers, D. L. (1995). A receptor guanylyl cyclase expressed specifically in olfactory sensory neurons. *Proceedings of the National Academy of Sciences of the United States of America*, *92*(8), 3571–3575.

Fujita, A. & Kurachi, Y. (2000). SAP family proteins. *Biochemical and Biophysical Research Communications*, *269*(1), 1–6.

Fung, B. K., Hurley, J. B., & Stryer, L. (1981). Flow of information in the light-triggered cyclic nucleotide cascade of vision. *Proceedings of the National Academy of Sciences of the United States of America*, *78*(1), 152–156.

Funke, L., Dakoji, S., & Bredt, D. S. (2005). Membrane-associated guanylate kinases regulate adhesion and plasticity at cell junctions. *Annual Review of Biochemistry*, *74*(1), 219–245.

Gage, R. M., Matveeva, E. A., Whiteheart, S. W., & Zastrow, M. v. (2005). Type i PDZ ligands are sufficient to promote rapid recycling of g protein-coupled receptors independent of binding to n-ethylmaleimide-sensitive factor. *Journal of Biological Chemistry*, *280*(5), 3305–3313.

Garbett, D. & Bretscher, A. (2012). PDZ interactions regulate rapid turnover of the scaffolding protein EBP50 in microvilli. *The Journal of Cell Biology*, *198*(2), 195–203.

Garbett, D., LaLonde, D. P., & Bretscher, A. (2010). The scaffolding protein EBP50 regulates microvillar assembly in a phosphorylation-dependent manner. *The Journal of Cell Biology*, *191*(2), 397–413.

Gardner, L. A., Naren, A. P., & Bahouth, S. W. (2007). Assembly of an SAP97-AKAP79-cAMP-dependent protein kinase scaffold at the type 1 PSD-95/DLG/ZO1 motif of the human Îš1-adrenergic receptor generates a receptosome involved in receptor recycling and networking. *Journal of Biological Chemistry*, *282*(7), 5085–5099. PMID: 17170109.

Georgescu, M.-M., Morales, F., Molina, J., & Hayashi, Y. (2008). Roles of NHERF1/EBP50 in cancer. *Current Molecular Medicine*, *8*(6), 459–468.

Good, M. C., Zalatan, J. G., & Lim, W. A. (2011). Scaffold proteins: Hubs for controlling the flow of cellular information. *Science*, *332*(6030), 680–686.

Graham, F. L., Smiley, J., Russell, W. C., & Nairn, R. (1977). Characteristics of a human cell line transformed by DNA from human adenovirus type 5. *Journal of General Virology*, *36*(1), 59–72. PMID: 886304.

Graziadei, P. P. C. & Monti Graziadei, A. G. (1983). Regeneration in the olfactory system of vertebrates. *American Journal of Otolaryngology*, *4*(4), 228–233.

Grubb, S., Poulsen, K. A., Juul, C. A., Kyed, T., Klausen, T. K., Larsen, E. H., & Hoffmann, E. K. (2013). TMEM16F (anoctamin 6), an anion channel of delayed ca2+ activation. *The Journal of General Physiology*, *141*(5), 585–600. PMID: 23630341.

Hall, R. A., Ostedgaard, L. S., Premont, R. T., Blitzer, J. T., Rahman, N., Welsh, M. J., & Lefkowitz, R. J. (1998). A c-terminal motif found in the Îš2-adrenergic receptor, P2Y1 receptor and cystic fibrosis transmembrane conductance regulator determines binding to the Na+/H+ exchanger regulatory factor family of PDZ proteins. *Proceedings of the National Academy of Sciences*, *95*(15), 8496–8501. PMID: 9671706.

Halpern, M. & Martinez-Marcos, A. (2003). Structure and function of the vomeronasal system: an update. *Progress in Neurobiology*, *70*(3), 245–318.

Hanahan, D. (1983). Studies on transformation of escherichia coli with plasmids. *Journal of Molecular Biology*, *166*(4), 557–580.

Hardie, R. C. & Raghu, P. (2001). Visual transduction in drosophila. *Nature*, *413*(6852), 186–193.

Hartzell, C., Putzier, I., & Arreola, J. (2005). Calcium-activated chloride channels. *Annual Review of Physiology*, *67*(1), 719–758.

He, J., Bellini, M., Inuzuka, H., Xu, J., Xiong, Y., Yang, X., Castleberry, A. M., & Hall, R. A. (2006). Proteomic analysis of Îš1-adrenergic receptor interactions with PDZ scaffold proteins. *Journal of Biological Chemistry*, *281*(5), 2820–2827. PMID: 16316992.

Heinze, C., Seniuk, A., Sokolov, M. V., Huebner, A. K., Klementowicz, A. E., SzijÃąrtÃş, I. A., Schleifenbaum, J., Vitzthum, H., Gollasch, M., Ehmke, H., Schroeder, B. C., & HÃijbner, C. A. (2014). Disruption of vascular ca2+-activated chloride currents lowers blood pressure. *Journal of Clinical Investigation*, *124*(2), 675–686.

Hensel, M., Klingauf, J., & Piehler, J. (2013). Imaging the invisible: resolving cellular microcompartments by superresolution microscopy techniques. *Biological Chemistry*, *394*(9), 1097âĂŞ1113.

Heydorn, A., SÃÿndergaard, B. P., ErsbÃÿll, B., Holst, B., Nielsen, F. C., Haft, C. R., Whistler, J., & Schwartz, T. W. (2004). A library of 7TM receptor c-terminal

tails INTERACTIONS WITH THE PROPOSED POST-ENDOCYTIC SORTING PROTEINS ERM-BINDING PHOSPHOPROTEIN 50 (EBP50), n-ETHYLMALEIMIDE-SENSITIVE FACTOR (NSF), SORTING NEXIN 1 (SNX1), AND g PROTEIN-COUPLED RECEPTOR-ASSOCIATED SORTING PROTEIN (GASP). *Journal of Biological Chemistry*, *279*(52), 54291–54303.

Horowitz, L. F., Montmayeur, J.-P., Echelard, Y., & Buck, L. B. (1999). A genetic approach to trace neural circuits. *Proceedings of the National Academy of Sciences*, *96*(6), 3194–3199. PMID: 10077660.

Huang, P. (2004). Opioid receptor interacts with Na+/H+-exchanger regulatory factor-1/Ezrin-Radixin-Moesin-binding phosphoprotein-50 (NHERF-1/EBP50) to stimulate Na+/H+ exchange independent of Gi/Go proteins. *Journal of Biological Chemistry*, *279*(24), 25002–25009.

Huard, J. M. T. & Schwob, J. E. (1995). Cell cycle of globose basal cells in rat olfactory epithelium. *Developmental Dynamics*, *203*(1), 17–26.

Huber, A. (2001). Scaffolding proteins organize multimolecular protein complexes for sensory signal transduction. *European Journal of Neuroscience*, *14*(5), 769âĂŞ776.

Ingraffea, J., Reczek, D., & Bretscher, A. (2002). Distinct cell type-specific expression of scaffolding proteins EBP50 and E3KARP: EBP50 is generally expressed with ezrin in specific epithelia, whereas E3KARP is not. *European Journal of Cell Biology*, *81*(2), 61–68.

Ishikawa, H. & Marshall, W. F. (2011). Ciliogenesis: building the cell's antenna. *Nature Reviews Molecular Cell Biology*, *12*(4), 222–234.

Jang, Y. & Oh, U. (2014). Anoctamin 1 in secretory epithelia. *Cell Calcium*.

Jelen, F., Oleksy, A., Smietana, K., & Otlewski, J. (2003). PDZ domains - common players in the cell signaling. *Acta biochimica Polonica*, *50*(4), 985–1017.

Jeon, J. H., Paik, S. S., Chun, M.-H., Oh, U., & Kim, I.-B. (2013). Presynaptic localization and possible function of calcium-activated chloride channel anoctamin 1 in the mammalian retina. *PLoS ONE*, *8*(6), e67989.

Jia, C. & Halpern, M. (1996). Subclasses of vomeronasal receptor neurons: differential expression of g proteins (giÎś2 and goÎś) and segregated projections to the accessory olfactory bulb. *Brain Research*, *719*(1âĂŞ2), 117–128.

Jin, X., Shah, S., Liu, Y., Zhang, H., Lees, M., Fu, Z., Lippiat, J. D., Beech, D. J., Sivaprasadarao, A., Baldwin, S. A., & others (2013). Activation of the cl-channel ANO1 by localized calcium signals in nociceptive sensory neurons requires coupling with the IP3 receptor. *Science signaling*, *6*(290), ra73.

Jones, D. T. & Reed, R. R. (1989). Golf: an olfactory neuron specific-g protein involved in odorant signal transduction. *Science (New York, N.Y.)*, *244*(4906), 790–795. PMID: 2499043.

Jung, J., Nam, J. H., Park, H. W., Oh, U., Yoon, J.-H., & Lee, M. G. (2013). Dynamic modulation of ANO1/TMEM16A HCO3âĹŠ permeability by ca2+/calmodulin. *Proceedings of the National Academy of Sciences*, *110*(1), 360–365.

Juul, C. A., Grubb, S., Poulsen, K. A., Kyed, T., Hashem, N., Lambert, I. H., Larsen, E. H., & Hoffmann, E. K. (2014). Anoctamin 6 differs from VRAC and VSOAC but is involved in apoptosis and supports volume regulation in the presence of ca2+. *PflÃijgers Archiv - European Journal of Physiology*, 1–12.

Karthikeyan, S., Leung, T., Birrane, G., Webster, G., & Ladias, J. A. A. (2001). Crystal structure of the PDZ1 domain of human Na+/H+ exchanger regulatory factor provides insights into the mechanism of carboxyl-terminal leucine recognition by class i PDZ domains. *Journal of Molecular Biology*, *308*(5), 963–973.

Kim, J. K., Choi, J. W., Lim, S., Kwon, O., Seo, J. K., Ryu, S. H., & Suh, P.-G. (2011). Phospholipase c-Îů1 is activated by intracellular ca2+ mobilization and enhances GPCRs/PLC/Ca2+ signaling. *Cellular Signalling*, *23*(6), 1022–1029.

Kim, J. K., Lim, S., Kim, J., Kim, S., Kim, J. H., Ryu, S. H., & Suh, P.-G. (2011). Subtype-specific roles of phospholipase c-Îš via differential interactions with PDZ domain proteins. *Advances in Enzyme Regulation*, *51*(1), 138–151.

Kim, M. J., Min, D. S., Ryu, S. H., & Suh, P.-G. (1998). A cytosolic, gÎśq- and ÎšÎş-insensitive splice variant of phospholipase c-Îš4. *Journal of Biological Chemistry*, *273*(6), 3618–3624. PMID: 9452490.

Kim, S., Ma, L., & Yu, C. R. (2011). Requirement of calcium-activated chloride channels in the activation of mouse vomeronasal neurons. *Nature Communications*, *2*, 365.

Kim, Y., Chattopadhyay, S., Locke, S., & Pearce, D. A. (2005). Interaction among btn1p, btn2p, and ist2p reveals potential interplay among the vacuole, amino acid levels, and ion homeostasis in the yeast saccharomyces cerevisiae. *Eukaryotic Cell*, *4*(2), 281–288.

Kimoto, H., Haga, S., Sato, K., & Touhara, K. (2005). Sex-specific peptides from exocrine glands stimulate mouse vomeronasal sensory neurons. *Nature*, *437*(7060), 898–901.

Kirkup, A. J., Edwards, G., Green, M. E., Miller, M., Walker, S. D., & Weston, A. H. (1996). Modulation of membrane currents and mechanical activity by niflumic acid in rat vascular smooth muscle. *European Journal of Pharmacology*, *317*(1), 165–174.

Kleene, S. J. (2008). The electrochemical basis of odor transduction in vertebrate olfactory cilia. *Chemical Senses*, *33*(9), 839–859. PMID: 18703537.

Kleene, S. J. & Gesteland, R. C. (1991). Calcium-activated chloride conductance in frog olfactory cilia. *The Journal of Neuroscience*, *11*(11), 3624–3629.

Kleene, S. J., Gesteland, R. C., & Bryant, S. H. (1994). An electrophysiological survey of frog olfactory cilia. *The Journal of Experimental Biology*, *195*(1), 307–328. PMID: 7964415.

Klenoff, J. R. & Greer, C. A. (1998). Postnatal development of olfactory receptor cell axonal arbors. *The Journal of Comparative Neurology*, *390*(2), 256–267.

Kmit, A., van Kruchten, R., Ousingsawat, J., Mattheij, N. J. A., Senden-Gijsbers, B., Heemskerk, J. W. M., Schreiber, R., Bevers, E. M., & Kunzelmann, K. (2013). Calcium-activated and apoptotic phospholipid scrambling induced by ano6 can occur independently of ano6 ion currents. *Cell Death & Disease*, *4*(4), e611.

Kobayakawa, K., Kobayakawa, R., Matsumoto, H., Oka, Y., Imai, T., Ikawa, M., Okabe, M., Ikeda, T., Itohara, S., Kikusui, T., Mori, K., & Sakano, H. (2007). Innate versus learned odour processing in the mouse olfactory bulb. *Nature*, *450*(7169), 503–508.

Kolnberger, I. (1971). Vergleichende untersuchungen am riechepithel, insbesondere des jacobsonschen organs von amphibien, reptilien und saugetieren. *Z. Zellforsch.*, *122*, 53–67.

Kott, J. N. & Westrum, L. E. (1996). Developmental localization of GAP-43 and olfactory marker protein in rat olfactory bulb transplants. *International journal of developmental neuroscience: the official journal of the International Society for Developmental Neuroscience*, *14*(7-8), 961–970. PMID: 9010738.

Kozubowski, L., Saito, K., Johnson, J. M., Howell, A. S., Zyla, T. R., & Lew, D. J. (2008). Symmetry-breaking polarization driven by a cdc42p GEF-PAK complex. *Current biology: CB*, *18*(22), 1719–1726.

Kuhlmann, K., Tschapek, A., Wiese, H., Eisenacher, M., Meyer, H. E., Hatt, H. H., Oeljeklaus, S., & Warscheid, B. (2014). The membrane proteome of sensory cilia to the depth of olfactory receptors. *Molecular & Cellular Proteomics*, mcp.M113.035378.

Kunzelmann, K., Nilius, B., Owsianik, G., Schreiber, R., Ousingsawat, J., Sirianant, L., Wanitchakool, P., Bevers, E. M., & Heemskerk, J. W. M. (2014). Molecular functions of anoctamin 6 (TMEM16F): a chloride channel, cation channel, or phospholipid scramblase? *PflÃijgers Archiv - European Journal of Physiology*, *466*(3), 407–414.

Kunzelmann, K., Schreiber, R., Kmit, A., Jantarajit, W., Martins, J. R., Faria, D., Kongsuphol, P., Ousingsawat, J., & Tian, Y. (2011). Expression and function of epithelial anoctamins. *Experimental Physiology*, no–no.

Kunzelmann, K., Tian, Y., Martins, J. R., Faria, D., Kongsuphol, P., Ousingsawat, J., Thevenod, F., Roussa, E., Rock, J., & Schreiber, R. (2011). Anoctamins. *PflÃijgers Archiv - European Journal of Physiology*, *462*(2), 195–208.

LaLonde, D. P., Garbett, D., & Bretscher, A. (2010). A regulated complex of the scaffolding proteins PDZK1 and EBP50 with ezrin contribute to microvillar organization. *Molecular Biology of the Cell*, *21*(9), 1519–1529.

Lau, A. G. & Hall, R. A. (2001). Oligomerization of NHERF-1 and NHERF-2 PDZ domains:âĂĽ differential regulation by association with receptor carboxyl-termini and by phosphorylationâĂă. *Biochemistry*, *40*(29), 8572–8580.

Lauffer, B. E. L., Chen, S., Melero, C., Kortemme, T., Zastrow, M. v., & Vargas, G. A. (2009). Engineered protein connectivity to actin mimics PDZ-dependent recycling of g protein-coupled receptors but not its regulation by hrs. *Journal of Biological Chemistry*, *284*(4), 2448–2458.

Lee, S., Fan, S., Makarova, O., Straight, S., & Margolis, B. (2002). A novel and conserved protein-protein interaction domain of mammalian lin-2/CASK binds and recruits SAP97 to the lateral surface of epithelia. *Molecular and Cellular Biology*, *22*(6), 1778–1791. PMID: 11865057.

Leinders-Zufall, T., Brennan, P., Widmayer, P., S, P. C., Maul-Pavicic, A., JÃďger, M., Li, X.-H., Breer, H., Zufall, F., & Boehm, T. (2004). MHC class i peptides as chemosensory signals in the vomeronasal organ. *Science*, *306*(5698), 1033–1037. PMID: 15528444.

Leinders-Zufall, T., Lane, A. P., Puche, A. C., Ma, W., Novotny, M. V., Shipley, M. T., & Zufall, F. (2000). Ultrasensitive pheromone detection by mammalian vomeronasal neurons. *Nature*, *405*(6788), 792–796.

Lenfant, N., Polanowska, J., Bamps, S., Omi, S., Borg, J.-P., & Reboul, J. (2010). A genome-wide study of PDZ-domain interactions in c. elegans reveals a high frequency of non-canonical binding. *BMC Genomics*, *11*(1), 671.

L'Etoile, N. D. & Bargmann, C. I. (2000). Olfaction and odor discrimination are mediated by the c. elegans guanylyl cyclase ODR-1. *Neuron*, *25*(3), 575–586.

Liberles, S. D. & Buck, L. B. (2006). A second class of chemosensory receptors in the olfactory epithelium. *Nature*, *442*(7103), 645–650.

Liebman, P. A. & Pugh Jr, E. N. (1979). The control of phosphodiesterase in rod disk membranes: Kinetics, possible mechanisms and significance for vision. *Vision Research*, *19*(4), 375–380.

Liman, E. R., Corey, D. P., & Dulac, C. (1999). TRP2: a candidate transduction channel for mammalian pheromone sensory signaling. *Proceedings of the National Academy of Sciences*, *96*(10), 5791–5796. PMID: 10318963.

Lindemann, B. (2001). Predicted profiles of ion concentrations in olfactory cilia in the steady state. *Biophysical Journal*, *80*(4), 1712–1721.

Lucas, P., Ukhanov, K., Leinders-Zufall, T., & Zufall, F. (2003). A diacylglycerol-gated cation channel in vomeronasal neuron dendrites is impaired in TRPC2 mutant mice: Mechanism of pheromone transduction. *Neuron*, *40*(3), 551–561.

Luck, K., Charbonnier, S., & TravÃľ, G. (2012). The emerging contribution of sequence context to the specificity of protein interactions mediated by PDZ domains. *FEBS Letters*, *586*(17), 2648–2661.

Mahon, M. J. & Segre, G. V. (2004). Stimulation by parathyroid hormone of a NHERF-1-assembled complex consisting of the parathyroid hormone i receptor, phospholipase cÎš, and actin increases intracellular calcium in opossum kidney cells. *Journal of Biological Chemistry*, *279*(22), 23550–23558. PMID: 15037630.

Marg, A., Haase, H., Neumann, T., Kouno, M., & Morano, I. (2010). AHNAK1 and AHNAK2 are costameric proteins: AHNAK1 affects transverse skeletal muscle fiber stiffness. *Biochemical and Biophysical Research Communications*, *401*(1), 143–148.

Martins, J. R., Faria, D., Kongsuphol, P., Reisch, B., Schreiber, R., & Kunzelmann, K. (2011). Anoctamin 6 is an essential component of the outwardly rectifying chloride channel. *Proceedings of the National Academy of Sciences*, *108*(44), 18168–18172. PMID: 22006324.

Mashukova, A., Spehr, M., Hatt, H., & Neuhaus, E. M. (2006). Îš-arrestin2-mediated internalization of mammalian odorant receptors. *The Journal of Neuroscience*, *26*(39), 9902–9912.

Menco, B. P. (1984). Ciliated and microvillous structures of rat olfactory and nasal respiratory epithelia. a study using ultra-rapid cryo-fixation followed by freeze-substitution or freeze-etching. *Cell and tissue research*, *235*(2), 225–241. PMID: 6367994.

Menco, B. P. M., Carr, V. M., Ezeh, P. I., Liman, E. R., & Yankova, M. P. (2001). Ultrastructural localization of g-proteins and the channel protein TRP2 to microvilli of rat vomeronasal receptor cells. *Journal of Comparative Neurology*, *438*(4), 468âĂŞ489.

Milenkovic, V. M., Brockmann, M., StÃűhr, H., Weber, B. H., & Strauss, O. (2010). Evolution and functional divergence of the anoctamin family of membrane proteins. *BMC evolutionary biology*, *10*(1), 319.

Mombaerts, P. (2004). Genes and ligands for odorant, vomeronasal and taste receptors. *Nature Reviews Neuroscience*, *5*(4), 263–278.

Montell, C. (1998). TRP trapped in fly signaling web. *Current Opinion in Neurobiology*, *8*(3), 389–397.

Montell, C. (2012). Drosophila visual transduction. *Trends in Neurosciences*, *35*(6), 356–363.

Morales, F. C., Takahashi, Y., Kreimann, E. L., & Georgescu, M.-M. (2004). EzrinâĂŞradixinâĂŞmoesin (ERM)-binding phosphoprotein 50 organizes ERM proteins at the apical membrane of polarized epithelia. *Proceedings of the National Academy of Sciences of the United States of America*, *101*(51), 17705–17710.

Morales, F. C., Takahashi, Y., Momin, S., Adams, H., Chen, X., & Georgescu, M.-M. (2007). NHERF1/EBP50 head-to-tail intramolecular interaction masks association with PDZ domain ligands. *Molecular and Cellular Biology*, *27*(7), 2527–2537. PMID: 17242191.

Mostarda, S., Gfeller, D., & Rao, F. (2012). Beyond the binding site: The role of the Îš2 âĂŞ Îš3 loop and extra-domain structures in PDZ domains. *PLoS Comput Biol*, *8*(3), e1002429.

Moulton, D. G. & Beidler, L. M. (1967). Structure and function in the peripheral olfactory system. *Physiological Reviews*, *47*(1), 1–52. PMID: 5343221.

Muller, B. M., Kistner, U., Veh, R. W., Cases-Langhoff, C., Becker, B., Gundelfinger, E. D., & Garner, C. C. (1995). Molecular characterization and spatial distribution of SAP97, a novel presynaptic protein homologous to SAP90 and the drosophila discs-large tumor suppressor protein. *The Journal of Neuroscience*, *15*(3), 2354–2366.

Munger, S. D., Leinders-Zufall, T., & Zufall, F. (2009). Subsystem organization of the mammalian sense of smell. *Annual Review of Physiology*, *71*(1), 115–140. PMID: 18808328.

Nakagawa, T., Futai, K., Lashuel, H. A., Lo, I., Okamoto, K., Walz, T., Hayashi, Y., & Sheng, M. (2004). Quaternary structure, protein dynamics, and synaptic function of SAP97 controlled by l27 domain interactions. *Neuron*, *44*(3), 453–467.

Naren, A. P., Cobb, B., Li, C., Roy, K., Nelson, D., Heda, G. D., Liao, J., Kirk, K. L., Sorscher, E. J., Hanrahan, J., & Clancy, J. P. (2003). A macromolecular complex of ?2 adrenergic receptor, CFTR, and ezrin/radixin/moesin-binding phosphoprotein 50 is regulated by PKA. *Proceedings of the National Academy of Sciences of the United States of America*, *100*(1), 342–346. PMID: 12502786 PMCID: PMC140971.

Nooh, M. M., Naren, A. P., Kim, S.-J., Xiang, Y. K., & Bahouth, S. W. (2013). SAP97 controls the trafficking and resensitization of the beta-1-adrenergic receptor through its PDZ2 and i3 domains. *PLoS ONE*, *8*(5), e63379.

Nourry, C., Grant, S. G. N., & Borg, J.-P. (2003). PDZ domain proteins: Plug and play! *Science Signaling*, *2003*(179), re7.

Oberland, S. (2014). A novel olfactory subset: Cd36-expressing neurons and their role in murine suckling. *PhD Thesis, Department of Biology, Chemistry and Pharmacy, Freie Universitaet Berlin*.

Oliveria, S. F., Gomez, L. L., & Dell'Acqua, M. L. (2003). Imaging kinaseâĂŞAKAP79âĂŞphosphatase scaffold complexes at the plasma membrane in living cells using FRET microscopy. *The Journal of Cell Biology*, *160*(1), 101–112. PMID: 12507994.

Pak, W. L., Grossfield, J., & Arnold, K. S. (1970). Mutants of the visual pathway of drosophila melanogaster. *Nature*, *227*(5257), 518–520.

Pawson, T. & Nash, P. (2003). Assembly of cell regulatory systems through protein interaction domains. *Science*, *300*(5618), 445–452.

Pedemonte, N. & Galietta, L. J. V. (2014). Structure and function of TMEM16 proteins (anoctamins). *Physiological Reviews*, *94*(2), 419–459.

Pifferi, S., Dibattista, M., & Menini, A. (2009). TMEM16B induces chloride currents activated by calcium in mammalian cells. *PflÃijgers Archiv - European Journal of Physiology*, *458*(6), 1023–1038.

Ponissery Saidu, S., Stephan, A. B., Talaga, A. K., Zhao, H., & Reisert, J. (2013). Channel properties of the splicing isoforms of the olfactory calcium-activated chloride channel anoctamin 2. *The Journal of General Physiology*, *141*(6), 691–703.

Potter, S. M., Zheng, C., Koos, D. S., Feinstein, P., Fraser, S. E., & Mombaerts, P. (2001). Structure and emergence of specific olfactory glomeruli in the mouse. *The Journal of Neuroscience*, *21*(24), 9713–9723. PMID: 11739580.

Ranganathan, R., Harris, G. L., Stevens, C. F., & Zuker, C. S. (1991). A drosophila mutant defective in extracellular calcium-dependent photoreceptor deactivation and rapid desensitization. *Nature*, *354*(6350), 230–232. PMID: 1961249.

Rankin, M. L., Alvania, R. S., Gleason, E. L., & Bruch, R. C. (1999). Internalization of g protein-coupled receptors in single olfactory receptor neurons. *Journal of Neurochemistry*, *72*(2), 541–548.

Rasche, S., Toetter, B., Adler, J., Tschapek, A., Doerner, J. F., Kurtenbach, S., Hatt, H., Meyer, H., Warscheid, B., & Neuhaus, E. M. (2010). Tmem16b is specifically expressed in the cilia of olfactory sensory neurons. *Chemical Senses*, *35*(3), 239–245. PMID: 20100788.

Reczek, D., Berryman, M., & Bretscher, A. (1997). Identification of EBP50: a PDZ-containing phosphoprotein that associates with members of the ezrin-radixin-moesin family. *The Journal of Cell Biology*, *139*(1), 169–179.

Reisert, J. (2003). The ca-activated cl channel and its control in rat olfactory receptor neurons. *The Journal of General Physiology*, *122*(3), 349–364.

Reuver, S. M. & Garner, C. C. (1998). E-cadherin mediated cell adhesion recruits SAP97 into the cortical cytoskeleton. *Journal of Cell Science*, *111*(8), 1071–1080.

Riviere, S., Challet, L., Fluegge, D., Spehr, M., & Rodriguez, I. (2009). Formyl peptide receptor-like proteins are a novel family of vomeronasal chemosensors. *Nature*, *459*(7246), 574–577.

Roepman, R. & Wolfrum, U. (2007). Protein networks and complexes in photoreceptor cilia. *Sub-cellular biochemistry*, *43*, 209–235. PMID: 17953396.

Sabio, G., Arthur, J. S. C., Kuma, Y., Peggie, M., Carr, J., Murray-Tait, V., Centeno, F., Goedert, M., Morrice, N. A., & Cuenda, A. (2005). p38? regulates the localisation of SAP97 in the cytoskeleton by modulating its interaction with GKAP. *The EMBO Journal*, *24*(6), 1134–1145. PMID: 15729360 PMCID: PMC556394.

Sanders, K. M., Zhu, M. H., Britton, F., Koh, S. D., & Ward, S. M. (2011). Anoctamins and gastrointestinal smooth muscle excitability. *Experimental Physiology*, no–no.

Sans, N., Racca, C., Petralia, R. S., Wang, Y.-X., McCallum, J., & Wenthold, R. J. (2001). Synapse-associated protein 97 selectively associates with a subset of AMPA receptors early in their biosynthetic pathway. *The Journal of Neuroscience*, *21*(19), 7506–7516. PMID: 11567040.

Schroeder, B. C., Cheng, T., Jan, Y. N., & Jan, L. Y. (2008). Expression cloning of TMEM16A as a calcium-activated chloride channel subunit. *Cell*, *134*(6), 1019–1029.

Shenolikar, S., Voltz, J. W., Minkoff, C. M., Wade, J. B., & Weinman, E. J. (2002). Targeted disruption of the mouse NHERF-1 gene promotes internalization of proximal tubule sodium-phosphate cotransporter type IIa and renal phosphate wasting. *Proceedings of the National Academy of Sciences of the United States of America*, *99*(17), 11470–11475. PMID: 12169661 PMCID: PMC123280.

Sheridan, J. T., Worthington, E. N., Yu, K., Gabriel, S. E., Hartzell, H. C., & Tarran, R. (2011). Characterization of the oligomeric structure of the ca2+-activated clâĹŠ channel Ano1/TMEM16A. *Journal of Biological Chemistry*, *286*(2), 1381–1388. PMID: 21056985.

Shieh, B.-H. & Zhu, M.-Y. (1996). Regulation of the TRP ca2+ channel by INAD in drosophila photoreceptors. *Neuron*, *16*(5), 991–998.

Singer, S. J. & Nicolson, G. L. (1972). The fluid mosaic model of the structure of cell membranes. *Science (New York, N.Y.)*, *175*(4023), 720–731.

Songyang, Z., Fanning, A. S., Fu, C., Xu, J., Marfatia, S. M., Chishti, A. H., Crompton, A., Chan, A. C., Anderson, J. M., & Cantley, L. C. (1997). Recognition of

unique carboxyl-terminal motifs by distinct PDZ domains. *Science*, *275*(5296), 73–77.

Spehr, J., Hagendorf, S., Weiss, J., Spehr, M., Leinders-Zufall, T., & Zufall, F. (2009). Ca2+âĂŞCalmodulin feedback mediates sensory adaptation and inhibits pheromone-sensitive ion channels in the vomeronasal organ. *The Journal of Neuroscience*, *29*(7), 2125–2135.

Spehr, M. & Munger, S. D. (2009). Olfactory receptors: G protein-coupled receptors and beyond. *Journal of Neurochemistry*, *109*(6), 1570–1583.

Stein, A. & Aloy, P. (2008). Contextual specificity in peptide-mediated protein interactions. *PLoS ONE*, *3*(7), e2524.

Stephan, A. B., Shum, E. Y., Hirsh, S., Cygnar, K. D., Reisert, J., & Zhao, H. (2009). ANO2 is the cilial calcium-activated chloride channel that may mediate olfactory amplification. *Proceedings of the National Academy of Sciences*, *106*(28), 11776–11781. PMID: 19561302.

Stiffler, M. A., Chen, J. R., Grantcharova, V. P., Lei, Y., Fuchs, D., Allen, J. E., Zaslavskaia, L. A., & MacBeath, G. (2007). PDZ domain binding selectivity is optimized across the mouse proteome. *Science*, *317*(5836), 364–369.

Stoehr, H., Heisig, J. B., Benz, P. M., SchÃűberl, S., Milenkovic, V. M., Strauss, O., Aartsen, W. M., Wijnholds, J., Weber, B. H. F., & Schulz, H. L. (2009). TMEM16B, a novel protein with calcium-dependent chloride channel activity, associates with a presynaptic protein complex in photoreceptor terminals. *The Journal of Neuroscience*, *29*(21), 6809–6818.

Suzuki, J., Fujii, T., Imao, T., Ishihara, K., Kuba, H., & Nagata, S. (2013). Calcium-dependent phospholipid scramblase activity of TMEM16 protein family members. *Journal of Biological Chemistry*, *288*(19), 13305–13316. PMID: 23532839.

Suzuki, J., Umeda, M., Sims, P. J., & Nagata, S. (2010). Calcium-dependent phospholipid scrambling by TMEM16F. *Nature*, *468*(7325), 834–838.

Suzuki, Y., Takeda, M., & Farbman, A. I. (1996). Supporting cells as phagocytes in the olfactory epithelium after bulbectomy. *The Journal of comparative neurology*, *376*(4), 509–517. PMID: 8978466.

Takahashi, Y., Morales, F. C., Kreimann, E. L., & Georgescu, M.-M. (2006). PTEN tumor suppressor associates with NHERF proteins to attenuate PDGF receptor signaling. *The EMBO Journal*, *25*(4), 910–920. PMID: 16456542 PMCID: PMC1383560.

Taouil, K., Hinnrasky, J., Hologne, C., Corlieu, P., Klossek, J.-M., & Puchelle, E. (2003). Stimulation of Îš2-adrenergic receptor increases cystic fibrosis transmembrane conductance regulator expression in human airway epithelial cells through a cAMP/Protein kinase a-independent pathway. *Journal of Biological Chemistry*, *278*(19), 17320–17327. PMID: 12621035.

Thomas-Gatewood, C., Neeb, Z. P., Bulley, S., Adebiyi, A., Bannister, J. P., Leo, M. D., & Jaggar, J. H. (2011). TMEM16A channels generate ca2+-activated cl- currents in cerebral artery smooth muscle cells. *AJP: Heart and Circulatory Physiology*, *301*(5), H1819–H1827.

Tian, Y., Schreiber, R., & Kunzelmann, K. (2012). Anoctamins are a family of ca2+-activated clâĹŠ channels. *Journal of Cell Science*, *125*(21), 4991–4998. PMID: 22946059.

Tien, J., Lee, H. Y., Minor, D. L., Jan, Y. N., & Jan, L. Y. (2013). Identification of a dimerization domain in the TMEM16A calcium-activated chloride channel (CaCC). *Proceedings of the National Academy of Sciences*, *110*(16), 6352–6357. PMID: 23576756.

Tirindelli, R., Dibattista, M., Pifferi, S., & Menini, A. (2009). From pheromones to behavior. *Physiological Reviews*, *89*(3), 921–956.

Tong, Q., Chu, X., Cheung, J. Y., Conrad, K., Stahl, R., Barber, D. L., Mignery, G., & Miller, B. A. (2004). Erythropoietin-modulated calcium influx through TRPC2 is mediated by phospholipase cÎş and IP3R. *American Journal of Physiology - Cell Physiology*, *287*(6), C1667–C1678.

Tonikian, R., Zhang, Y., Sazinsky, S. L., Currell, B., Yeh, J.-H., Reva, B., Held, H. A., Appleton, B. A., Evangelista, M., Wu, Y., Xin, X., Chan, A. C., Seshagiri, S., Lasky, L. A., Sander, C., Boone, C., Bader, G. D., & Sidhu, S. S. (2008). A specificity map for the PDZ domain family. *PLoS Biol*, *6*(9), e239.

Trotier, D., Doving, K. B., Ore, K., & Shalchian-Tabrizi, C. (1998). Scanning electron microscopy and gramicidin patch clamp recordings of microvillous receptor neurons dissociated from the rat vomeronasal organ. *Chemical Senses*, *23*(1), 49–57.

Trudeau, M. C. & Zagotta, W. N. (2003). Calcium/Calmodulin modulation of olfactory and rod cyclic nucleotide-gated ion channels. *Journal of Biological Chemistry*, *278*(21), 18705–18708. PMID: 12626507.

Tsao, P. I. & Zastrow, M. v. (2000). Type-specific sorting of g protein-coupled receptors after endocytosis. *Journal of Biological Chemistry*, *275*(15), 11130–11140.

Ullmer, C., Schmuck, K., Figge, A., & LÃijbbert, H. (1998). Cloning and characterization of MUPP1, a novel PDZ domain protein. *FEBS Letters*, *424*(1âĂŞ2), 63–68.

Umino, Y., Solessio, E., & Barlow, R. B. (2008). Speed, spatial, and temporal tuning of rod and cone vision in mouse. *The Journal of Neuroscience*, *28*(1), 189–198.

Valentine, C. D. & Haggie, P. M. (2011). Confinement of Îš1- and Îš2-adrenergic receptors in the plasma membrane of cardiomyocyte-like h9c2 cells is mediated by selective interactions with PDZ domain and a-kinase anchoring proteins but not caveolae. *Molecular Biology of the Cell*, *22*(16), 2970–2982.

Valtschanoff, J. G., Burette, A., Davare, M. A., Leonard, A. S., Hell, J. W., & Weinberg, R. J. (2000). SAP97 concentrates at the postsynaptic density in cerebral cortex. *European Journal of Neuroscience*, *12*(10), 3605–3614.

Verpy, E., Leibovici, M., Zwaenepoel, I., Liu, X. Z., Gal, A., Salem, N., Mansour, A., Blanchard, S., Kobayashi, I., Keats, B. J., Slim, R., & Petit, C. (2000). A defect in harmonin, a PDZ domain-containing protein expressed in the inner ear sensory hair cells, underlies usher syndrome type 1C. *Nature genetics*, *26*(1), 51–55. PMID: 10973247.

von Zastrow, M. (2001). Role of endocytosis in signalling and regulation of g-protein-coupled receptors. *Biochemical Society transactions*, *29*(Pt 4), 500–504.

Wang, C. K., Pan, L., Chen, J., & Zhang, M. (2010). Extensions of PDZ domains as important structural and functional elements. *Protein & Cell*, *1*(8), 737–751.

Wang, L., Piserchio, A., & Mierke, D. F. (2005). Structural characterization of the intermolecular interactions of synapse-associated protein-97 with the NR2B subunit of n-methyl-d-aspartate receptors. *Journal of Biological Chemistry*, *280*(29), 26992–26996. PMID: 15929985.

Wang, S., Raab, R. W., Schatz, P. J., Guggino, W. B., & Li, M. (1998). Peptide binding consensus of the NHE-RF-PDZ1 domain matches the c-terminal sequence of cystic fibrosis transmembrane conductance regulator (CFTR). *FEBS letters*, *427*(1), 103–108. PMID: 9613608.

Wang, Y., Alam, T., Hill-Harfe, K., Lopez, A. J., Leung, C. K., Iribarne, D., Bruggeman, B., Miyamoto, M. M., Harfe, B. D., & Choe, K. P. (2013). Phylogenetic, expression, and functional analyses of anoctamin homologs in caenorhabditis elegans. *AJP: Regulatory, Integrative and Comparative Physiology*, *305*(11), R1376–R1389.

Weinman, E. J., Mohanlal, V., Stoycheff, N., Wang, F., Steplock, D., Shenolikar, S., & Cunningham, R. (2006). Longitudinal study of urinary excretion of phosphate, calcium, and uric acid in mutant NHERF-1 null mice. *American Journal of Physiology - Renal Physiology*, *290*(4), F838–F843.

Wheeler, D. S., Barrick, S. R., Grubisha, M. J., Brufsky, A. M., Friedman, P. A., & Romero, G. (2011). Direct interaction between NHERF1 and frizzled regulates Îš-catenin signaling. *Oncogene*, *30*(1), 32–42.

Wloga, D. & Gaertig, J. (2010). Post-translational modifications of microtubules. *Journal of Cell Science*, *123*(20), 3447–3455. PMID: 20930140 PMCID: PMC2951466.

Wong, G. T., Gannon, K. S., & Margolskee, R. F. (1996). Transduction of bitter and sweet taste by gustducin. *Nature*, *381*(6585), 796–800.

Wong, X. M., Younger, S., Peters, C. J., Jan, Y. N., & Jan, L. Y. (2013). Subdued, a TMEM16 family ca2+-activated cl- channel in drosophila melanogaster with an unexpected role in host defense. *eLife*, *2*.

Wu, H., Reuver, S. M., Kuhlendahl, S., Chung, W. J., & Garner, C. C. (1998). Subcellular targeting and cytoskeletal attachment of SAP97 to the epithelial lateral membrane. *Journal of Cell Science*, *111*(16), 2365–2376. PMID: 9683631.

Xiao, Q., Yu, K., Perez-Cornejo, P., Cui, Y., Arreola, J., & Hartzell, H. C. (2011). Voltage- and calcium-dependent gating of TMEM16A/Ano1 chloride channels are physically coupled by the first intracellular loop. *Proceedings of the National Academy of Sciences*, *108*(21), 8891–8896.

Xu, X.-Z. S., Choudhury, A., Li, X., & Montell, C. (1998). Coordination of an array of signaling proteins through homo- and heteromeric interactions between PDZ domains and target proteins. *The Journal of Cell Biology*, *142*(2), 545–555.

Yan, X., Zhou, H., Zhang, J., Shi, C., Xie, X., Wu, Y., Tian, C., Shen, Y., & Long, J. (2009). Molecular mechanism of inward rectifier potassium channel 2.3 regulation by tax-interacting protein-1. *Journal of Molecular Biology*, *392*(4), 967–976.

Yang, H., Kim, A., David, T., Palmer, D., Jin, T., Tien, J., Huang, F., Cheng, T., Coughlin, S. R., Jan, Y. N., & Jan, L. Y. (2012). TMEM16F forms a ca2+-activated cation channel required for lipid scrambling in platelets during blood coagulation. *Cell*, *151*(1), 111–122.

Yang, Y. D., Cho, H., Koo, J. Y., Tak, M. H., Cho, Y., Shim, W.-S., Park, S. P., Lee, J., Lee, B., Kim, B.-M., Raouf, R., Shin, Y. K., & Oh, U. (2008). TMEM16A confers receptor-activated calcium-dependent chloride conductance. *Nature*, *455*(7217), 1210–1215.

Ye, F. & Zhang, M. (2013). Structures and target recognition modes of PDZ domains: recurring themes and emerging pictures. *Biochemical Journal*, *455*(1), 1–14.

Yeomans, M. R. (2006). Olfactory influences on appetite and satiety in humans. *Physiology & Behavior*, *87*(4), 800–804.

Yu, K., Duran, C., Qu, Z., Cui, Y.-Y., & Hartzell, H. C. (2012). Explaining calcium-dependent gating of anoctamin-1 chloride channels requires a revised topology. *Circulation research*, *110*(7), 990–999.

Zeke, A., LukÃącs, M., Lim, W. A., & RemÃľnyi, A. (2009). Scaffolds: interaction platforms for cellular signalling circuits. *Trends in Cell Biology*, *19*(8), 364–374.

Zhang, J., Yan, X., Shi, C., Yang, X., Guo, Y., Tian, C., Long, J., & Shen, Y. (2008). Structural basis of Îš-catenin recognition by tax-interacting protein-1. *Journal of Molecular Biology*, *384*(1), 255–263.

Zhang, M. & Wang, W. (2003). Organization of signaling complexes by PDZ-domain scaffold proteins. *Accounts of Chemical Research*, *36*(7), 530–538.

Zheng, J. & Zagotta, W. N. (2004). Stoichiometry and assembly of olfactory cyclic nucleotide-gated channels. *Neuron*, *42*(3), 411–421.

Zufall, F., Kelliher, K. R., & Leinders-Zufall, T. (2002). Pheromone detection by mammalian vomeronasal neurons. *Microscopy Research and Technique*, *58*(3), 251–260.

Zufall, F., Ukhanov, K., Lucas, P., & Leinders-Zufall, T. (2005). Neurobiology of TRPC2: from gene to behavior. *PflÃijgers Archiv*, *451*(1), 61–71.

Zuker, C. S. (1996). The biology of vision of drosophila. *Proceedings of the National Academy of Sciences*, *93*(2), 571–576. PMID: 8570597.

Appendix

List of Abbreviations

Table 5.1: Abbrivations

Abbreviation	Denotation
°C	degree celsius
ACIII	adenylate cylcase type III
AcTub	acetylated tubulin
ANO	Anoctamin
ATP	adenosine-5-triphosphate
bp	base pairs
BRET	bioluminescence resonance energy transfer
CaCC	calcium-gated chloride channel
CaM	calmodulin
cAMP	cyclic adenosine monophosphate
CNG	cyclic nucleotide-gated
C-terminus	carboxy terminus
DAG	diacylglycerol
DLG1	disc large-1
EC_{50}	effective concentration of 50%
ERM	ezrin/radixin/moesin
Fig.	figure
GFP	green fluorescent protein
GPCR	G protein-coupled receptor
GST	glutathione-S-transferase
HA	hemmaglutini
HEK293	human embryonic kidney cells
INAD	inactivation no after potential D
IP3	inositol 1,4,5-trisphosphate
Luc	*Renilla* luciferase
MAGUK	membrane-associated guanylate kinase

Continued on next page

Abbreviation	Denotation
MOE	main olfactory epithelium
MUPP1	multiple PDZ domain protein 1
NHERF	Na^+/H^+ exchanger regulatory factor 1
NINAC	neither nor after potential C
N-terminus	amino terminus
OMP	olfactory marker protein
OSN	olfactory sensory neuron
PAGE	polyacrylamide gel electrophorese
PBS	phosphate-buffered saline
PCR	polymerasae chain reaction
PDE	phosphodiesterase
PDZ	postsynaptic densitiy-95/disc large-1/zona occludens 1
PID	protein interaction domain
PIP2	phosphoinositol-phosphate-2
PLC	phospholipase C
PSD-95	postsynaptic densitiy-95
RT-PCR	reverse transcription polymerase chain reaction
SAP	synapse associated protein
SD	standard deviation
SDS	sodium dodecyl sulfate
SEM	standard error of the mean
SH3	Src homology 3
STED	stimulated emission depletion
Tab.	table
TM	transmembrane
TRP	transient receptor potential
V1	vomeronasal receptor type 1
V2	vomeronasal receptor type 2
VNO	vomeronasal organ
VSN	vomeronasal sensory neuron
WT	wildtype
ZO-1	zona occludens-1

List of Figures

List of Tables

NHERF1 interaction partners

Table 5.2: Vomeronasal receptors bound to NHERF1

Receptor	Sequence	PDZ class	PDZ1	PDZ2
Vmn1ra10	IIKFLRSMCGRIANI	Class II	*	*
Vmn1r50	MIKFVTSMCGRIVNV	Class II	*	*
Vmn1r53	ITNFLRSMCGRIVNI	Class II	*	*
Vmn1r34	NYASRYFKKCNFPLI	Class II	*	*
Vmn1rb4	IIKFLRSMCGRIVNI	Class II	*	*
Vmn1rc9	LTVQKLVQPLWKSVF	Class I	*	*
Vmn1r31	LKNMHSKHHQSFF	Class I	*	*
Vmn1r5 / r6	MTKILRSVCTRIINI	Class II	*	*
Vmn1r40	IIKFWESKCGRIVNI	Class II	*	*
Vmn1rb10	RMIKFGGQCWQNINI	Class II	*	*
Vmn1r46	IIKFFWSLCGRIVNI	Class II	*	*
Vmn1r229	VSRFCFTCIGNLKLP	Class III	*	*
Vmn1r212	GDSSLELRINYKLTL	Class II	*	*
Vmn1r210	VKFWHAQWEKLRKCL	Class III	*	*
Vmn1r1 / r51 / ra1	KHIVNCLRSV	Class III	*	*
Vmn1r39	LKNMQKVCHQICKKV	Class III	*	*
Vmn1ra7	RITNLLISMYEKIVL	Class II	*	*
Vmn1r84	STPKNALPCCSRRNL	Class III	*	*
Vmn1re11	VRPRLSLVWMRNINP	Class II	*	*
Vmn1r168 / rd12 r177	SYPCSLIFNYKKPVI	Class II	*	
Vmn2r122	GKVMGGCGGFLHLGF	Class II	*	
Vmn1r63 / rd1	KGHCSLRIMSVWKSI	Class III	*	
Vmn1rc18	TSDERIINVLKNLWP	Class II	*	
Vmn1r228	DFTASRCCFTWIKII	Class III	*	
Vmn1re6	CFTWTRNIKIP	Class III		*
Vmn1rc4	NVQKFVSNAYPQLPL	Class II		*
Vmn2r53	QRRCVSSGESLGSSL	Class I	*	
Vmn2r110	IRDKTHSQRNTSLKI	Class II		*

Table 5.3: Further PDZ ligands bound to NHERF1

Protein	Sequence	PDZ class	PDZ1	PDZ2
ACCN4	HPHGPPGSLFEDFAC		*	*
PDE2A	DGTRAPVNGCCSLEG		*	*
ACCN1	VPLQTALGTLEEIAC		*	*
KCNMB2	LCERIQRINR		*	
Slc22a12	THDTPDGSILMSTRL	Class I	*	
D2R	IEFRKAFMKILHC		*	
AC 6	TYFLNGGPSS			*
AC 5	YFLNGGPPLS			*
CD36	YCACKSKNGK			*
TMEM17	SSAAVRRVRQCTEEL	Class III		*
ATP8a1	VIRAYDTTKQRPDEW			*
AC 2	RSLSQSNLAS			*
PLCβ1	LIEDPLHDKLWKCSL			*
Slc24a4 isoform b	VNLPMCREDD			*
Clic-like 1	AVAAHGTEPVSSPCG			*
PLCη1	DGKENCLVQI	Class II		*
$G_{\alpha t1}$ / $G_{\alpha t2}$ / $G_{\alpha t3}$	TDIIIKENLKDCGLF			*
Slc24a4 isoform c	SFCHFQTGAP			*
TRM3g	DRFLVCYLGGDNHCR			*
ATP8b3	ASSSPSQLEVPRKQS			*
CD9	SMILCCAIRRSREMV			*
ATP8b1	IIADGTAEYRRTVES			*
$G_{\alpha i3}$	TDVIIKNNLKECGLY			*
FPR3	GKSSNFSSCPADSEL	Class I		*
Clic1 iso a	WRPCCALPGTQSWLP			*
CaM	GQVNYEEFVQMMTAK			*
FPR6	ALNSDKTRNLSSQRL			*
DAGβ	TACVSCPGQGGSSVP	Class I		*
TMEM2	HRRDLDLLQQALKVL	Class III		*
TMEM111	HFEGMFKKELQTSIF	Class I		*

DLG1 interaction partners

Table 5.4: Vomeronasal receptors bound to DLG1 PDZ2 domain

Receptor	Sequence	PDZ class	also by NHERF1
Vmn1ra10	IIKFLRSMCGRIANI	Class II	*
Vmn1r53	ITNFLRSMCGRIVNI	Class II	*
Vmn1r1 / r51 / ra1	KHIVNCLRSV	Class II	*
Vmn1r40	IIKFWESKCGRIVNI	Class II	*
Vmn1r210	VKFWHAQWEKLRKCL	Class III	*
Vmn1r229	VSRFCFTCIGNLKLP	Class III	*
Vmn1r50	MIKFVTSMCGRIVNV	Class II	*
Vmn1r208	SKFWHAHWEKLSKCL	Class III	
Vmn1r34	NYASRYFKKCNFPLI	Class II	*
Vmn2r104	IRKKTQSRRKKSPKM	Class II	
Vmn2r96	YIRKKTPSRKNFPKI	Class II	

Table 5.5: Further PDZ ligands bound to DLG1 PDZ2 domain

Protein	Sequence	PDZ class	also by NHERF1
KCNMB2	LCERIQRINR		*
Kcnmb4	AEAMKKRKFS		
Slc22a12	THDTPDGSILMSTRL	Class I	*
TRPM3g	DRFLVCYLGGDNHCR		*
TMEM2	HRRDLDLLQQALKVL	Class III	*
Slc24a4 isoform c	SFCHFQTGAP		*
CD9	SMILCCAIRRSREMV		*
ACCN4	HPHGPPGSLFEDFAC		*
D2R	IEFRKAFMKILHC		*
PLC gamma 1	LIEDPLHDKLWKCSL		*
PLC beta 1	LIEDPLHDKLWKCSL	Class I	

PDZ interaction microarray - complete list

Name	Sequence	Accession No.	PDZ class
V1-receptors			
Vmn1r31	LKNMHSKHHQSFF	NM_001166729.1	Class I
Vmn1rc9	LTVQKLVQPLWKSVF	AF291505.1	Class I
Vmn1rc4	NVQKFVSNAYPQLPL	AF291500.1	Class II
Vmn1r212	GDSSLELRINYKLTL	NM_134241.1	Class II
Vmn1rc18	TSDERIINVLKNLWP	NM_134173.2	Class II
Vmn1c20	IMLKNLQSKHYHLYF	NM_134175.1	Class II
Vmn1ra7	RITNLLISMYEKIVL	AF291486.1	Class II
Vmn1rb10	RMIKFGGQCWQNINI	AF291496.1	Class II
Vmn1r5 r6	MTKILRSVCTRIINI	Y17566.1 Y17567.1	Class II
Vmn1r185	HLRKINLSPNLVINM	NM_134231.1	Class II
Vmn1re11	VRPRLSLVWMRNINP	NM_134230.3	Class II
Vmn1r34	NYASRYFKKCNFPLI	NM_001166719.1	Class II
Vmn1r168 rd12 r177	SYPCSLIFNYKKPVI	NM_001166842.1 CH466593.2 NM_206872.2	Class II
Vmn1rb4	IIKFLRSMCGRIVNI	AAI07185	Class II
Vmn1r53	ITNFLRSMCGRIVNI	NM_053226.2	Class II
Vmn1r40	IIKFWESKCGRIVNI	NM_053228.1	Class II
Vmn1r46	IIKFFWSLCGRIVNI	NM_053229.1	Class II
Vmn1r49	IIKFWESIFGRIVNI	NM_011911.1	Class II
Vmn1r50	MIKFVTSMCGRIVNV	NM_053225.1	Class II
Vmn1rc1	KHQQRFFNKDIFFSL	NM_053231.2	Class II
Vmn1r7	KCHPSFSLKDFFFFI	NM_001166710.1	Class II
Vmn1rc14	IKNMQKVCHQIFFKV	BC138428.1	Class II
Vmn1ra10	IIKFLRSMCGRIANI	BC151088.1	Class II
Vmn1r205	NKFWHAQWEKLRKYL	NM_134217.1	Class III
Vmn1r210	VKFWHAQWEKLRKCL	NM_134235.1	Class III
Vmn1r208	SKFWHAHWEKLSKCL	NM_134218.1	Class III
Vmn1rb11	ALKSI	AY065465.1	Class III
Vmn1r228	DFTASRCCFTWIKII	NM_134192.3	Class III
Vmn1r63 rd1	KGHCSLRIMSVWKSI	NM_030742.1 CH466627.1	Class III
Vmn1r60	KGHCSVHIMSVWKSM	NM_001166732.1	Class III
Vmn1r61	MSVWKSM	NM_001166733.1	Class III
Vmn1r229	VSRFCFTCIGNLKLP	NM_134190.1	Class III
Vmn1re6	CFTWTRNIKIP	NM_134195.2	Class III
Vmn1r36	LKSMQKLWHQIFKKV	NM_134166.1	Class III
Vmn1r39	LKNMQKVCHQICKKV	NM_001166720.1	Class III

Vmn1r84	STPKNALPCCSRRNL	NM_134233.1	Class III
Vmn1r1 r51 ra1	KHIVNCLRSV	BC046308.1 Q8VIC6 AF291481.1	Class III
Vmn1r17	LKNMHSKHHQRFF	NM_134171.1	Class III
Vmn1r20	VKNMYSKHHQRFF	NM_001101533.1	Class III
V1ra9	EKHIVNILRG	Q8VIC7	
V1rd3	GLEIHMTRGDITEEQ	NP_109665	
V1rd4	SMGIHVTGGAITEGQ	EDL31296	

V2-receptors			
Vmn2r53	QRRCVSSGESLGSSL	NM_001104644.1	Class I
Vmn2r99	IRKKTLSRRKNFSKI	NM_001104551.2	Class I
Vmn2r40 r41 r36 r47 r15 r34 r45 r14 r32 r49 r42 r51	PERNSTQKIREKSYF	NM_001105072.1 NM_001105073.1 NM_001105068.1 NM_001105151.1 NM_009490.3 NM_001105066.1 NM_001105075.1 NM_009489.2 NM_001105063.1 NM_001105156.1 NM_009493.2 NM_001105179.1	Class I
Vmn2r31 r44 r38 r33	KVRNSTQKIKEKSYF	NM_001105062.1 NM_001105074.1 NM_001105070.1 NM_001105065.2	Class I
Vmn2r35	KENNSTQKIKEKSYF	NM_001105067.1	Class I
Vmn2r50	KESNSTQKIKEKSNF	NM_001105178.1	Class I
Vmn2r29	PERNSTQKIKEKSYF	NM_001113468.1	Class I
Vmn2r28 r52	PERNSIKKIREKSHF	NM_001081405.1 NM_001105191.1	Class I
Vmn2r109	IRDKTHSRRNKSLKI	NM_001104571.1	Class II
Vmn2r110	IRDKTHSQRNTSLKI	NM_001104572.1	Class II
Vmn2r80	THNRDKRQHRSKILL	NM_001103368.1	Class II
Vmn2r97	IRKKTPTRKKNFPKI	NM_001104549.1	Class II
Vmn2r98	IRKKTPSRKKKFPKI	NM_001104550.1	Class II
Vmn2r102	IRKKTYSRRKNFPKI	NM_001104564.1	Class II
Vmn2r103	HVRKKTYSRKNYPKI	NM_001104565.1	Class II
Vmn2r101	IQKKTHSRRKNFPKI	NM_001104563.1	Class II
Vmn2r92	RKKKTHSKRKIFPKI	NM_001104541.1	Class II
Vmn2r93	IRRKQHTRRKNSPKI	NM_001104542.1	Class II

Vmn2r96	YIRKKTPSRKNFPKI	NM_001104547.1	Class II
Vmn2r54	QRRYKFSGESPEPNI	NM_001081449.2	Class II
Vmn2r104	IRKKTQSRRKKSPKM	NM_001104566.1	Class II
Vmn2r91	FRHTRKKNHIPVAKI	NM_001104540.1	Class II
Vmn2r64 r62	RLDIRHKIHSRRVVI	NM_001105061.1 NM_001105059.1	Class II
Vmn2r63	CLDIRHKIHSRKVVI	NM_001105060.1	Class II
Vmn2r27	SGGYSRKKFFKSVSP	NM_001104642.1	Class II
Vmn2r60	PEKNSYLGVRHKII	NM_001105057.1	Class III
Vmn2r57	RNKIHSRRSSHLKFI	NM_177764.4	Class III
Vmn2r116	LEMIRVKSSSNVHVS	NP_001098050	
Vmn2r122 kurz	PDSNFIQNHKGKLLY	AAH38260	
Vmn2r122	GKVMGGCGGFLHLGF	NP_033518	Class II
Vmn2r1 r2	SSELNSTTVSTVLDE	NP_064302 NP_001098062	

Formyl-petide receptors			
FPR1	TNLASLPEDIEIKAI	NP_032068	Class III
FPR2	TSSTSPPADIELKAP	NP_032065	Class III
FPR3	GKSSNFSSCPADSEL	NP_032066	Class I
FPR4	IYSLYASLERALRED	EDL20517	
FPR5	GTNSTSLSENTLNAM	AAA16110	
FPR6	ALNSDKTRNLSSQRL	NP_796290	
FPR7	SALNSDKIRNLSSQT	AF437513_1	

Trace amino associated receptors			
TAAR1	GKIFQKDSSRSKLFL	NP_444435	Class II
TAAR2	SHFHNTNLFTQKETE	NP_001007267	
TAAR3	FRSNSDTANLFPEAH	NP_001008429	
TAAR4	FRSDSSTSSLHPAHP	NP_001008499	Class II
TAAR5	EIFSPRTPTVDLYHD	NP_001009574	
TAAR6	FKNSSATMNLFSEQI	NP_001010828	Class III
TAAR7a-f	KILRENSSTTNLFPE	NP_001010829 NP_001010827 NP_001010838 NP_001010835 NP_001010839	
TAAR8a/b	EILKGHSSTANLFSE	NP_001010830 NP_001010837	
TAAR8c	KILKGHSSTTNLFSE	NP_001010840	
TAAR9	DSSTTNLFSEEAGAG	NP_001010831	

Olfactory receptors			
Olfr726	KPGQVSELIRNVLFM	NP_666428	Class II
Olfr727	QVSALIRNVLFLETK	NP_666431	
Olfr1348	NKEVHTVLKKTLHWP	NP_667124	

other receptors			
Pgrmc1	SDDEEPKDETARKNE	NP_058063	
D2R	IEFRKAFMKILHC	NP_034207	
Edg1	NPETIMSSGNVNSSS	EDL12402	
M3	RQSVIFHKRVPEQAL	NP_150372	

VSN signaling cascade			
PLC beta	EIERENPGREFDTPL	AAH58710.1	Class I
PLC gamma	LIEDPLHDKLWKCSL	NP_067255.2	
DAG alpha	GASPTKQDDLVISAR	NP_932782.2	
DAG beta	TACVSCPGQGGSSVP	NP_659164.2	Class I
TRPC2 beta	GDLPLEGDLETKGES	AAG29951.1	
GC-D	GLAEPRKSGEAGPGP	NP_001124165	Class II
PDE2A	DGTRAPVNGCCSLEG	AAH86800	
CA2	PAQPLKNRKIKASFK	NP_033931	

OSN signaling cascade			
CNGB1	TLSVEVLEEKKEGAE	AAH45114.1	
CNGA4	DGEEKAGQEGPSGLE	NP_001028489.1	
CNGA2	YLSDGINTPEPAVAE	NP_031750.2	
CNGA3	FSPDRENSEDASKTD	NP_034048	
AC III	NGSSVTLPHQVVDNP	NP_612178.2	Class III
PDE1C2	SNTGNESKKTDDPEE	NP_001020739	
PDE4A	VISAPGRWGSGGDPA	AAF14519	Class III

TMEM proteins			
TMEM16a	DGSPVPSYEYHGDAL	Q8BHY3	Class III
TMEM16b	QPGSIASSGSQHTNV	NP_705817	Class I
TMEM16f	RIGGTVDNSVRPKLE	EDL04250	
TMEM16k	ENLKEEYQEDGKEAT	NP_598740	
TMEM30a	HKYRNSSNTADITI	AAH18491	Class II
TMEM30b	YQDQDDDDNDDE	AAI19225	
TMEM30c	SISYSILLCHAPSSE	CAP19187	
TMEM67	KNLATKTLVDERFLI	Q8BR76	Class II
TMEM67 iso c	CCSSVLWIWLARTLF	EDL05629	Class I
TMEM111	HFEGMFKKELQTSIF	NP_780310	Class I
TMEM214	TVAFLDWALTMISQQ	NP_653108	
TMEM168	PTVLDTGQGFKLVKS	NP_083266	

TMEM165	ALFISPESGF	NP_035756	Class I
TMEM17	SSAAVRRVRQCTEEL	NP_705824	Class III
TMEM24	FKSKPKANGNPSPQL	NP_082185	Class II
TMEM2	HRRDLDLLQQALKVL	NP_114386	Class III
TMEM32	SNTSLKLRKFDSLRR	NP_666346	
TMEM57	SGLDPNASVYQPLKK	CAM26943	
TMEM43	RTRVPAKKLE	NP_083042	
TMEM33	LQSIAFISRLAPTVA	NP_083251	Class I
TMEM109	RQRRAAKMPRSMEEE	NP_598903	
TMEM85	EPPERMEFSGGGLLL	NP_080795	Class II
TMEM115	VPESSLITLETAPLL	NP_062678	Class II
TMEM205	VGLALGLRSL	NP_848692	Class III
TMEM63a	AQDPSGTAAYAYQES	NP_659043	
TMEM147	LYVAVVNVHS	NP_081491	
TMEM122	GLLNAHQAASSQNKR	NP_001032723	
TMEM199	RAMEGELGEL	NP_954669	
REEPs			
REEP1	MSRSASESAGSSGTA	AAT70674	
REEP2	KTRPKKKSSGGGDSA	AAT70675	Class III
REEP3	GSLKYKVKKRPQVYF	AAT70676	Class II
REEP4	KVRTRKKAMPSDMDS	AAT70677	
REEP5	VKKATVNLLGDEKKS	AAT70678	
REEP6	ASTSEPPAALELDPK	AAT70679	
TRP channels			
TRPC1	LGFRTSKYAMFYPRN	EDL20938	
TRPV1	EDAEVFKDSMAPGEK	NP_001001445	
TRPM2	KTILQKVASLFGAHF	EDL31768	Class II
TRPM3a (a-e)	LSRTSAFHSFESKHN	NP_001030316	
TRPM3f	LQESIDPAEHPFYSV	NP_796315	
TRPM3g	DRFLVCYLGGDNHCR	NP_001030321	
TRPM3h	AFGHKYSEEGGIYFL	NP_001030322	
TRPM3i	SDILAFGHKYSEEGG	NP_001030323	
TRPM4	PPGAPPPPSPTGSKD	AAH96475	
TRPM5	RDREYLESGLPPSDT	NP_064673	
Amyloride sensitive cation channels			
ACCN1	VPLQTALGTLEEIAC	NP_031410	

ACCN2	LPHHPARGTFEDFTC	NP_033727	
ACCN3a	TLAASHRTCYLVTRL	EDL03130	Class I
ACCN3b	EQKAAYEVSELLGVY	EDL03131	
ACCN3d	NGHRTHVPHLSLGPR	EDL03133	
ACCN4	HPHGPPGSLFEDFAC	NP_898843	
other channels / trans-porters			
KCNMA1	RESRDKQNRKEMVYR	NP_034740.2	
KCNA5	SLYALCLDTSRETDL	NP_666095	Class I
ERG1	LTSQPLHRHGSDPGS	O35219.2	
ERG3	LGLHRHVSDPGLPGK	Q9ER47.1	
SLCO2A1	KNREYSLQENASGLI	NP_201571.2	
Slc27a2	TENIYNAIIDKTLKL	AAH24735	Class II
Slc12a2	LLVRGNHQSVLTFYS	NP_033220	
Slc24a4 isoform b	VNLPMCREDD	EDL18869	
Slc24a4 isoform c	SFCHFQTGAP	EDL18870	
Slc4a11	IESKYLDVMDAEHRP	AAI11885	
Clic1 iso a	WRPCCALPGTQSWLP	EDL26683	
Clic1 iso b	EQRLCPGRICLHLSR	EDL26684	
Clic1 iso c	EEIELAYEQVARALK	EDL26685	
Clic4	EVEIAYSDVAKRLTK	CAJ18487	
Clic6	REIEHAYSDAAKRMK	NP_766057	
Clic-like 1	AVAAHGTEPVSSPCG	NP_001171241	
Vdac-1	NAGGHKLGLGLEFQA	NP_035824	Class II
Catsper2	LQEFAVQALMSFEDK	NP_694715	
ATPases			
ATP1a1	IRRRPGGWVEKETYY	AAH25037	
ATP8a2	IVRAYDTTKENSRKK	NP_056618	
ATP8b1	IIADGTAEYRRTVES	AAR90342	
ATP8b3	ASSSPSQLEVPRKQS	AAI18978	
ATP8a1	VIRAYDTTKQRPDEW	AAI29873	
Signal regulation			
CaM	GQVNYEEFVQMMTAK	NP_031615.1	
Camk2b	NVHFHCSGAPVAPLQ	CAI24954	
PLC beta2	QEPLVSKADTQESRL	AAI45250	Class I
Pde6h	FSHLELHELAQFGII	NP_076387	

Sac-1	DFVDAPRLVQKEKID	NP_109617	
Orai1	DHRGDHSLTPGTHYA	BAF47905.1	
STIM1	RKKFPLKIFKKPLKK	AAH21644.1	
Ezrin	RQGNTKQRIDEFEAM	NP_033536	Class III
Sans	RQALERPLALEDTEL	BAC57430	Class I
Ck2 alpha	CAENTVLSSGLTAAR	NP_034104	
Ck2 protein 2	ALLRYFQTKFQNEKS	NP_776286	
Ppp1r9b	ELEGNLQTLRNSNST	CAI23964	
Rgs20	YKDLLTSLAEKTVEA	NP_001171266	Class II
Gipc1	FDVWGAIGDAKVGRY	NP_061241	
Lipid regulation			
CD36	YCACKSKNGK	AAH10262	
Cav1	GKIFSNIRISTQKEI	AAR16290	Class III
Cav2 isoform a	VGRSFSSVSMQLSHD	AAR16289	
Cav2 isoform b	FATLSCLHIW	EDL13889	
Cav3	GQVCSNIKVVLRREG	NP_031643	
Misc I			
Ror2	DTLQVTEAAHVQLEA	AB010384.1	Class II
Stoml3	GGISYGNNKKVTAKA	NP_694796	Class II
Stomatin	PLPVDMLQGIMGSNH	CAM16868.1	
SPP beta H13	STEASASKRLEKKEK	NP_034506	
GRP78	PPPTGEEDTSEKDEL	NP_001156906	Class III
Ncam	VPNDATQTKENESKA	P13595	Class I
Tmed10	RFFKAKKLIE	NP_081051	
Spef-1	DDLSRRLQQAERKQR	NP_081917	
Lbra alpha	YNDFNRWHHEYQTRY	NP_109620	
Lbra beta	SAVGSTLFLLLGSSK	NP_001071156	
Lbra gamma	DPLIGLSLLSLFAIH	NP_001071155	
Pacs-1	VKHFPVGLFSGSKTT	NP_694769	
Cep290	EHSEDGESPHSFPIY	NP_666121	
Cd225	IVLNAQNLHT	NP_079654	
S100A13	AKEVRKEKALGIRKK	NP_033139	
G-alpha			
Golf	RDIIQRMHLKQYELL	Q8CGK7	Class III
Gnas1 short Gnas1 long	RDIIQRMHLRQYELL	AAH62654 Q6R0H7	
Gnai1	TDVIIKNNLKDCGLF	AAI38866	
Gnai2	VTDVIIKNNLKDCGLF	NP_032164.2	

Gnai3	TDVIIKNNLKECGLY	AAH41107	
Gnaio1	TDIIIANNLRGCGLY	EDL11107	
Gnat1 Gnat2 Gnat3	TDIIIKENLKDCGLF	AAH58810 AAH16272 AAI47842	
Gnaz	TDVIIQNNLKYIGLC	AAH14702	
Gnaq Gnaq11	KDTILQLNLKEYNLV	AAH57583 NP_034431.1	
Gnaq14	KDTILQLNLREFNLV	AAH27015	
Gnaq15	RDSVLARYLDEINLL	AAH11098	
Gna12	DTILQENLKDIMLQ	NP_034432	
Gna13	KDTILHDNLKQLMLQ	EDL34354	

controls			
HA-Tag	YPYDVPDYA		
myc-Tag	EQKLISEEDL		
FLAG-Tag	DYKDDDDK		
EBP50	PQMDWSKKNELFSNL	NP_036160	Class I
EBP50 -PDZ	PQMDWSKKNELF	NP_036160	
PDZK1	STASHSSSNSEDTEM	NP_001139473	
beta-catenin	PPGDSNQLAWFDTDL	AAH53065	Class I
CFTR	ALKEETEEEVQETRL	NP_066388	Class I
PTEN	NEPFDEDQHSQITKV	NP_032986	Class I
SR-B1	MSPAAKGTVLQEAKL	NP_058021	Class II
SR-B1 -PDZ letzte AS	MSPAAKGTVLQEAK	NP_058021	Class II
Slc34a3 (NaP2c)	AHCYENPQVIASQQL	NM_080854	
NaP2a	ENVLEEEGRVRSTPM	NP_001158029	Class I
Slc22a5	KDGEESPTVLKSTAF	NP_035526	Class I
Slc15a2	IQGNMINLETKNTRL	NP_067276	Class I
Slc22a12	THDTPDGSILMSTRL	NP_033229	Class I

Misc II			
Frizzled 1	FYTRLTNSKQGETTV		Class I
Frizzled 3	GTSMNRVIEEDGTSA		Class I
Frizzled 7	FYHRLSHSSKGETAV		Class I

Curriculum vitae

For reasons of data protection,
the curriculum vitae is not included in the online version